Modeling optical inscription of complex surface patterns in azobenzene-containing materials

Dissertation

zur Erlangung des akademischen Grades
Doctor rerum naturalium
(Dr. rer. nat.)
vorgelegt
dem Bereich Mathematik und Naturwissenschaften
Fakultät Physik
Institut für Theoretische Physik
der Technischen Universität Dresden

Von
Bharti Yadav
geboren am 24.02.1995 in Nawta Ki Dhani, India

Eingereicht am
Erster Gutachter
Prof. Dr. Jens-Uwe Sommer
Zweiter Gutachter
Prof. Dr. Svetlana Santer

Acknowledgement

I greatly wish to thank my supervisors PD Dr. Marina Grenzer (Saphiannikova) and Prof. Dr. Jens-Uwe Sommer. I also gratefully acknowledge the help and support by all my colleagues, who have contributed in the successful completion of this work. I would like to thank Jan Domurath, Nina Tverdokhleb, Markus Koch, Ankush Checkervarty and Abhinav Sharma for fruitful discussions and for sharing their experiences and thoughts on various topics. I further thank Sarah Loebner for interesting discussions over experimental observations. I appreciate the interdisciplinary atmosphere in the Leibniz Institute of Polymer Research, Dresden.
I would like to thank my friends in Dresden, Abhinav bhaiya and Arsha for their love and support. Last but not the least, I would like to thank my family, my parents, my sister Bhawna and my brother Dev, without them it was not possible. I would like to thank my husband, Avinash for his immense love, understanding and support.

Abstract

Azopolymers represent a wide class of polymeric systems in which the azobenzene chromophores are either incorporated into the main chain or covalently attached to it as a part of side chain. Light with an appropriate wavelength induces cyclic trans-cis isomerization, which results in preferred orientation of the trans-isomers perpendicular to the light polarization. Most azopolymer materials directionally deform in the presence of various light polarizations.

In this thesis, a study is presented for photoinduced deformations in glassy side-chain azopolymers under different irradiation patterns. In particular, the photodeformations are investigated under homogeneous irradiation with linearly and circularly polarized light, and under inhomogeneous irradiation with intensity and polarization interference patterns. It is proposed to explain these mechanical deformations using the orientation approach, which takes into account the reorientation of the chromophores. Due to the rigid attachment of the chromophores with the main chain, the backbone segments in side-chain azopolymers should reorient into the polarization plane, which is accompanied by appearance of light induced stress. To describe the time evolution of light induced stresses, the side-chain azopolymers are modeled as an ensemble of rigid segments in presence of the effective orientation potential. Implementing the stress in a viscoplastic material model of the finite element software ANSYS, it is shown that a square azopolymer post elongates along the polarization for the linearly polarized light and contracts along the propagation direction for the circularly polarized light. Also, the deformations in the elongated oriented colloids under intensity interference patterns are modeled and it is found that the formation of beads and wave-like structures are in accordance with the experiment. The orientation approach also reproduces the peculiar structures at the edges of thin azopolymer film under polarization interference patterns. Hence, the orientation approach correctly predicts local variations of the light induced stress in each illumination pattern for both initially isotropic and highly oriented materials.

With this, it is proved that the orientation approach implements a self-sufficient and convincing mechanism to describe photoinduced deformation in azopolymer materials, which does not rely on the photo-fluidization concept. The viscoplastic material modeling, developed in this thesis, can be used to describe the inscription of intricate surface structures under complex interference patterns.

Contents

Acknowledgement **i**

Abstract **ii**

1 Introduction **2**
1.1 Motivation . . . 3
1.2 Goals . . . 5
1.3 Outline of thesis . . . 5

2 Azopolymer properties and behaviour **8**
2.1 Models to explain photodeformations . . . 8
2.2 Order parameter . . . 12
2.3 Light polarizations . . . 15
2.3.1 Linear polarization of light . . . 15
2.3.2 Circular polarization of light . . . 16
2.3.3 Light interference patterns . . . 18
2.4 Effective orientation potential for linearly polarized light . . . 21
2.5 Magnitude of light-induced stress and yield stress in glassy azopolymers . . . 24

3 Light-induced orientation and stress **26**
3.1 Effective orientation potential for circularly polarized light . . . 26
3.2 Derivation of stress tensor . . . 28
3.2.1 Derivation of time-dependent orientation tensor . . . 31
3.3 Closure approximations for orientation tensor . . . 33
3.3.1 Uniaxial orientation order . . . 34
3.3.2 Biaxial orientation order . . . 36
3.4 Calculation of orientation tensor . . . 37
3.4.1 Uniaxial orientation order . . . 37
3.4.2 Biaxial orientation order . . . 38

4 Viscoplastic modeling of glassy azopolymers **41**
4.1 Viscoplastic material modeling . . . 41
4.2 Material modeling in ANSYS . . . 42
4.3 Application of light-induced stress in ANSYS . . . 44

5 Directional deformations under homogeneous light illumination **46**
5.1 Light-induced stress tensor 47
5.1.1 Linearly polarized light 47
5.1.2 Circularly polarized light 50
5.2 Cuboid azopolymer sample 52
5.2.1 Effect of linearly polarized light 53
5.2.2 Effect of circularly polarized light 53

6 Stripe patterns under Gaussian distributed light intensity **56**
6.1 Strongly focused beam 56
6.2 Light-induced stress field 57
6.3 Modeling conditions 60
6.4 Modeling results 62

7 Complex photodeformations under intensity interference patterns **69**
7.1 Formation of ellipsoidal colloid and effect of spatially varying light intensity 71
7.1.1 Spherical azopolymer colloid in the presence of linearly polarized light 71
7.1.2 Light-induced stress for spatially varying intensity 75
7.2 Surface relief gratings 81

8 Summary and outlook **89**
8.1 Summary 89
8.2 Outlook 91

List of Publications **93**

A Time dependent components of the stress tensor **95**
A.1 Calculations of stress tensor components 95

B APDL commands and subroutine computational codes **97**
B.1 Mechanical APDL code for implementation of homogeneous stress 97
B.2 Mechanical APDL code used in workbench 98
B.3 Definition of initial state variables 99
B.4 Userthstrain subroutine 100

Bibliography **112**

List of figures **117**

List of Tables **118**

List of Symbols **120**

Chapter 1

Introduction

Azobenzene containing polymers or shortly azopolymers represent a wide class of polymeric systems in which the azobenzene chromophores are either incorporated into the main chain or covalently attached to it as a part of the side chain. The azobenzene chromophores are photosensitive, i.e. in the presence of light the azobenzene molecule isomerizes between trans and cis states. Additionally, when azobenzenes are irradiated with linearly polarized light, they reorient preferentially perpendicular to the light polarization direction[1, 2]. Such sensitivity of the azobenzene chromophores makes the whole azopolymer system photosensitive. Even chirality, solubility and polarity can be changed by applying the light to the photo-switchable compounds. In principle, the melting point and hence mechanical properties (viscosity, moduli) of azobenzene containing materials can be changed using light of appropriate wavelength, which results in photoinduced solid to liquid transitions [3]. These solid to liquid transitions can be manipulated in such a way to imprint nanopatterns on the surface of the azopolymeric materials [4].

Photosensitive azopolymers are known as highly versatile systems which have many applications in different fields. These materials can be used as molecular switches [5, 6] and fancy molecular motors [7, 8], because the parent azobenzene exists in two isomeric forms, which can be interchanged using light of appropriate wavelength or heat [9]. The light-responsive materials made of azopolymers are used in medicine [10], nano and liquid crystalline technology [11, 12, 13], as smart polymers for soft-robotics [1, 14, 15], large-scale multiplexed gratings for photonic applications [16] and intelligent enzymes [17]. Also azo-structures can be used in devices with light-controlled wettability [18, 19, 20]. Some natural phenomena like fly trapping plants [21] can be mimicked by designing micro-robotic systems incorporating azobenzene chromophores.

Azopolymers are used in the various branches of biology. For DNA compacting, azobenzene containing surfactants are developed which can have application in the drug delivery [22, 23]. In the past two decades, many techniques are being developed to engineer biological membranes using azobenzene systems to produce light-gated ion channels [24, 25, 26]. Many such applications

of azopolymers in the biological systems are discussed in the review of Barrett et al. [27].

Azopolymers have played a very important role in electronics and modern photonics which can not be ignored. The azopolymers can be used as an optical storage medium [28, 29, 30, 31, 32], liquid crystal anchoring and to structure waveguides and waveguide couplers [33, 34]. The azobenzene liquid-crystal films can be used for optical switching and image storage [35]. Due to the photo-switching ability of azobezene, the light energy can be transformed into the mechanical energy which makes the system a prototype of light-powered engine [36].

The use of light as an external stimulus is rather attractive, as it can provide a remote control of the device or help to restore its function, for example, to heal the electrical conductivity after mechanical failure [37]. With this aim, photo-sensitive azopolymers, which deform in the presence of light, can be used. Such polymers exhibit considerable photodeformations even below the glass transition temperature T_G, because the light-induced mechanical stress can be larger than the yield stress. The azopolymers were observed to experience photomechanical bending under light irradiation; with this property there are possibilities that they can be used as fluid actuators [38]. A very interesting research is ongoing for light driven artificial muscles made of azobenzene containing materials [1, 39].

Unusual photo-mechanical effects have been observed in side-chain azobenzene containing polymers. First of all, they include inscription of surface relief gratings on the top of azopolymer films [40, 41], the efficiency of which depends on the light interference pattern [42]. Secondly, response of azopolymers with different chemical architecture was studied under linearly polarized light in thin azopolymer films placed on the water surface [43]. The deformations had an opposite sign depending on the polymer architecture: the polymer with rigid back backbone deformed in the direction of light polarization, whereas the polymer with flexible backbone deformed in the direction perpendicular to the light polarization [43]. The efficiency of surface relief grating inscription also depends on the architecture of the used azopolymer [42, 44, 45, 46]. Recently, formation of triangular and hexagonal shaped pillars was found in the azo-molecular glasses when irradiated with circularly polarized light [47, 48]. All these phenomena await an explanation on the molecular level.

1.1 Motivation

As we have discussed in the previous section, azobenzene containing polymers exhibit a versatile behaviour when irradiated by polarized light. Below we mention few experiments which excite the most, as the light-induced deformations in these polymers take place much below the glass transition temperature.

- **Inscription of surface relief gratings**

  The phenomenon was discovered in 1995, when two research groups [41,

40] reported independently about the formation of surface relief gratings. Inscription was done by exposing an azopolymer film to periodic intensity or polarization patterns that resulted from the interference of two polarized laser beams. The wavelength of the laser was in the absorption region associated with the cyclic trans-cis-trans isomerization of the azo dye. Following these initial reports, not only one dimensional linear gratings but also two-dimensional periodic structures were inscribed onto film surfaces [41, 49, 50].

- **Uniaxial deformations of azopolymer posts**

  An epoxy-based side-chain azopolymer with $T_G = 120\,^{\circ}\mathrm{C}$ deforms vertically/horizontally for the vertical/horizontal linear polarization. In the case of circularly polarized light, an initially square post is deformed radially [37].

- **Inscription of stripe patterns by moving laser beam**

  A puzzling phenomenon was discovered by Ambrosio et al. [51]. When a highly focused linearly polarized Gaussian beam is moved over a thin azo-polyurethane film in two different directions, parallel and perpendicular to the light polarization, the film surface deforms differently. In the case of parallel movement, the material deforms in the direction of light polarization by making an elongated protrusion [51]. In case of the movement perpendicular to the light polarization, a groove was observed. The authors checked that in both cases the overall volume stays conserved. Interestingly, the depth of the grooves has been found to be much larger than the height of the protrusions.

- **Structuring of spherical colloids by interference patterns**

  An experiment was conducted in the group of Santer [52] on the spherically shaped azopolymer colloids, which were first illuminated with the horizontally polarized light. After some time the colloid elongates in the polarization direction, reaching an aspect ratio up to 5. In a second step the elongated colloid was illuminated with the light having sinusoidal intensity distribution. Formations of beads and wave-like structure were observed for light polarized along and perpendicular to the long axis of the colloid, respectively.

Several models of grating inscription [53, 43, 54] have been proposed but none of these provided a satisfactory explanation at a molecular level. At present, the models based on the light-induced reorientation of azobenzene moieties look as the most promising explanation [55, 43, 49]. The reorientation arises statistically, after a number of isomerization cycles, with the long axis of trans-isomers lying preferably perpendicular to the light polarization. This causes a reorientation of the polymer backbones to which the azobenzenes are attached and appearance of the light-induced stress which dictates a direction of the macroscopic deformation. Our motivation in this thesis is to explain the directional

deformations in azopolymers, as listed above, using this orientational hypothesis.

1.2 Goals

In this thesis, we aim to provide an explanation for some of the above discussed puzzling phenomena. To explain directional deformations induced by the polarized light, it is necessary to establish a relation between the light characteristics and the properties of azopolymer material. For this purpose, orientation approach is used in which the trans-cis photo-isomerization events are described by the effective orientation potential acting on the azobenzene chromophores [56].

As in this thesis we focus on the side-chain azopolymers, the effective orientation potential should be recalculated for the main chain, for that the chemical architecture of the azopolymer is taken into account. The main chains reorient under the polarized light, which results in induction of light-induced stress. Our goal is to predict the time dependent orientation tensor of polymer backbones and corresponding stress tensor.

Different azopolymers were used in the experiments mentioned in Motivation, and all of them are glassy materials. Therefore, to explain the movement of material under various polarizations, we model it as a viscoplastic solid. By using the orientation approach, we aim to explain the following phenomena:

- Directional deformations in the square post under homogeneous light intensity,
- Formation of grooves and hills under moving light beam with horizontal and vertical polarization,
- Bead and wave-like structure formation in spherical colloids under intensity interference patterns,
- Structuring of film edges under polarization interference patterns.

To achieve this goal, we implement the stress fields induced in these experiments, in finite element modeling software (ANSYS). Finally, the deformations achieved in the material modeling are compared with the experimental ones to check the validity of the orientation approach.

1.3 Outline of thesis

After introducing the background of the thesis work in the present chapter, the following points will be explained in the next chapters:

- In Chapter 2 azopolymers are introduced as glassy materials with the help of experiments that support the thermal stability of the azopolymers at temperatures below the glass transition temperature. Further,

we discuss the uniaxial and biaxial orientational states observed in these materials under light irradiation. Later the experimental setup and electric field vector distributions corresponding to various polarizations are described. Then we introduce the effective orientation potential originating from cyclic trans-cis isomerization of azobenzenes in the presence of linearly polarized light. The last part of this chapter is devoted to the experiments which confirm that the magnitude of light-induced stresses in azopolymers is larger than the yield stress.

- In the first part of Chapter 3 the effective orientation potential for the circularly polarized light is calculated based on the angular hole burning effect. Later this chapter is focused on the derivation of time dependent orientation and stress tensors for uniaxial and biaxial orientational states. For calculating these tensors, the azopolymers are modeled as an ensemble of rigid Kuhn segments in the presence of external orientation potential. To calculate the components of orientation tensor, suitable closure approximations are developed for uniaxial and biaxial order.

- In Chapter 4 the description of the methods which we have developed is given. To calculate the light-induced deformations, the finite element modeling software ANSYS is used, in which the viscoplastic Perzyna model is applied to describe material properties of glassy azopolymers. In ANSYS, we implement the light-induced stress either directly in case of homogeneous stresses or indirectly using Userthstrain subroutine in case of spatially dependent stresses.

- In Chapter 5, we study the directional deformations in the azopolymer square post irradiated with the linearly and circularly polarized light. In this case, the mechanical strains can be calculated analytically and compared with the predictions from finite element modeling in ANSYS. With the help of this comparison the mesh size and the length of time steps are calibrated in ANSYS to reproduce the exact analytical solution. After that, using the orientation approach we reproduce the directional deformations observed in the experiment done by Lee et al.[37].

- In Chapter 6, we model the effect of fast moving light beam on the azopolymer surface, for the case of horizontally and vertically polarized light. In accordance with the experiment, [57] we observe formation of grooves and hills under irradiation with Gaussian distributed light intensity.

- Further, in Chapter 7 we focus on the modeling of azopolymer structuring under light interference patterns. The first part of the chapter is about elongation of spherical colloids in the presence of linearly polarized light, similar to the experiment of Santer et al.[52]. Later, we model the deformations in the elongated spherical colloids under intensity interference patterns and observe the formation of beads and wave-like structures in accordance with the experiment. In the last part of the chapter the formation of peculiar structures at the edges of thin film under polarization

interference patterns is modeled. A striking resemblance between the real and modelled structures is established.

- In chapter 8 the thesis work is summarized by emphasizing on the importance of the orientation approach to explain the directional deformations under various light polarizations and interference patterns. The thesis is closed by a brief outlook.

Chapter 2

Azopolymer properties and behaviour

Azobenzene containing polymers are defined as polymeric systems in which the azobenzene chromophores are incorporated into the main chain or covalently attached to it as a part of the side chain. Azobenzene molecules are made of two phenyl rings that have a nitrogen double bond between them, called the azo-bond, see Figure 2.1. Azobenzene chromophores tend to switch between trans- and cis-isomeric states in the presence of polarized light and the rate of isomerization depends on the polarization direction [58, 59, 60, 61, 62, 63, 64]. The cis-isomers have a bent structure because the two phenyl rings are attached at 90^0 but the trans isomers have a straight rode-like structure, as shown in Figure 2.1.

As mentioned in Chapter 1, azopolymer materials show directional deformations when irradiated with polarized light. In this chapter, we focus on the light characteristics and the properties of azopolymer material to set up a background for modeling the directional deformations.

2.1 Models to explain photodeformations

The photodeformations in azopolymer materials are stable below the glass transition temperature and can not be further changed in the absence of the light irradiation [37]. To explain the directional photodeformations in azopolymers, several models are proposed. Here, in this section, a brief discussion about the models and their shortcomings is provided.

Photo-softening models [65, 66, 67]

The inscription of surface relief gratings is done at room temperature which is far below the glass transition temperature. The azopolymers are in glassy state which means that their Young's modulus and viscosity are extremely large. The

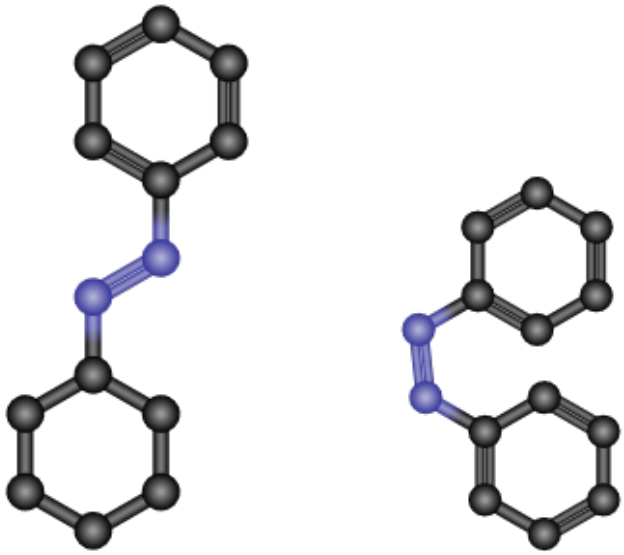

(a) **(b)**

Figure 2.1: Chemical structure of azobenzene chromophore a) in the straight trans-state and b) in the bent cis-state.

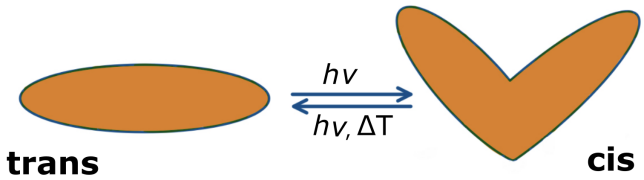

Figure 2.2: Isomerization between trans- and cis-isomers of azobenzene chromophore in the presence of light.

material displacement in the glassy state is assumed to be due to the photo-softening effect, either due to light-induced mobility of the main chains or due to formation of a thermal gradient that results in the surface relief gratings. Still, these models can not explain the photodeformations due to following reasons.

Shortcomings

- It was observed that Young's modulus of polymer materials decreases under light irradiation from 3.4 GPa to 0.9 GPa [66, 68, 69]. This is not enough to induce the transition from glassy state into low viscosity polymer melt [70], characterized by high mobility of the main chains.
- During formation of surface relief gratings, the thermal gradient is below 10 K and can not explain the material displacement below the glass transitions temperature [71].
- The dependence of photodeformations on light polarization is not taken into account.

Gradient force model [65, 72, 54, 73, 74]

To explain the grating formation, Kumar et al. proposed that the electric field vector $\mathbf{E}$ in the direction of mass migration is required. Also, it was assumed that the material is polarized by the electric field and the spatially dependent light intensity I changes the material susceptibility tensor χ. With these assumptions, the polarization $\mathbf{P}$ is defined as follows:

$$\mathbf{P} = \epsilon_0 \chi(I) \mathbf{E} \tag{2.1}$$

Here, ϵ_0 is the vacuum permittivity.
The time averaged force $\mathbf{F}$ generated in the material under electric field gradient is [73]:

$$\mathbf{F} = \langle (\mathbf{P} \cdot \nabla) \mathbf{E} \rangle \tag{2.2}$$

Hence, the gradient force depends on the material susceptibility, magnitude and gradient of the electric field vector. The gradient force model predicts the formation of surface relief gratings depending on the light polarization.

Shortcoming

- It has been calculated that the magnitude of force density is of the order of 100 N/m^3, which is even smaller than the gravitational force. With this it can be concluded that the gradient force concept can not explain the material movement under light irradiation [75].

Asymmetric diffusion theory [65, 72, 76, 77]

In this model, it was assumed that the orientational concentration gradient is responsible for the material movement. It was proposed that the trans-cis cyclic photo-isomerization enables the random motion of azobenzene molecules along the longer axis of the chromophore. The probability of the random-walk step is directly proportional to the probability of isomerization which depends on the light intensity and the angle between the electric field vector and chromophore dipole. The theory predicts the movement of molecules from illuminated area to the dark area, which explains some of the experimental observations.

Shortcomings

- This model can explain the grating formation in a system of small molecules but for larger molecules and polymer chains it becomes a tug of war situation which can defeat the net movement of the main chains [72]. Thus, asymmetric diffusion is not sufficient to explain the formation of surface relief gratings in azopolymers.

Isomerization pressure approach [65, 72, 78, 79]

Barrett et al. were one of the first who tried to explain the formation of surface relief gratings by the generation of pressure gradient because of the free volume required in the isomerization process, which is directly proportional to the intensity of light. Thus, the formation of surface relief gratings can be explained by assuming that the pressure generated is larger than the yield point. The following Navier-Stokes equation is used to describe the viscous flow of polymer material under pressure gradient:

$$\rho \frac{\partial \mathbf{v}}{\partial t} = -\nabla P + \mu \Delta \mathbf{v} \tag{2.3}$$

Here, ρ is the density, $\mathbf{v}$ refers to the velocity, P is the pressure and μ is the viscosity of the material.

Shortcomings

- This approach can not explain the photodeformations under polarization inference patterns with constant light intensity.
- The assumption that the pressure generated is larger than the yield point was not verified.

Mean-field theory [65, 72, 80, 81]

The mean-field theory takes into account the intensity and polarization of spatially distributed light field. In this model, the chromophores are considered as liquid crystalline moieties and each chromophore is assumed to experience a net

or mean-field potential resulting from all the chromophore dipoles in the material. The mean-field potential is given by the Maier-Saupe approximation. The light irradiation is responsible for the reorientation and alignment of the chromophores. The azobenzenes, which are aligned parallelly, experience a strong attractive force between them due to the mean-field potential. Hence, the chromophores accumulate in higher light intensity regions. Thus, the peaks in the surface relief grating appear at the light maxima.

Shortcomings

- The mean-field theory is consistent with some experiments on liquid crystal systems but can not explain the deformations in the amorphous samples, particularly in glassy azopolymer samples.
- This model does not differentiate between isomerising and non-isomerising liquid crystal systems. Also, the formation of gratings is not observed yet for the non-isomerising systems which do not contain azobenzene chromophores.

Orientation approach [82, 56, 83, 84]

The formation of surface relief gratings is assumed to be caused by an external potential which is called the effective orientation potential. It results from the kinetics of trans-cis photo-isomerization and reorients the chromophores perpendicular to the light polarization. As chromophores are attached to the main chains, they will be reoriented too. The orientation potential approach explains the following points.

- In this approach, the spatially dependent polarization and intensity of light are taken into account.
- Chemical architecture of the azopolymers is taken into account.
- This is the first theory that explains the photodeformations in the glassy azopolymers due to light-induced stresses (10 - 50 MPa) which are considerably larger than the yield stress [56, 52].

It can be concluded that the orientation approach is very promising to explain the light-induced deformations in the glassy azopolymers. Because of this reason, we will use the orientation approach to model the directional deformations observed in the experiments mentioned in Chapter 1. Later in the current chapter, the effective orientation potential is introduced in detail.

2.2 Order parameter

The orientation order in azobenzene containing side-chain azopolymers is defined via the order parameter for rigid segments (Kuhn segments) comprising

the polymer backbones [85]. The orientation of each Kuhn segment is represented by the unit vector **u**, which makes an angle θ with the preferential orientation direction (nematic director), see Figure 2.3. The direction of nematic vector **n** is along the x axis. The projection of the unit orientation vector on x, y and z axes around the nematic director **n** can be written as follows:

$$u_x = \cos\theta \tag{2.4}$$

$$u_y = \sin\theta \sin\phi \tag{2.5}$$

$$u_z = \sin\theta \cos\phi \tag{2.6}$$

Here, θ is the polar angle and ϕ is the azimuthal angle. General form of nematic order parameter can be represented by the following tensor [86]:

$$\mathbf{Q} = \frac{3}{2}\langle \mathbf{uu} \rangle - \frac{1}{2}\boldsymbol{\delta}, \tag{2.7}$$

where $\langle \mathbf{uu} \rangle$ is the 2nd order orientation tensor and $\boldsymbol{\delta}$ is a unit tensor. The angular brackets describe the averaging over the ensemble of Kuhn segments.

For the azobenzene chromophores the probability to find a dipole in direction **p** is the same as -**p**. With this, it can be concluded that the nematic directors **n** and -**n** are indistinguishable [87]. We assume the distribution function of orientation vector to be f(θ, ϕ)dΩ, where $d\Omega = \sin\theta d\theta d\phi$. The indistinguishable property of nematic directors provides the following symmetry of the distribution function: $f(\theta, \phi) = f(\pi - \theta, \phi) = f(\pi, 2\pi - \phi)$. To simplify the 2nd order tensor $\langle \mathbf{uu} \rangle$, we calculate first the following moment:

$$\langle \mathbf{u} \cdot \mathbf{n} \rangle = \langle \cos\theta \rangle = \int f(\theta, \phi) \cos\theta d\Omega \tag{2.8}$$

It vanishes as a result of the $f(\theta, \phi) = f(\pi - \theta, \phi)$ property of the distribution function. Similarly, the other moments can be calculated: $\langle \sin^2\theta \sin\phi \cos\phi \rangle = \langle \cos\theta \sin\theta \sin\phi \rangle = \langle \cos\theta \sin\theta \cos\phi \rangle = 0$. Thus, it can be shown that the off-diagonal components of 2nd order orientation tensor $\langle \mathbf{uu} \rangle$ and hence the nematic order tensor **Q** are zero.The xx component of the nematic order tensor defines the nematic order parameter Q:

$$Q_{xx} = \frac{3}{2}\langle \cos^2\theta \rangle - \frac{1}{2} = \langle P_2(\cos\theta) \rangle = Q \tag{2.9}$$

Here, $P_2(\cos\theta) = \frac{3\cos^2\theta - 1}{2}$ is the 2nd order Lagrange polynomial.

Uniaxial order: Conventional nematics are characterised by the uniaxial order, when the distribution function $f(\theta, \phi)$ is independent of ϕ [87]. To simplify

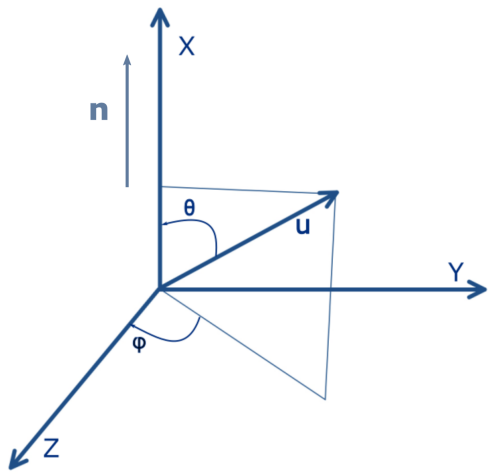

Figure 2.3: Representation of the orientation vector $\boldsymbol{u}$ in the polar co-ordinate system. The nematic director $\mathbf{n}$ is along the x axis.

the nematic order tensor let us calculate the following moments:

$$\langle u_y^2 \rangle = \langle \sin^2 \theta \rangle \langle \sin^2 \phi \rangle = \frac{\langle \sin^2 \theta \rangle}{2} \tag{2.10}$$

$$\langle u_z^2 \rangle = \langle \sin^2 \theta \rangle \langle \cos^2 \phi \rangle = \frac{\langle \sin^2 \theta \rangle}{2} \tag{2.11}$$

Here, $\int \sin^2 \phi d\phi = \int \cos^2 \phi d\phi = \frac{1}{2}$. Further, the diagonal components of the nematic order tensor can be written as $Q_{yy} = Q_{zz} = -Q/2$. The nematic order tensor in the uniaxial order case is as follows:

$$\mathbf{Q} = \begin{bmatrix} Q & 0 & 0 \\ 0 & -Q/2 & 0 \\ 0 & 0 & -Q/2 \end{bmatrix} \tag{2.12}$$

Biaxial order: For azobenzene chromophores with strong orientational interactions, the light can induce a uniaxial to biaxial phase transition with two distinct axes [84]. One is given by $\mathbf{E}$ and another is perpendicular to it. The chromophores will be oriented preferentially in the plane perpendicular to the polarization direction $\mathbf{E}$. However, in case of biaxial nematic order θ and ϕ are not independent anymore, which makes the yy and zz components to be dependent on each other. With this, the nematic order tensor can be written

as follows [84]:

$$\mathbf{Q} = \begin{bmatrix} Q & 0 & 0 \\ 0 & -\frac{Q}{2} + \frac{3\mu}{4} & 0 \\ 0 & 0 & -\frac{Q}{2} - \frac{3\mu}{4} \end{bmatrix} \tag{2.13}$$

Here, $\mu = \langle u_z^2 \rangle - \langle u_y^2 \rangle$ is the biaxial order parameter, it becomes zero for the uniaxial order. The orientation tensor is trace-less for all cases, see Equations 2.12 and 2.13.

2.3 Light polarizations

In this thesis, we perform modeling of the experiments in which the azopolymer samples are irradiated with different kind of polarized light that leads to specific structure formation.
As we know, light is an electromagnetic wave that is comprised of coupled magnetic and electric fields oscillating in perpendicular planes. By convention the polarization direction is along the electric field vector. In the experiments by varying the direction of electric field vector with time or space the resultant polarization of light can be manipulated. To create light interference patterns, a special optical setup is required which is called a two-beam interferometer [44]. By setting up different polarizations of two light beams in the interferometer, a large variety of intensity and polarization interference patterns can be produced. Below we describe the light polarizations and patterns, relevant to the experiments we aim to model.

2.3.1 Linear polarization of light

The linearly polarized light is the one which has electric field vector only in one direction which does not change with time and space. One of the example of linear polarization is as follows.

Polarization along y direction:

When light is polarized along the y-direction, the electric field vector **E** is also along the y-direction. The propagation direction is assumed to be in the z-direction, as shown in Figure 2.4. Thus, components of the electric field vector can be written as follows:

$$E_x(z,t) = 0 \tag{2.14}$$

$$E_y(z,t) = E_0 \cos(kz - \omega t) \tag{2.15}$$

$$E_z(z,t) = 0 \tag{2.16}$$

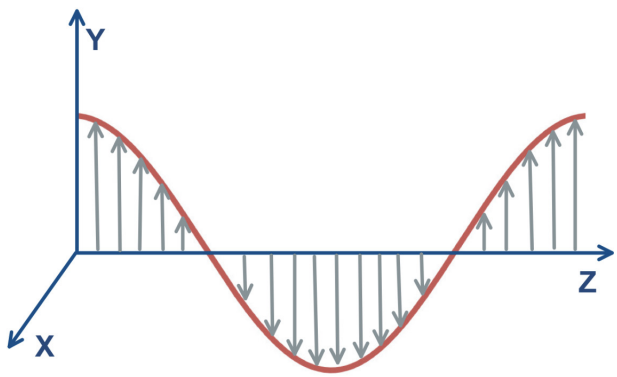

Figure 2.4: The linearly polarized light is propagating in the z direction and its electric field vector (represented with gray arrows) lies along the y direction.

$$\mathbf{E}(z,t) = E_y(z,t)\mathbf{y} \tag{2.17}$$

Here, $\mathbf{E}$ is the polarization vector and E_0 is its amplitude, $\mathbf{y}$ is the unit vector in the y direction, $k = 2\pi/\lambda$ is the wave number, λ is the wavelength of light and ω is the angular frequency. The light polarized in the x or z-direction is the $\pi/2$ rotation of the coordinate system around the z-axis and x-axis, respectively.

2.3.2 Circular polarization of light

In the case of circularly polarized light, the electric field vector rotates around the propagation direction with time. The electric field vector $\mathbf{E}$ for the circularly polarized light propagating in z direction can be written as follows:

$$\mathbf{E}(z,t) = E_x(z,t)\mathbf{x} + E_y(z,t)\mathbf{y} \tag{2.18}$$

Here $\mathbf{x}$ and $\mathbf{y}$ represent the unit vectors along x and y directions, respectively. For left handed circularly polarized light:

$$E_y(z,t) = E_0 \cos(kz - \omega t)$$

and

$$E_x(z,t) = E_0 \cos(\pi/2 + kz - \omega t)$$

for right handed circularly polarized light:

$$E_y(z,t) = E_0 \cos(kz - \omega t)$$

and

$$E_x(z,t) = -E_0 \cos(\pi/2 + kz - \omega t)$$

The x and y components of the electric field vector are with $\pi/2$ phase difference. This makes the electric field vector rotating around the propagation direction, as shown in Figures 2.5 and 2.6.

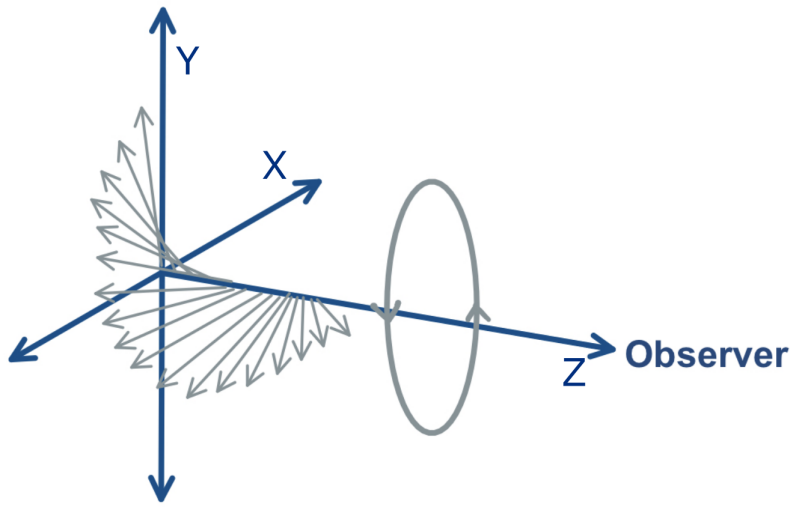

Figure 2.5: In left handed circularly polarized light, the electric field vectors, represented by gray color, rotate anti-clockwise with respect to the observer and the light propagates along the z direction.

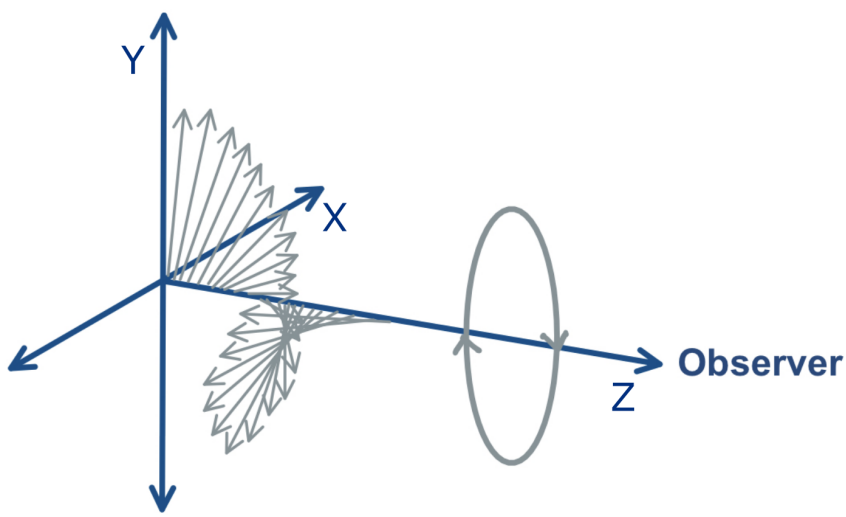

Figure 2.6: In right handed circularly polarized light, the electric field vectors, represented by gray color, rotate clockwise with respect to the observer and the light propagates along the z direction.

2.3.3 Light interference patterns

The light interference patterns are formed by two interfering coherent beams (coming from the same laser) with different polarization, as shown in Figure 2.7. The resultant electric field vector $\mathbf{E}$ for the interference pattern can be written as follows:

$$\mathbf{E} = \mathbf{E}_1 + \mathbf{E}_2 \tag{2.19}$$

Here, $\mathbf{E}_1$ and $\mathbf{E}_2$ represent the electric field vectors corresponding to first and second light beams. The interference patterns are of two types which are intensity and polarization interference patterns with polarization and intensity being constant in time and space, respectively.

SS and PP intensity interference patterns

SS and PP light interference patterns are produced in the experiments by interaction of S and P polarized light beams. Two propagating beams form the incidence plane, as shown in Figure 2.7. When the light beam is polarized in the direction perpendicular to the incident plane, it is called S polarized light and, when it is polarized along the incident plane, it is called the P polarized light beam.

Here, we assume the light beams are propagating in the xz plane. With this, the electric field vector for S polarized light beam is:

$$\mathbf{E} = E_0 \cos(\omega t - kr)\boldsymbol{y} \tag{2.20}$$

Here, r is the beam path along the propagation direction.
The electric field vector for P polarized light beam is:

$$\boldsymbol{E} = E_0 \cos(\omega t - kr)(\cos\theta \boldsymbol{x} + \sin\theta \boldsymbol{z}) \tag{2.21}$$

Here, $\mathbf{x}$ and $\mathbf{z}$ are the unit vectors in the x and z directions and θ is the incidence angle.

SS interference pattern

When two S polarized light beams interfere, the SS interference pattern forms. The electric field vectors for the beams in this case are:

$$\boldsymbol{E}_1 = E_0 \cos(\omega t - kr_1)\boldsymbol{y} \tag{2.22}$$

and

$$\boldsymbol{E}_2 = E_0 \cos(\omega t - kr_2)\boldsymbol{y} \tag{2.23}$$

Here, $\boldsymbol{r}_1 = z\cos^{-1}\theta + x\sin\theta$ and $\boldsymbol{r}_2 = z\cos^{-1}\theta - x\sin\theta$ are the beam paths.

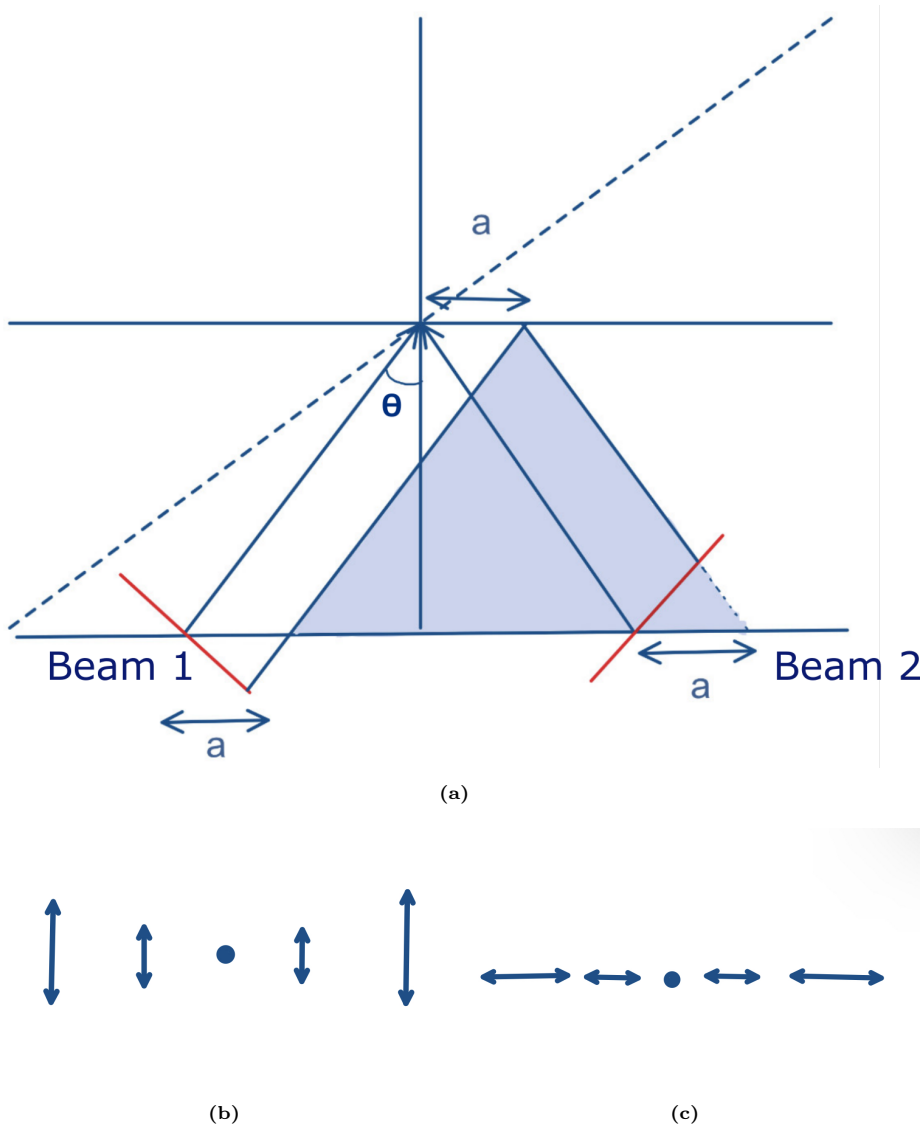

Figure 2.7: a) Typical setup for interference patterns where red lines represent the two light beams, whose wavefronts propagate in the shaded incidence plane. b) Representation of SS c) and PP interference patterns, where length of arrow represents the intensity of light and direction gives polarization.

Thus, the resultant electric field vector $\boldsymbol{E}$ can be written as follows:

$$\boldsymbol{E} = 2E_0 \cos(\omega t - kz\cos^{-1}\theta)\cos(kx\sin\theta)\boldsymbol{y} \tag{2.24}$$

Spatial distribution of light intensity corresponding to the resultant electric field vector is:

$$I(x) = E^2 \propto E_0^2 \cos^2(kx\sin\theta) \tag{2.25}$$

Introducing the grating period $D = \lambda/(2\sin\theta)$, the intensity of light can be written as follows:

$$I(x) \propto E_0^2 \cos^2(\frac{\pi x}{D}) \tag{2.26}$$

The optical period can be regulated by changing the angle θ between the beams, D is usually in the range of $0.5 - 4$ μm.

PP interference pattern

When two P polarized light beams interfere, the PP interference pattern forms. The electric field vectors for the beams are :

$$\boldsymbol{E}_1 = E_0 \cos(\omega t - kr_1)(\cos\theta\boldsymbol{x} + \sin\theta\boldsymbol{z}) \tag{2.27}$$

and

$$\boldsymbol{E}_2 = E_0 \cos(\omega t - kr_2)(\cos\theta\boldsymbol{x} + \sin\theta\boldsymbol{z}) \tag{2.28}$$

Under an assumption θ to be very small, the z component of $\boldsymbol{E}_1$ and $\boldsymbol{E}_2$ can be neglected. Thus, the resultant electric field vector for PP interference pattern can be written as follows:

$$\boldsymbol{E} = 2E_0 \cos(\omega t - kz\cos^{-1}\theta)\cos(kx\sin\theta)\boldsymbol{x} \tag{2.29}$$

Intensity of light corresponding to the resultant electric field vector is:

$$I \propto E_0^2 \cos^2(\frac{\pi x}{D}) \tag{2.30}$$

For SS and PP interference patterns, the polarization direction is constant but the intensity has spatial dependence as can be seen from Equation 2.26 and 2.30. Therefore, they are called intensity interference patterns.

RL and LR polarization interference patterns

RL and LR interference patterns are formed when left and right hand circularly polarized light beams interfere. The electric field vector for right hand circularly polarized light (RCP) beam is:

$$\boldsymbol{E}_{rcp} = E_0(\cos(\omega t - kr_1)\cos\theta\boldsymbol{x} + \sin(\omega t - kr_1)\boldsymbol{y} - \cos(\omega t - kr_1)\sin\theta\boldsymbol{z}) \tag{2.31}$$

The electric field vector for left hand circularly polarized (LCP) light beam is:

$$\boldsymbol{E}_{lcp} = E_0(\cos(\omega t - k\boldsymbol{r}_1)\cos\theta\boldsymbol{x} - \sin(\omega t - k\boldsymbol{r}_1)\boldsymbol{y} + \cos(\omega t - k\boldsymbol{r}_1)\sin\theta\boldsymbol{z}) \tag{2.32}$$

The position of LCP and RCP, see Figure 2.5 and 2.6, defines the resultant interference pattern, as explained below.

RL interference pattern
When the beam 1 is the right circularly polarized and beam 2 is left circularly polarized, the resultant interference pattern is called the RL interference pattern and its electric field vector is as follows:

$$\boldsymbol{E} = 2E_0\cos(\omega t - kz\cos^{-1}\theta)(\cos(kx\sin\theta)\boldsymbol{x} - \sin(kx\sin\theta)\boldsymbol{y}) \tag{2.33}$$

The intensity of light corresponding to the resultant electric field vector $\boldsymbol{E}$ is:

$$I = E^2 \propto 2E_0^2 \tag{2.34}$$

LR interference pattern
When the beam 1 is the left circularly polarized and beam 2 is right circularly polarized, the resultant interference pattern is called the LR interference pattern and its electric field vector is as follows:

$$\boldsymbol{E} = 2E_0\cos(\omega t - kz\cos^{-1}\theta)(\cos(kx\sin\theta)\boldsymbol{x} + \sin(kx\sin\theta)\boldsymbol{y}) \tag{2.35}$$

The intensity of light corresponding to the resultant electric field vector $\boldsymbol{E}$ is:

$$I = E^2 \propto 2E_0^2 \tag{2.36}$$

As it can be seen from Equation 2.34 and 2.36, the intensity of light is constant for RL and LR interference patterns. On the other side, from Equations 2.33 and 2.35 it follows that the polarization of light is varying in the xy plane (the substrate plane). Therefore, the RL and LR patterns are called polarization interference patterns.

2.4 Effective orientation potential for linearly polarized light

As discussed in the Section 2.1, the orientation approach is very promising to explain the photodeformations in azopolymers. A theoretical formalism for the "hole burning" effect for the azo dyes in amorphous polymers was introduced by Dumont et al. [88]. As the azobenzene chromophores isomerize in the presence of light, the isomerization events depend on the probability of absorption. The

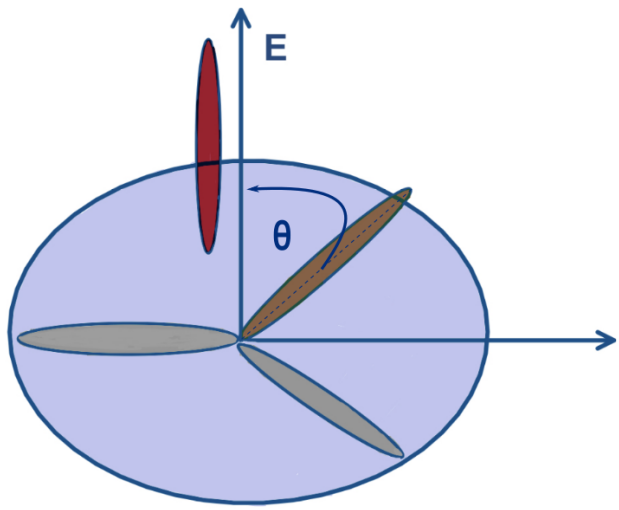

Figure 2.8: Light-induced orientation of azobenzenes in the plane perpendicular to the light polarization $\boldsymbol{E}$ of the linearly polarized light.

mechanism of angular hole-burning becomes clear if one considers the probability of absorption by trans- and cis-isomers:

$$P_J(\theta) = I_P \sigma_J [1 + \frac{1}{2} \epsilon a_J (3\cos^2(\Theta) - 1)] \tag{2.37}$$

Here, I_P is the flux of photons proportional to the intensity of a pumping beam in W/cm^2, σ_J and a_J are the average absorption cross-section and the molecular anisotropy of trans ($J = T$) and cis ($J = C$) isomers, respectively. Θ is the angle between the transition dipole moment of the chromophores (for the trans isomer it is oriented along the long molecular axis) and the symmetry axis that lies along the polarization direction, for the linearly polarized light it is defined by the electric field vector $\boldsymbol{E}$. The molecular anisotropy of axially symmetrical trans-isomers $a_T = 1$ [88]. It is reasonable to consider an angular independent absorption by bent cis-isomers due to their isotropic polarizability tensor [37, 89]. The molecular anisotropy of cis-isomers $a_C = 0$ and the probability of absorption by cis-isomers for linearly polarized light is: $P_C = I_P \sigma_C$, the parameter $\epsilon = 2$ for linearly polarized beam [90]. Probability of absorption by trans-isomers when irradiated with linearly polarized light is:

$$P_{T,lin} = 3 I_P \sigma_T \cos^2(\Theta) \tag{2.38}$$

Hence, the probability of excitation $P_{T,lin}$ by linearly polarized light is pro-

portional to $\cos^2(\Theta)$, where the angle Θ is counted from the direction of light polarization $\boldsymbol{E}$, as shown in Figure 2.8. From Equation (2.38), it can be seen that the chromophores which are oriented perpendicular to the light polarization do not absorb light [56]. The probability to be excited is highest for the trans-isomer oriented parallel to $\boldsymbol{E}$ (it is marked as a red "hot" isomer). Therefore, starting from a sample with an isotropic distribution of chromophores, multiple trans-cis-trans photo-isomerizations will result in a preferential orientation of the chromophores in the plane perpendicular to the vector $\boldsymbol{E}$ (those are marked as gray "cold" isomers).
The azobenzene chromophores reorient under irradiation with polarized light due to angular selective isomerization process [83, 56, 1, 2]. Using kinetic equations for the photo-isomerization dynamics, it has been explained theoretically and using computer simulations that the action of polarized light on azobenzene chromophores is as effective as application of external potential u_{eff}, which reorients the chromophores perpendicular to the polarization direction [56]:

$$u_{eff} = V_0 \cos^2(\Theta), \qquad V_0 = \frac{p_T kT \langle \sin^2 \chi \rangle}{4D_r} \tag{2.39}$$

The potential acts on each azobenzene and its strength V_0 depends on the probability of trans-cis isomerization $p_T \approx I_P \sigma_T$, magnitude of stochastic jumps χ performed during photo-isomerization and the orientation diffusion coefficient D_r of the azobenzene, which is defined by the viscosity of the material.
The effective potential acting on the backbone segments can be obtained as the sum of potentials acting on each chromophore present in the segment [83]:

$$U_{eff} = mV_0 \langle \cos^2(\Theta) \rangle \tag{2.40}$$

Here, m is the number of azobenzenes in the backbone segment. After averaging over all possible chromophore orientations, the effective orientation potential for the backbone segments can be written as follows:

$$U_{eff} = qmV_0 \cos^2(\theta) \tag{2.41}$$

Here, $q = [3\langle \cos^2 \alpha \rangle - 1]/2$ is the shape factor, α is the angle at which the chromophores are attached to the backbone. For the side-chain polymers α is close to $\pi/2$, which makes $q \approx -0.5$. θ is the angle between the orientation of the segment and the electric field vector, as represented in Figure 2.9. Thus, Equation (2.41) can be redefined as:

$$U_{eff} = qmV_0 (\hat{\mathbf{E}} \cdot \boldsymbol{u})^2 \tag{2.42}$$

where $\hat{\mathbf{E}} = \boldsymbol{E}/|\boldsymbol{E}|$ is the unit vector of light polarization. From Equation (2.42), it can be seen that the effective potential for the segment is minimum when the

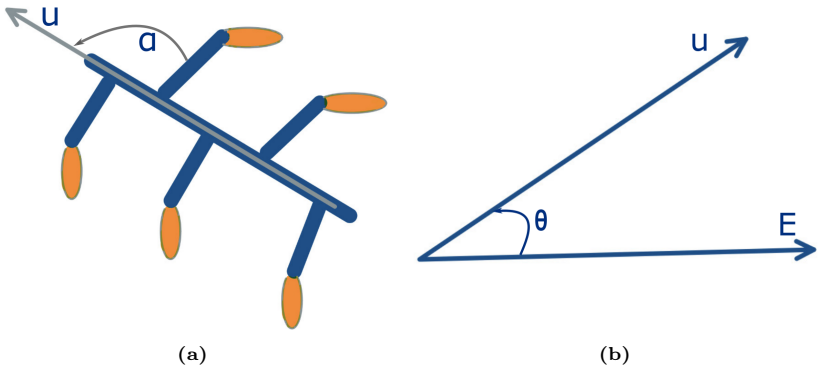

Figure 2.9: a) Representation of the azopolymer Kuhn segment, the orange-colored chromophores are rigidly attached to the main chain via a spacer (both are represented by blue color), the gray arrow represents the orientation vector for the Kuhn segment and b) the electric field vector makes an angle θ with the unit orientation vector.

segment is aligned along the electric field vector, and maximum when the segment is perpendicular to the electric field vector. As every system tries to minimise its potential energy for attaining the equilibrium, it can be concluded that the preferred direction for the segment is along the electric field vector. In the reorientation process of polymer backbones, the light-induced stress should appear in the material, as we discuss below.

2.5 Magnitude of light-induced stress and yield stress in glassy azopolymers

It was observed in the experiments that the deformations induced in glassy azopolymer materials by the polarized light stay preserved even after removing the light source [37, 52, 91, 92]. With this particular observation it can be concluded that the deformations are not elastic but plastic. To attain plastic deformations the stress induced in the material should be larger than the yield stress [93]. As mentioned above, the already existing theories other than the orientation approach do not predict sufficient light-induced stress or force for the structuring of azopolymer materials.
The yield stress for azopolymers was estimated in the range of $20 - 30$ MPa [94]. The magnitude of light-induced potential ($\approx 7 \times 10^{-18}$ J) was predicted using the orientation approach, which provided the light-induced stress of about 4 GPa [56]. In Ref. [85], the authors estimated the light-induced stress using computer simulations, which is in the range 50 MPa - 5 GPa. Also, it was shown experimentally that the light-induced stress can be as large as 2 GPa and was capable of breaking the metallic layer on the surface of a glassy azo-polymer as

well as of deforming the covalent bonds [95, 91, 96]. Hence, it was shown that the light-induced stress in azopolymers can be much larger than the yield stress. The orientation approach provides the effective potential, as described by Equation (2.42), which depends on the azopolymer material properties as well as on the characteristics of linearly polarized light. As mentioned in section 1.2, we aim to model the experiments performed using variously polarized light, especially circularly polarized one. The time-dependent stress induced under linearly and circularly polarized light is derived in the next chapter.

Chapter 3

Light-induced orientation and stress

Azobenzene chromophores isomerise cyclically in the presence of light with an appropriate wavelength. Due to the cyclic isomerization, the chromophores will gradually reorient themselves in a preferred direction which is perpendicular to the light polarization [1, 2]. Because of this reorientation, a light-induced stress will appear which can be defined via the introduction of the effective orientation potential, for linearly polarized light it is already discussed in Chapter 2. In the present chapter the orientation potential for circularly polarized light will be introduced. Further, the time dependent light-induced orientation and stress tensors are calculated for the linearly and circularly polarized light.

3.1 Effective orientation potential for circularly polarized light

The probability of absorption by trans- and cis-isomers is given by Equation (2.37) from Chapter 2. The molecular anisotropy of cis-isomers $a_C = 0$ and the probability of absorption by cis-isomers is the same for linearly and circularly polarized light: $P_C = I_P \sigma_C$. According to Dumont et al. [90], the parameter $\epsilon = -1$ for circularly polarized (or unpolarized) beam propagating along $\boldsymbol{k}$. With this, the probability of absorption for trans-isomers under circularly polarized light can be written as follows:

$$P_{T,circ} = \frac{3}{2} I_P \sigma_T \sin^2(\Theta) \tag{3.1}$$

This probability $P_{T,circ}$ is proportional to $\sin^2(\Theta)$, where angle Θ is counted from the direction of light propagation $\boldsymbol{k}$, as shown in Figure 3.1. The probability to be excited is highest for the trans-isomers (red "hot" isomers) oriented in the plane with rapidly rotating electric field vector $\boldsymbol{E}$. Therefore, multiple

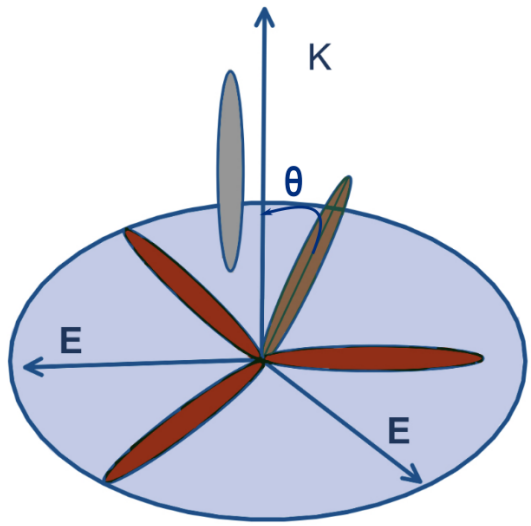

Figure 3.1: Light-induced orientation of azobenzenes along the propagation direction $\boldsymbol{k}$ of the circularly polarized light.

trans-cis photo-isomerizations caused by the circularly polarized light will result in the preferential orientation of a chromophore (a gray "cold" isomer) along the direction of light propagation $\boldsymbol{k}$. In analogy to linearly polarized light, the process of time dependent orientation induced by the circularly polarized light should be described by the effective orientation potential:

$$u_{circ}(\Theta) = \frac{V_0}{2}\sin^2(\Theta) \tag{3.2}$$

Here, V_0 is the strength of the orientation potential which is defined by the same Equation (2.39). Also, u_{circ} can be derived directly by averaging orientation potential (2.39) over all polarizations in the plane perpendicular to the propagation direction.

This thesis is focused on the modeling of amorphous azopolymers in which the chromophores are attached to the main chain either directly or via a very short spacer. Similar as it was done for the linearly polarized light, the effective orientation potential u_{circ} acting on the azobenzenes can be recalculated to the orientation potential acting on the backbone segments:

$$U_{circ}(\theta) = qm\frac{V_0}{2}\sin^2(\theta) = qm\frac{V_0}{2}[1-(\hat{\mathbf{k}}\cdot\boldsymbol{u})]^2 \tag{3.3}$$

Here, θ is counted between the orientation of rigid segment and light propagation direction $\boldsymbol{k}$. Further, $\sin(\theta)$ is expressed through the scalar product between

the unit vectors of light propagation $\hat{\mathbf{k}} = \boldsymbol{k}/|\boldsymbol{k}|$ and the orientation vector $\boldsymbol{u}$ of the rigid segment. We remind that in the above equation m is the number of azobenzenes in the backbone segment and q is the shape factor which defines the direction of the backbone reorientation and its effectiveness.
As we discussed in Chapter 2, the azobenzene chromophores are attached preferentially perpendicularly to the main chain which results in a negative shape factor, $q \approx -0.5$. This means that the main chains will reorient perpendicular to the direction of azobenzene orientation. Therefore, the effective potential (3.3) should reorient the main chains in the polarization plane. The reorientation of the main chain results in appearance of light-induced stress. Further, in the next section we focus on calculation of the time dependent light-induced stress.

3.2 Derivation of stress tensor

In this thesis, we model azopolymers as an ensemble of rigid rod-like (Kuhn) segments. The internal stress induced in the ensemble of rod-like particles in the presence of external potential U_{eff} is given by Equation (A) from Table 14.3-1 in the text book of R.B. Bird [97]:

$$\boldsymbol{\tau} = -3nkT\langle \boldsymbol{uu} \rangle + nkt\boldsymbol{\delta} - n\langle \boldsymbol{u}\frac{\partial U_{eff}}{\partial \boldsymbol{u}} \rangle \tag{3.4}$$

Here, n is the number density of the rigid segments, each characterized by the unit orientation vector $\boldsymbol{u}$, and $\boldsymbol{\delta}$ is the unit tensor. The angular brackets indicate averaging over the ensemble of rigid segments. The time evolution of 2nd order orientation tensor $\langle \boldsymbol{uu} \rangle$, which describes an average orientation state of the segments, is given by Equation (14.2-11) from the same book [97]:

$$\frac{\partial}{\partial t}\langle \boldsymbol{uu} \rangle = \frac{1}{3\lambda}\boldsymbol{\delta} - \frac{1}{\lambda}\langle \boldsymbol{uu} \rangle - \frac{1}{6kT\lambda}\langle \frac{\partial U_{eff}}{\partial \boldsymbol{u}}\boldsymbol{u} + \boldsymbol{u}\frac{\partial U_{eff}}{\partial \boldsymbol{u}} \rangle \tag{3.5}$$

Here, λ is the rotational time of the rigid segment in the absence of external potential. It characterizes the relaxation of the 2nd order Legendre polynomial $\langle P_2(\boldsymbol{u}(t)\cdot\boldsymbol{u}(0)) \rangle = \exp(-6D_r t)$ [98], and is related to the rotation diffusivity D_r:

$$\lambda = \frac{1}{6D_r} = \frac{\pi\eta L^3}{18kT(\ln r + C)} \tag{3.6}$$

Here, L and r are the length and aspect ratio of the rod-like particle; the constant $C = 0.662 + 0.917/r - 0.05/r^2$ takes into account the end-effect terms for short rods [99]. Using parameters of the rigid segment $L \approx 3.52$ nm and $r \approx 5.8$ obtained for the side-chain azopolymer in Ref. [52], it can be shown that the viscosity of the plastic flow $\eta = C_\eta \lambda$, where C_η is about 0.68 MPa.
It can be seen from Equations (3.4) and (3.5) that the orientation tensor is symmetric, while a contribution to the stress tensor from the external potential, given by the third term in Equation (3.4) is not necessarily symmetric. One

finds publications that claim this contribution should be also symmetric [100]. To simplify the analysis, in the present study it will be assumed that the stress tensor is symmetric and Equation (3.4) can be rewritten as follows:

$$\boldsymbol{\tau} = -3nkT\langle \boldsymbol{uu} \rangle + nkt\boldsymbol{\delta} + \boldsymbol{\tau}_{light} \tag{3.7}$$

The total internal stress $\boldsymbol{\tau}$ takes into account the entropic contribution described by the first two terms in the above equation. The third term $\boldsymbol{\tau}_{light}$ represents the light-induced stress which is given by the following relation:

$$\boldsymbol{\tau}_{light} = -\frac{n}{2}\langle \frac{\partial U_{eff}}{\partial \boldsymbol{u}}\boldsymbol{u} + \boldsymbol{u}\frac{\partial U_{eff}}{\partial \boldsymbol{u}} \rangle \tag{3.8}$$

Firstly, it can be seen from Equation (3.7) that in the absence of light, the sample of amorphous azopolymer with initially isotropic orientation of side chains and backbones ($\langle \boldsymbol{uu} \rangle = \boldsymbol{\delta}/3$) is stress free. Secondly, a relatively high stress appears in a sample of strongly oriented azopolymer due to the entropic contribution. For example, for perfect uniaxial orientation along the x-axis, $u_x^2 = 1$, in the absence of light the tensile stress $\tau_{tens} = \tau_{xx} - \tau_{yy}$ has the magnitude of $3nkT$ [101]. Considering a typical number density of the azobenzenes $n \approx 1.0 \times 10^{21}$ cm^{-3}, the magnitude of tensile stress at room temperature, $kT \approx 4.1 \times 10^{21}$J, reaches 12 MPa. To be able to withstand such internal stress, the glassy azopolymer should have the yield stress above this value. Indeed, tensile measurements of azo-containing polyamides provide the yield stresses of $20 - 35$ MPa, [83, 82, 56] quite close to our simple estimate.

Stress tensor calculations for linearly polarized light

The action of linearly polarized light on the rigid backbone segments is described by the effective potential U_{lin}, see Equation (2.42). Its derivative over the unit vector $\boldsymbol{u}$ is defined by the term:

$$\frac{\partial}{\partial \boldsymbol{u}}(\hat{\mathbf{E}}\cdot\boldsymbol{u})^2 = 2(\hat{\mathbf{E}}\cdot\boldsymbol{u})(\frac{\partial \hat{\mathbf{E}}\cdot\boldsymbol{u}}{\partial \boldsymbol{u}}) = 2(\hat{\mathbf{E}}\cdot\boldsymbol{u})\hat{\mathbf{E}}\cdot(\boldsymbol{\delta}-\boldsymbol{uu}) = 2(\hat{\mathbf{E}}\cdot\boldsymbol{u}\hat{\mathbf{E}}-\hat{\mathbf{E}}\cdot\boldsymbol{u}\hat{\mathbf{E}}\cdot\boldsymbol{uu}) \tag{3.9}$$

To derive the above equation, we used that $\frac{\partial}{\partial \boldsymbol{u}}\boldsymbol{u} = \boldsymbol{\delta} - \boldsymbol{uu}$ [97]. Thus, the derivative of U_{lin} over $\boldsymbol{u}$ can be written as follows:

$$\frac{\partial U_{lin}}{\partial \boldsymbol{u}} = 2qmV_0(\hat{\mathbf{E}}\cdot\boldsymbol{u}\hat{\mathbf{E}} - \hat{\mathbf{E}}\cdot\boldsymbol{u}\hat{\mathbf{E}}\cdot\boldsymbol{uu}) \tag{3.10}$$

Multiplying Equation (3.10) by the unit vector $\boldsymbol{u}$ from the right and using the tensor equalities $(\boldsymbol{b}\cdot\boldsymbol{c})\boldsymbol{ad} = \boldsymbol{a}(\boldsymbol{b}\cdot\boldsymbol{c})\boldsymbol{d}$ and $\boldsymbol{ab}:\boldsymbol{cd} = \boldsymbol{a}\cdot\boldsymbol{db}\cdot\boldsymbol{c}$, we obtain:

$$\begin{aligned}\frac{\partial U_{lin}}{\partial \boldsymbol{u}}\boldsymbol{u} &= 2qmV_0(\hat{\mathbf{E}}\cdot\boldsymbol{u}\hat{\mathbf{E}}\boldsymbol{u} - \hat{\mathbf{E}}\cdot\boldsymbol{u}\hat{\mathbf{E}}\cdot\boldsymbol{uuu}) \\ &= 2qmV_0(\hat{\mathbf{E}}\hat{\mathbf{E}}\cdot\boldsymbol{uu} - \hat{\mathbf{E}}\hat{\mathbf{E}}:\boldsymbol{uuuu})\end{aligned} \tag{3.11}$$

Multiplying Equation (3.10) by the unit vector $\boldsymbol{u}$ from the left and using the tensor equalities $\boldsymbol{a}(\boldsymbol{b}\cdot\boldsymbol{c})\boldsymbol{d} = \boldsymbol{a}(\boldsymbol{c}\cdot\boldsymbol{b})\boldsymbol{d}$ and $\boldsymbol{ab}:\boldsymbol{cd} = \boldsymbol{a}\cdot\boldsymbol{db}\cdot\boldsymbol{c}$, we obtain

$$\begin{aligned}\boldsymbol{u}\frac{\partial U_{lin}}{\partial \boldsymbol{u}} &= 2qmV_0(\boldsymbol{u}\hat{\mathbf{E}}\cdot\hat{\mathbf{E}}\boldsymbol{u} - \boldsymbol{u}\hat{\mathbf{E}}\cdot\boldsymbol{u}\hat{\mathbf{E}}\cdot\boldsymbol{uu}) \\ &= 2qmV_0(\boldsymbol{uu}\cdot\hat{\mathbf{E}}\hat{\mathbf{E}} - \hat{\mathbf{E}}\hat{\mathbf{E}}:\boldsymbol{uuuu})\end{aligned} \tag{3.12}$$

Thus, the stress induced by the linearly polarized light is given by:

$$\begin{aligned}\boldsymbol{\tau}_{light} &= -\frac{n}{2}\langle\frac{\partial U_{eff}}{\partial \boldsymbol{u}}\boldsymbol{u} + \boldsymbol{u}\frac{\partial U_{eff}}{\partial \boldsymbol{u}}\rangle \\ &= -nqmV_0\langle\boldsymbol{uu}\cdot\hat{\mathbf{E}}\hat{\mathbf{E}} + \hat{\mathbf{E}}\hat{\mathbf{E}}\cdot\boldsymbol{uu} - 2\hat{\mathbf{E}}\hat{\mathbf{E}}:\boldsymbol{uuuu}\rangle\end{aligned} \tag{3.13}$$

Taking the average from each of the three terms on the right hand side of Equation (3.13), we finally obtain:

$$\boldsymbol{\tau}_{light} = -nqmV_0(\langle\boldsymbol{uu}\rangle\cdot\hat{\mathbf{E}}\hat{\mathbf{E}} + \hat{\mathbf{E}}\hat{\mathbf{E}}\cdot\langle\boldsymbol{uu}\rangle - 2\hat{\mathbf{E}}\hat{\mathbf{E}}:\langle\boldsymbol{uuuu}\rangle) \tag{3.14}$$

Here, the 2nd and 4th order orientation tensors $\langle\boldsymbol{uu}\rangle$ and $\langle\boldsymbol{uuuu}\rangle$ describe an average orientation state of the ensemble of rigid backbone segments. Note, the light-induced stress tensor can be concisely expressed as a contraction of the orientation tensors with the dyadic product of light polarization $\hat{\mathbf{E}}$.

Stress tensor calculations for circularly polarized light

The action of circularly polarized light on the rigid backbone segments is described by the effective potential U_{circ}, see Equation (3.3). The derivative of U_{circ} over the unit vector $\boldsymbol{u}$ is defined by the term:

$$\begin{aligned}\frac{\partial}{\partial \boldsymbol{u}}[1-(\hat{\mathbf{k}}\cdot\boldsymbol{u})^2] &= -(\hat{\mathbf{k}}\cdot\boldsymbol{u})(\hat{\mathbf{k}}\cdot\frac{\partial}{\partial \boldsymbol{u}}\boldsymbol{u}) = -(\hat{\mathbf{k}}\cdot\boldsymbol{u})\hat{\mathbf{k}}\cdot(\boldsymbol{\delta}-\boldsymbol{uu}) \\ &= -(\hat{\mathbf{k}}\cdot\boldsymbol{u}\hat{\mathbf{k}} - \hat{\mathbf{k}}\cdot\boldsymbol{u}\hat{\mathbf{k}}\cdot\boldsymbol{uu})\end{aligned} \tag{3.15}$$

As this derivative has the same form as in Equation (3.9), we can immediately write an expression for the stress induced by the circularly polarized light:

$$\boldsymbol{\tau}_{light} = nqm\frac{V_0}{2}(\langle\boldsymbol{uu}\rangle\cdot\hat{\mathbf{k}}\hat{\mathbf{k}} + \hat{\mathbf{k}}\hat{\mathbf{k}}\cdot\langle\boldsymbol{uu}\rangle - 2\hat{\mathbf{k}}\hat{\mathbf{k}}:\langle\boldsymbol{uuuu}\rangle) \tag{3.16}$$

Again we note that the light-induced stress tensor can be concisely expressed as a contraction of the orientation tensors with the dyadic product of the light propagation direction $\hat{\mathbf{k}}$.
Next, we focus on the time dependence of the orientation tensor $\langle\boldsymbol{uu}\rangle$, which leads to induction of light-induced stress in the azopolymer materials.

3.2.1 Derivation of time-dependent orientation tensor

The light induced stress is time dependent, because the 2nd and 4th order orientation tensors evolve with time. First we calculate the time evolution of $\langle \boldsymbol{uu} \rangle$ and then show how the 4th order orientation tensor depends on it.

Linearly polarized light

By substituting Equations (3.11) and (3.12) into Equation (3.5), the time evolution of $\langle \boldsymbol{uu} \rangle$ can be written as follows:

$$\frac{\partial}{\partial t_\lambda}\langle \boldsymbol{uu} \rangle = -\frac{qmV_0}{3kT}[\langle \boldsymbol{uu} \rangle \cdot \hat{\mathbf{E}}\hat{\mathbf{E}} + \hat{\mathbf{E}}\hat{\mathbf{E}} \cdot \langle \boldsymbol{uu} \rangle - 2\hat{\mathbf{E}}\hat{\mathbf{E}} : \langle \boldsymbol{uuuu} \rangle] - \langle \boldsymbol{uu} \rangle + \frac{\boldsymbol{\delta}}{3} \tag{3.17}$$

Circularly polarized light

Similarly, the time evolution of $\langle \boldsymbol{uu} \rangle$ for circularly polarized light can be obtained:

$$\frac{\partial}{\partial t_\lambda}\langle \boldsymbol{uu} \rangle = \frac{qmV_0}{6kT}[\langle \boldsymbol{uu} \rangle \cdot \hat{\mathbf{k}}\hat{\mathbf{k}} + \hat{\mathbf{k}}\hat{\mathbf{k}} \cdot \langle \boldsymbol{uu} \rangle - 2\hat{\mathbf{k}}\hat{\mathbf{k}} : \langle \boldsymbol{uuuu} \rangle] - \langle \boldsymbol{uu} \rangle + \frac{\boldsymbol{\delta}}{3} \tag{3.18}$$

To simplify the above equations, the time derivative has been defined in the units of rotational time λ of the rigid segment. As it is already mentioned, this time is related with the rotational diffusivity D_r. Importantly, after multiplying the right hand sides of Equations (3.17) and (3.18) by $3nkT$ and comparing the results with Equations (3.14) and (3.16), the total stress tensor can be directly related to the time evolution of the 2nd order orientation tensor:

$$\boldsymbol{\tau} = 3nkT\frac{\partial}{\partial t_\lambda}\langle \boldsymbol{uu} \rangle \tag{3.19}$$

This is so-called Giesekus form of the stress tensor [97], which will be used in the following analysis, as it allows together with Equations (3.17) and (3.18) straightforward calculation of the stress tensor.
Let us calculate the components of the orientation tensor for linearly polarized light. Assuming the light is polarized in the x direction, $\hat{\mathbf{E}} = (1, 0, 0)$, the dyadic product of $\hat{\mathbf{E}}$ is

$$\hat{\mathbf{E}}\hat{\mathbf{E}} = \begin{bmatrix} 1 & 0 & 0 \\ 0 & 0 & 0 \\ 0 & 0 & 0 \end{bmatrix} \tag{3.20}$$

The dyadic product of the unit orientation vector $\boldsymbol{u}$ is:

$$\boldsymbol{uu} = \begin{bmatrix} u_x^2 & u_x u_y & u_x u_z \\ u_x u_y & u_y^2 & u_y u_z \\ u_x u_z & u_y u_z & u_z^2 \end{bmatrix} \tag{3.21}$$

Its average defines the 2nd order orientation tensor, multiplying it from left and right side by the dyadic product $\hat{\mathbf{E}}\hat{\mathbf{E}}$, we can write the following relation:

$$\hat{\mathbf{E}}\hat{\mathbf{E}} \cdot \langle \boldsymbol{uu} \rangle + \langle \boldsymbol{uu} \rangle \cdot \hat{\mathbf{E}}\hat{\mathbf{E}} = \begin{bmatrix} \langle 2u_x^2 \rangle & 0 & 0 \\ 0 & 0 & 0 \\ 0 & 0 & 0 \end{bmatrix} \tag{3.22}$$

Using the tensor equality $\hat{\mathbf{E}}\hat{\mathbf{E}} : \boldsymbol{uuuu} = \hat{\mathbf{E}} \cdot \boldsymbol{u}\hat{\mathbf{E}} \cdot \boldsymbol{uuu}$ and $\hat{\mathbf{E}} \cdot \boldsymbol{u} = u_x$, we can write the tensor product in simplified way:

$$\hat{\mathbf{E}}\hat{\mathbf{E}} : \boldsymbol{uuuu} = u_x^2 \boldsymbol{uu} \tag{3.23}$$

Finally from Equation (3.17), we receive the time evolution of diagonal components of orientation tensor.

$$\frac{\partial}{\partial t_\lambda} \langle u_x^2 \rangle = -\frac{2qmV_0}{3kT} [\langle u_x^2 \rangle - \langle u_x^4 \rangle] - \langle u_x^2 \rangle + \frac{1}{3} \tag{3.24}$$

$$\frac{\partial}{\partial t_\lambda} \langle u_y^2 \rangle = \frac{2qmV_0}{3kT} \langle u_x^2 u_y^2 \rangle - \langle u_y^2 \rangle + \frac{1}{3} \tag{3.25}$$

$$\frac{\partial}{\partial t_\lambda} \langle u_z^2 \rangle = \frac{2qmV_0}{3kT} \langle u_x^2 u_z^2 \rangle - \langle u_z^2 \rangle + \frac{1}{3} \tag{3.26}$$

As mentioned in Chapter 2, the off-diagonal components of the orientation tensor are null ($\langle u_x u_y \rangle = \langle u_x u_z \rangle = \langle u_y u_z \rangle = 0$).
Similarly, we can calculate the time derivative of components of the orientation tensor under circularly polarized light. Let us assume that the circularly polarized light is propagating in the z direction, $\hat{\mathbf{k}} = (0, 0, 1)$, with this the dyadic product is:

$$\hat{\mathbf{k}}\hat{\mathbf{k}} = \begin{bmatrix} 0 & 0 & 0 \\ 0 & 0 & 0 \\ 0 & 0 & 1 \end{bmatrix} \tag{3.27}$$

After multiplying the 2nd order orientation tensor from left and right side by the dyadic product $\hat{\mathbf{k}}\hat{\mathbf{k}}$, we can write the following relation:

$$\hat{\mathbf{k}}\hat{\mathbf{k}} \cdot \langle \boldsymbol{uu} \rangle + \langle \boldsymbol{uu} \rangle \cdot \hat{\mathbf{k}}\hat{\mathbf{k}} = \begin{bmatrix} 0 & 0 & 0 \\ 0 & 0 & 0 \\ 0 & 0 & \langle 2u_z^2 \rangle \end{bmatrix} \tag{3.28}$$

Using the tensor equality $\hat{\mathbf{k}}\hat{\mathbf{k}} : \boldsymbol{uuuu} = \hat{\mathbf{k}} \cdot \boldsymbol{u}\hat{\mathbf{k}} \cdot \boldsymbol{uuu}$ and $\hat{\mathbf{k}} \cdot \boldsymbol{u} = u_z$, we can write the tensor product in simplified way:

$$\hat{\mathbf{k}}\hat{\mathbf{k}} : \boldsymbol{uuuu} = u_z^2 \boldsymbol{uu} \tag{3.29}$$

From Equation (3.18), the time evolution of diagonal components of the orientation tensor can be obtained as follows:

$$\frac{\partial}{\partial t_\lambda} \langle u_y^2 \rangle = -\frac{qmV_0}{3kT} \langle u_z^2 u_y^2 \rangle - \langle u_y^2 \rangle + \frac{1}{3} \tag{3.30}$$

$$\frac{\partial}{\partial t_\lambda} \langle u_x^2 \rangle = -\frac{qmV_0}{3kT} \langle u_z^2 u_x^2 \rangle - \langle u_x^2 \rangle + \frac{1}{3} \tag{3.31}$$

$$\frac{\partial}{\partial t_\lambda} \langle u_z^2 \rangle = \frac{qmV_0}{3kT} [\langle u_z^2 \rangle - \langle u_z^4 \rangle] - \langle u_z^2 \rangle + \frac{1}{3} \tag{3.32}$$

It is not trivial to solve the above differential equations, as they contain the components of 4th order orientation tensor. Thus, we propose to use suitable closure approximations to reduce its order to components of 2nd order orientation tensor.

3.3 Closure approximations for orientation tensor

For a quantitative analysis of the light-induced orientation process, it is necessary to eliminate the 4th order terms $\langle u_x^4 \rangle$, $\langle u_x^2 u_y^2 \rangle$, $\langle u_x^2 u_z^2 \rangle$ from Equations (3.24), (3.25), (3.26), (3.30), (3.31) and (3.32). Otherwise, it would not be possible to solve the ordinary differential equations containing 4th order terms. To truncate higher order terms in the ordinary differential equations, closure approximations are usually applied. We will use the simplified closure approximations which provide nearly the same functional dependence as a more elaborated closure based on the effective orientation potential [101]. In this section, we find out the best suitable closure approximation for uniaxial and biaxial orientation order.

3.3.1 Uniaxial orientation order

The light polarized in the x direction induces uniaxial order with the 2nd order orientation tensor to be symmetric around x, which means $\langle u_y^2 \rangle = \langle u_z^2 \rangle$. Hence, the following relation can be written:

$$\langle u_y^2 \rangle = \langle u_z^2 \rangle = \frac{1 - \langle u_x^2 \rangle}{2} \tag{3.33}$$

and we need to calculate only the time dependence of $\langle u_x^2 \rangle$. Later, $\langle u_y^2 \rangle$ and $\langle u_z^2 \rangle$ can be expressed in terms of $\langle u_x^2 \rangle$.
For the linearly polarized light, the closure approximation based on the effective orientation potential U_{lin} has been introduced in ref. [101]. This closure agrees well with the results of direct numerical calculations. It is based on the following distribution function:

$$\eta(\theta) = \frac{1}{z} \exp\left(-U_{lin}\right) = \frac{1}{z} \exp\left(-V_0 \cos^2(\theta)\right) \tag{3.34}$$

Here, $z = \int \eta(\theta) \sin\theta d\theta$ is the normalization factor. Using the above distribution function, the components of 2nd and 4th order orientation tensor can be calculated as follows:

$$\langle u_x^n \rangle = \int \cos^n(\theta) \eta(\theta) \sin\theta d\theta, \qquad n = 2, 4 \tag{3.35}$$

From the above equation, the dependence of 4th order term on the 2th order term can be established numerically, as shown in Figure 3.2. The moments corresponding to different limits of orientation potential strength are:

- a) $V_0 \to -\infty$, $\langle u_x^2 \rangle = 1$ and $\langle u_x^4 \rangle = 1$
- b) $V_0 \to 0$, $\langle u_x^2 \rangle = 1/3$ and $\langle u_x^4 \rangle = 1/5$
- c) $V_0 \to \infty$, $\langle u_x^2 \rangle = 0$ and $\langle u_x^4 \rangle = 0$

It can be seen that the exact solutions for the perfect uniaxially oriented state, isotropic state and perfect orientation in the plane perpendicular to the polarization direction $\boldsymbol{x}$ are reproduced by cases a), b) and c), respectively. However, it is difficult to use this closure in the differential equations (3.24) and (3.32) , as it does not provide analytical solution for the 4th order terms. Therefore, we focus further on finding a simpler closure approximation which on one side fits well the results of closure based on the effective orientation potential but on the other side can be represented by analytical expression. With this purpose, next in this chapter, we define and compare the two types of closure approximations

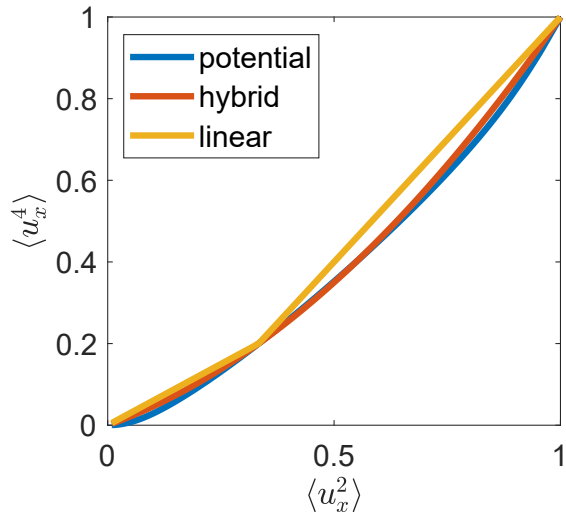

Figure 3.2: Comparison of the linear and hybrid closure approximations with the closure based on the effective orientation potential, as assigned in the legend.

which are linear and hybrid closure approximations.

- **Linear closure approximation**

  In the linear closure approximation a linear fit connects the exact solution points $\langle u_x^2 \rangle = 0$, $1/3$, 1 for three different cases discussed above.

$$\langle u_x^4 \rangle = \begin{cases} \frac{3}{5}\langle u_x^2 \rangle, & \langle u_x^2 \rangle < \frac{1}{3} \\ \frac{6}{5}\langle u_x^2 \rangle - \frac{1}{5}, & \langle u_x^2 \rangle \geq \frac{1}{3} \end{cases} \tag{3.36}$$

  Using the above equation, $\langle u_x^4 \rangle$ dependence on $\langle u_x^2 \rangle$ is plotted, see the yellow line in Figure 3.2.

- **Hybrid closure approximation**

  The name hybrid closure suggests that this approximation is a combination of linear and quadratic terms. In particular, we will use the following expression:

$$\langle u_x^4 \rangle = \frac{3}{5}\langle u_x^2 \rangle^2 + \frac{2}{5}\langle u_x^2 \rangle \tag{3.37}$$

  Using the hybrid closure approximation, $\langle u_x^4 \rangle$ depending on $\langle u_x^2 \rangle$ is plotted, see the red line in Figure 3.2.

Further, we compare linear and hybrid closure approximations with the closure approximation corresponding to the effective potential. It can be seen from

Figure 3.2 that the hybrid closure is the better fit to the orientation potential closure. Thus, we choose to use the hybrid closure approximation for the 4th order terms, such as $\langle u_x^4 \rangle$, $\langle u_y^4 \rangle$ and $\langle u_z^4 \rangle$.

3.3.2 Biaxial orientation order

When the azopolymer segments oriented along the x axis are irradiated with the light polarized in the $\boldsymbol{y}$ direction, the initial orientation tensor becomes asymmetric around the polarization of light $\boldsymbol{y}$. This results in biaxial orientation order and the time evolution of $\langle u_x^2 \rangle$ and $\langle u_z^2 \rangle$ can not be written in terms of $\langle u_y^2 \rangle$, as it is done for the uniaxial orientation order (3.33). It is required to truncate all 4th order orientation tensor components like $\langle u_y^2 u_z^2 \rangle$ and $\langle u_x^2 u_y^2 \rangle$ to 2nd order terms. In this section, we develop additional closure approximations for the biaxial orientation order.
For unit orientation vector the following relation is always valid:

$$u_x^2 + u_y^2 + u_z^2 = 1 \tag{3.38}$$

First squaring and then averaging Equation (3.38), the following expression is obtained:

$$\begin{aligned} \langle u_x^4 \rangle + \langle u_y^4 \rangle + \langle u_z^4 \rangle + 2\langle u_x^2 u_y^2 \rangle \\ + 2\langle u_y^2 u_z^2 \rangle + 2\langle u_x^2 u_z^2 \rangle = 1 \end{aligned} \tag{3.39}$$

Alternatively, first averaging and then squaring Equation (3.38), the following relation can be written:

$$\begin{aligned} \langle u_x^2 \rangle^2 + \langle u_y^2 \rangle^2 + \langle u_z^2 \rangle^2 \\ +2\langle u_x^2 \rangle \langle u_y^2 \rangle \\ + 2\langle u_y^2 \rangle \langle u_z^2 \rangle + 2\langle u_x^2 \rangle \langle u_z^2 \rangle = 1 \end{aligned} \tag{3.40}$$

Using Equations (3.39) and (3.40), we can write:

$$\begin{aligned} \langle u_x^4 \rangle + \langle u_z^4 \rangle = \frac{3}{5}\langle u_x^2 \rangle^2 + \frac{2}{5}\langle u_x^2 \rangle + \frac{3}{5}\langle u_z^2 \rangle^2 \\ + \frac{2}{5}\langle u_z^2 \rangle + \frac{6}{5}\langle u_x^2 \rangle \langle u_z^2 \rangle - 2\langle u_x^2 u_z^2 \rangle \end{aligned} \tag{3.41}$$

The above equation can be split in two parts by noticing that equal correction terms are added to $\langle u_x^4 \rangle$ and $\langle u_z^4 \rangle$ from the hybrid closure approximation (3.37):

$$\langle u_x^4 \rangle = \frac{3}{5}\langle u_x^2 \rangle^2 + \frac{2}{5}\langle u_x^2 \rangle + \frac{3}{5}\langle u_x^2 \rangle \langle u_z^2 \rangle - \langle u_x^2 u_z^2 \rangle \tag{3.42}$$

and

$$\langle u_z^4 \rangle = \frac{3}{5}\langle u_z^2 \rangle^2 + \frac{2}{5}\langle u_z^2 \rangle + \frac{3}{5}\langle u_x^2 \rangle \langle u_z^2 \rangle - \langle u_x^2 u_z^2 \rangle \tag{3.43}$$

Substituting Equations (3.40) and (3.39) into Equation (3.42) we get:

$$\langle u_x^2 u_y^2 \rangle = \frac{3}{5}\langle u_x^2 \rangle \langle u_y^2 \rangle \tag{3.44}$$

Substituting Equations (3.40) and (3.39) into Equation (3.43) we get:

$$\langle u_y^2 u_z^2 \rangle = \frac{3}{5}\langle u_y^2 \rangle \langle u_z^2 \rangle \tag{3.45}$$

Let us check the validity of the obtained closure approximations for the case of initial isotropic orientation with $\langle u_x^2 \rangle = \langle u_y^2 \rangle = \langle u_z^2 \rangle = \frac{1}{3}$. From Equation (3.44) we get:

$$\langle u_x^2 u_y^2 \rangle = \frac{1}{15} \tag{3.46}$$

On the other side, the hybrid closure (3.37) can be used to calculate $\langle u_x^2 u_y^2 \rangle$ for the case of initial isotropic orientation:

$$\langle u_x^2 u_y^2 \rangle = \frac{\langle u_x^2 \rangle - \langle u_x^4 \rangle}{2} = \frac{1}{15} \tag{3.47}$$

Comparing Equations (3.46) and (3.47), it can be seen that the proposed closure approximations for the biaxial orientation order provide the correct result for initial isotropic state. Similarly, it can be shown that they are valid for description of two other limiting cases with $\langle u_y^2 \rangle = 0, 1$.

3.4 Calculation of orientation tensor

To solve the system of differential Equations (3.24) - (3.26) and (3.30) - (3.32), the 4th order terms are truncated to 2nd order terms using the closure approximations defined above. The time dependent components of the orientation tensor for the uniaxial and biaxial order are calculated in this section.

3.4.1 Uniaxial orientation order

For the light linearly polarized in the x direction, the time derivative of the orientation tensor components is represented by Equations (3.24) - (3.26). As there is a symmetry in diagonal components of initial orientation tensor around x axis, as shown in Equation (3.33), it is enough to solve Equation (3.24) using

the hybrid closure approximation (3.37). The evolution of $\langle u_x^2 \rangle$ is described by the 2nd order differential equation [101]:

$$\frac{\partial}{\partial t_\lambda}\langle u_x^2 \rangle = -\frac{2qmV_0}{5kT}[\langle u_x^2 \rangle - \langle u_x^2 \rangle^2] - \langle u_x^2 \rangle + \frac{1}{3} \tag{3.48}$$

For $V_0 > 0$, the solution for the time-dependent xx orientation tensor component under the linearly polarized light is as follows:

$$\langle u_x^2 \rangle(t) = \frac{u_1 - u_2 \frac{u_0 - u_1}{u_0 - u_1} e^{a(u_1 - u_2)t}}{1 - \frac{u_0 - u_1}{u_0 - u_1} e^{a(u_1 - u_2)t}} \tag{3.49}$$

Here, $u_0 = \langle u_x^2 \rangle(0)$ is the initial value in the absence of light and

$$u_{1,2} = \frac{1}{2} + \frac{1}{2V_r} \pm \frac{1}{2}\sqrt{(1 + \frac{1}{V_r})^2 - \frac{4}{3V_r}} \tag{3.50}$$

Here, u_1 and u_2 are the roots of the quadratic equation defined by the right hand side of Equation (3.48). Both, the reduced potential $V_r = \frac{2qmV_0}{5kT}$ and the exponent $a = \frac{V_r}{\lambda}$, introduced in Equations (A.2) and (3.50), take negative values for side-chain azopolymers because of the negative shape factor q. This solution provides the stationary orientation $\langle u_x^2 \rangle_{st} = u_1$ at $t \to \infty$, when both exponential terms in Equation (3.50) take zero values. As can be seen from Equation (A.2), $u_1 \to 1$ under strong irradiation, when $V_r \to -\infty$, and the stationary state of the ensemble of rigid backbone segments approaches a perfect uniaxial orientation along $\hat{\mathbf{E}}||\hat{\mathbf{x}}$. As $\langle u_x^2 \rangle$ increases with time by higher rate under larger reduced potential strength, the saturation point is attained at smaller time values, as shown in Figure 3.3(a).

Similarly the orientation tensor for circularly polarized light can be expressed as:

$$\langle u_z^2 \rangle(t) = \frac{u_1 - u_2 \frac{u_0 - u_1}{u_0 - u_2} e^{a(u_1 - u_2)t}}{1 - \frac{u_0 - u_1}{u_0 - u_2} e^{a(u_1 - u_2)t}} \tag{3.51}$$

Here, $u_0 = \langle u_z^2 \rangle(0)$ is the initial value in the absence of light and the roots are

$$u_{1,2} = \frac{1}{2} - \frac{1}{V_r} \pm \frac{1}{2}\sqrt{(1 - \frac{2}{V_r})^2 + \frac{8}{3V_r}} \tag{3.52}$$

3.4.2 Biaxial orientation order

For the light linearly polarized in the y-direction, the time derivative of the orientation tensor with $\langle u_x^2 \rangle \neq \langle u_z^2 \rangle$ is represented by Equations (3.24) - (3.26).

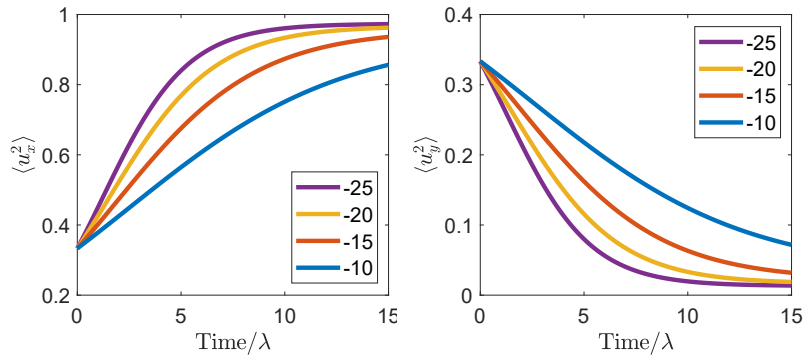

Figure 3.3: Time evolution of the orientation tensor components: a) $\langle u_x^2 \rangle$ and b) $\langle u_y^2 \rangle = \langle u_z^2 \rangle$ for different strengths of the reduced potential V_r. Time is expressed in the units of λ, rotational time of the rigid segments.

Applying the closure approximations (3.37) - (3.45), the orientation tensor components can be calculated by solving the following system of differential equations:

$$\frac{\partial}{\partial t_\lambda}\langle u_y^2 \rangle = -\frac{2qmV_0}{5kT}[\langle u_y^2 \rangle - \langle u_y^2 \rangle^2] - \langle u_y^2 \rangle + \frac{1}{3} \tag{3.53}$$

$$\frac{\partial}{\partial t_\lambda}\langle u_x^2 \rangle = \frac{2qmV_0}{5kT}\langle u_x^2 \rangle\langle u_y^2 \rangle - \langle u_x^2 \rangle + \frac{1}{3} \tag{3.54}$$

$$\frac{\partial}{\partial t_\lambda}\langle u_z^2 \rangle = \frac{2qmV_0}{5kT}\langle u_y^2 \rangle\langle u_z^2 \rangle - \langle u_z^2 \rangle + \frac{1}{3} \tag{3.55}$$

Equation (3.53) for $\langle u_y^2 \rangle$ can be solved analytically, similar as it was done for $\langle u_x^2 \rangle$ in Equation (3.48). The time dependent solution for $\langle u_y^2 \rangle$ can be written as follows:

$$\langle u_y^2 \rangle(t) = \frac{u_1 - u_2 \frac{u_0 - u_1}{u_0 - u_1} e^{a(u_1 - u_2)t}}{1 - \frac{u_0 - u_1}{u_0 - u_1} e^{a(u_1 - u_2)t}} \tag{3.56}$$

Here, $u_0 = \langle u_y^2 \rangle(0)$ is the initial value in the absence of light and the roots $u_{1,2}$ are given by Equation (3.50).
After that, $\langle u_x^2 \rangle$ and $\langle u_z^2 \rangle$ in Equations (3.54) and (3.55) are solved numerically using Euler's forward method:

$$\langle u_x^2 \rangle(t + dt) = \langle u_x^2 \rangle(t) + dt \frac{\partial}{\partial t_\lambda}\langle u_x^2 \rangle \tag{3.57}$$

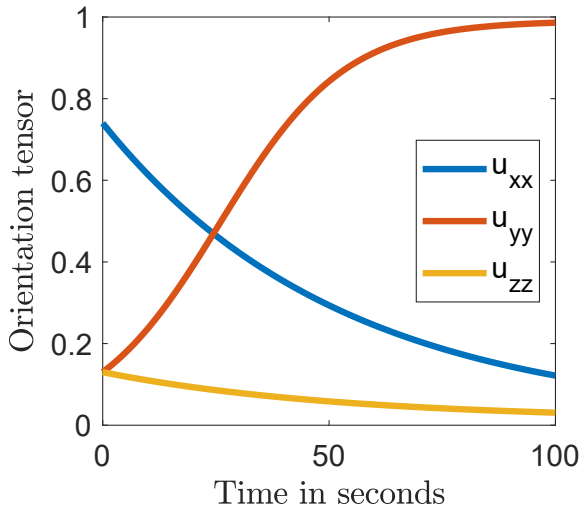

Figure 3.4: All three components of the orientation tensor corresponding to maximum stress under the SS interference pattern for $\tau_{xx,0} = 25$ MPa.

$$\langle u_z^2 \rangle (t + dt) = \langle u_z^2 \rangle (t) + dt \frac{\partial}{\partial t_\lambda} \langle u_z^2 \rangle \tag{3.58}$$

The exemplary solution for biaxial orientation order is represented in Figure 3.4. The initial conditions are $\langle u_x^2 \rangle = 0.74$, $\langle u_y^2 \rangle = \langle u_z^2 \rangle = 0.13$. It can be seen that in the case of biaxial order, the orientation component $\langle u_y^2 \rangle$ in the direction of light polarization increases and approaches to one, while two other diagonal components decrease from their different initial values. Hence, we observe here the reorientation transition: the segments, initially oriented in the x direction, gradually reorient in the light polarization direction $\boldsymbol{y}$.
The light-induced stress tensor can be calculated from the orientation tensor, as shown in Equation (3.19). To implement the light-induced stress, it is necessary to choose a proper simulation tool and to define the diverse material properties. With this purpose, we dedicate the next chapter to modeling the azopolymer material samples.

Chapter 4

Viscoplastic modeling of glassy azopolymers

In this present chapter, we focus on defining the azopolymer material model, which is necessary to implement the light-induced stress for different light polarizations and intensities. The glassy azopolymers remain in the solid state under illumination at moderate laser intensities, $0.1 - 0.2$ W/cm^2 [56, 83, 82]. This is especially true for the azopolymers, whose glass transition temperature is above 373 K [37]. Therefore, description of the light-induced deformation in glassy azo-materials should be based on a viscoplastic material model [101, 102, 103].
In this thesis we use the finite element modeling software ANSYS to model the viscoplastic response of glassy azopolymers under the light-induced stress. In particular, we choose Perzyna option which is suitable for modeling the viscoplastic materials under external applied stress.

4.1 Viscoplastic material modeling

Glassy azopolymers are viscoplastic materials and can be modelled as the Bingham solid [101, 103, 102]. It is a material that can support a finite stress elastically without flow and which flows with constant viscosity when the stresses are sufficiently large. The Bingham solid is defined by the following equation [104]:

$$\boldsymbol{\tau} = \begin{cases} 2G\boldsymbol{\epsilon}_{el}, & \tau_{eq} \leq \tau_{yield} \\ \boldsymbol{\tau}_{yield} + 2\eta\dot{\boldsymbol{\epsilon}}_{pl}, & \tau_{eq} > \tau_{yield} \end{cases} \tag{4.1}$$

Here, τ_{eq} is the equivalent stress, G is the shear modulus of the azopolymer, $\boldsymbol{\epsilon}_{el}$ is the elastic strain tensor, τ_{yield} is the yield stress of the azopolymer, η is the viscosity of the plastic flow and $\dot{\boldsymbol{\epsilon}}_{pl}$ is the rate of plastic strain tensor. Above the yield stress the total strain in the azopolymer is calculated as the sum of

elastic and true plastic strains:

$$\boldsymbol{\epsilon} = \boldsymbol{\epsilon}_{el} + \boldsymbol{\epsilon}_{pl} \tag{4.2}$$

where $\boldsymbol{\epsilon}_{el} = \boldsymbol{\tau}_{yield}/E$ and $\boldsymbol{\epsilon}_{pl} = \int \dot{\boldsymbol{\epsilon}}_{pl} dt$. A Young's modulus $E = 2G$ is about 2 GPa and the yield stress for azopolymers is of the order of 10 MPa [94]. Accordingly, an instantaneous elastic strain $\boldsymbol{\epsilon}_{el}$ should be considerably smaller than the plastic strain accumulated in the process of photodeformation.
It is assumed that the material yields when the stress state reaches the yield surface and further loading causes plastic deformation. The yield surface is commonly defined for isotropic polymers by the von Mises criterion $\tau_{eq} - \tau_{yield} = 0$ with the von Mises equivalent stress:

$$\tau_{eq} = \sqrt{\frac{3}{2}\boldsymbol{\tau} : \boldsymbol{\tau}} \tag{4.3}$$

The above relation can be written in terms of the stress tensor components:

$$\tau_{eq} = \sqrt{\frac{1}{2}((\tau_{11} - \tau_{22})^2 + (\tau_{22} - \tau_{33})^2 + (\tau_{33} - \tau_{11})^2 + 6(\tau_{12}^2 + \tau_{23}^2 + \tau_{31}^2))} \tag{4.4}$$

Using Bingham solid model, the plastic strain corresponding to the equivalent stress can be calculated for the homogeneous stress distribution. In the case when the light-induced stress tensor has spatial dependence, it is not possible to calculate the plastic strain analytically. Therefore, the light-induced deformations in the azopolymer material are modelled using a finite element modeling software ANSYS.

4.2 Material modeling in ANSYS

The ANSYS (Analysis System) software package is well suited for predicting material behaviour under complex mechanical deformations. In this work, Release 21.1 of ANSYS ©Academic Research Mechanical is used. To model azopolymers as viscoplastic solids, we apply the Perzyna option provided in the ANSYS software:

$$\dot{\epsilon}_{pl} = \gamma\Big(\frac{\tau_{eq}}{\tau_{yield}} - 1\Big)^{1/m} \tag{4.5}$$

Here, $\dot{\epsilon}_{pl}$ is the rate of equivalent plastic strain and $\gamma = \tau_{yield}/3\eta$ is the viscosity parameter which is related to the viscosity η in Equation (4.1). The Perzyna option with $m = 1$ describes the Bingham solid model. This option can be applied in two ways, which are mechanical APDL (ANSYS Parametric Design Language) and ANSYS workbench, to calculate the plastic deformation in the material. In both cases the command to switch on the Perzyna option is "Tb,

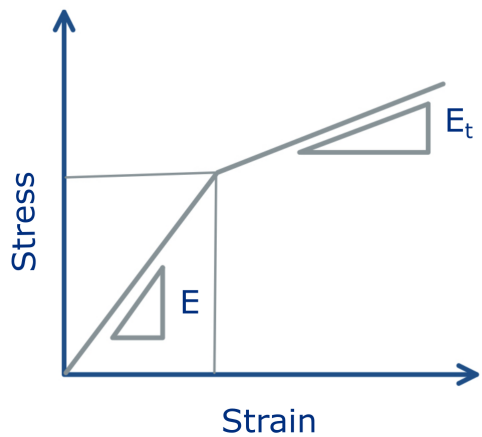

Figure 4.1: Dependence of stress on strain in the bilinear isotropic hardening (BISO) model: E is the Young's modulus and E_t is the tangent modulus.

rate".
Further, the material is characterised by the BISO command in ANSYS, which is bilinear isotropic hardening. It is defined via two parameters: the initial yield stress $\tau_{yield,ini}$ and the tangent modulus E_t which is the slope of stress-strain curve above the yield stress, see Figure 4.1. The value of τ_{yield} at any point of time is:

$$\tau_{yield} = \tau_{yield,ini} + E_t \epsilon_{pl} \tag{4.6}$$

The only information known about the yield stress of glassy azopolymers is its magnitude which is about $20-30$ MPa [94]. Due to that, we prefer to choose the yield stress to be constant under the influence of external applied stress. From Equation (4.6) it can be seen that the yield stress τ_{yield} grows with the plastic strain with the slope equal to the tangent modulus E_t. To keep the yield stress constant, we choose the value of the tangent modulus E_t four orders of magnitude smaller than the initial yield stress: $\tau_{yield,ini} = 10$ MPa and $E_t = 10^{-3}$ MPa. Even at large plastic strains, for example at $\epsilon_{pl} = 10$, the yield stress τ_{yield} remains constant for the chosen values of $\tau_{yield,ini}$ and E_t. Also, we define the Young's modulus ($E = 10^3$ MPa) and Poisson ratio ($= 0.49$) with the help of MP,Ex and MP,NUXY commands, respectively [105].
As mentioned in Chapter 3, the light-induced stress has time dependence which makes the rate of change of plastic strain also time dependent. The time dependent stress can be easily implemented in ANSYS for the homogeneous stress field, but it is not straightforward to implement the time as well as spatially dependent light induced stress field. For that, we collaborated with Dr. Hendrik Donner, who is responsible for the ANSYS maintenance and professional development at the CADFEM firm. It was suggested to use Userthstrain sub-

routine and explained in detail how to implement the spatially as well as time dependent light-induced stress in terms of thermal strain.

4.3 Application of light-induced stress in ANSYS

Exterior excitations like light-induced and thermal stresses can be incorporated in ANSYS using external subroutines like Usermat and Userthstrain. Implementation of Userthstrain subroutine is more simple and suitable for the application of light-induced stress in ANSYS. The main advantage of this subroutine is a simple combination with natively implemented material models via mechanical APDL.
The main idea of Userthstrain lies in the decomposition of the total strain tensor into mechanical $\boldsymbol{\epsilon}_{mech}$ and thermal $\boldsymbol{\epsilon}_{th}$ strain tensors:

$$\boldsymbol{\epsilon} = \boldsymbol{\epsilon}_{mech} + \boldsymbol{\epsilon}_{th} \tag{4.7}$$

Under suppressed deformations $\boldsymbol{\epsilon} = 0$, $\boldsymbol{\epsilon}_{mech} = -\boldsymbol{\epsilon}_{th}$. For isotropic linear elastic materials the light-induced stress can be written as follows:

$$\boldsymbol{\tau} = -E\boldsymbol{\epsilon}_{th} = E\boldsymbol{\epsilon}_{mech} \tag{4.8}$$

Hence, it can be concluded that a suitable thermal strain $\boldsymbol{\epsilon}_{th}$ can generate mechanical deformations which correspond to the light-induced stress.
In order to incorporate inelastic material properties, like plasticity, the total strain tensor for viscoplastic materials is decomposed by ANSYS as follows:

$$\boldsymbol{\epsilon} = \boldsymbol{\epsilon}_{el} + \boldsymbol{\epsilon}_{th} + \boldsymbol{\epsilon}_{pl} \tag{4.9}$$

For the inelastic case, under suppressed deformations $\boldsymbol{\epsilon} = 0$, $\boldsymbol{\epsilon}_{th} = -(\boldsymbol{\epsilon}_{el} + \boldsymbol{\epsilon}_{pl})$. For the viscoplastic materials, the thermal strain is chosen in the Userthstrain subroutine with the help of Perzyna option (see Equation (4.5)) in such a way that it produces the mechanical deformations prescribed locally by light-induced stress. With this implementation, the time dependent thermal strain can be defined at each material point. In this case, the temperature is used as a dummy variable to characterize the time range.
The final stress state depends not only on the applied light-induced stress but also on the boundary conditions. The different boundary conditions can produce different stress fields, as explained in Figure 4.2. It is very important to understand in ANSYS calculations that the final mechanical stress field, elastic and plastic strain fields are the results of modeling procedure at chosen boundary conditions, but not the initial input fields. Contrary, the external fields such as gravitational, magnetic or light-induced stress field, are the examples of the initial input fields.

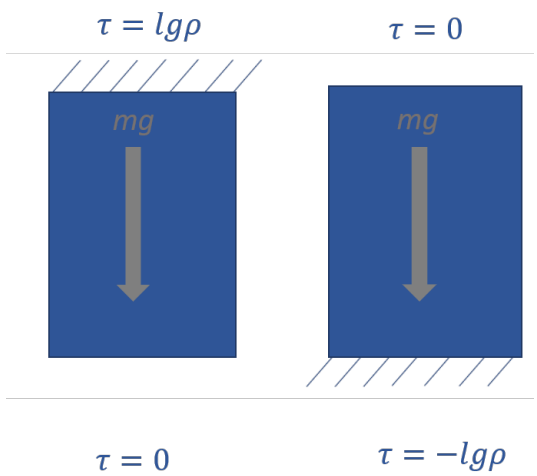

Figure 4.2: Distribution of stress fields $\boldsymbol{\tau}$ in the block a) hanging at the ceiling and b) lying on the ground, under the effect of gravitational force mg. Here, l is the length of the block, m is the mass and ρ is the density of the block.

Userthstrain is linked to mechanical APDL via some commands, which set material properties and state variables. State variables are needed to store values at previous time steps. Necessary material properties, for example, the shear modulus or the yield stress, can be put into the Mechanical APDL with the help of commands: TB, TBDATA, MP. The command INISTATE can prescribe initial stresses, strains, state variables and plastic strains, etc. Using INISTATE, spatially inhomogeneous stress field can be defined (for e.g. the stress field which appears under light interference patterns). The magnitudes of state variables can be defined node-wise, element-wise, for each Gauss point, and with respect to different coordinate systems.
To summarise, with the help of Userthstrain subroutine, the locally varying stress field corresponding to light-induced stress can be implemented in ANSYS using different Mechanical APDL commands under the influence of suitable boundary conditions.
Further, the material model should be calibrated with respect to the exact analytical solutions by adjusting the mesh and time step size. For viscoplastic materials, we mesh the sample with tetrahedral elements. In the next chapter, we focus on implementation of light-induced stress in ANSYS under homogeneous light intensity. For this case, the light-induced deformations can be calculated exactly and can be used to calibrate the ANSYS results. After that, the modeling results are compared with the experimental observations in azopolymer square posts under homogeneous light illuminations.

Chapter 5

Directional deformations under homogeneous light illumination

The photodeformation phenomenon of azopolymers under light illumination has been studied for the last three decades. Several interesting observations are made when samples are irradiated with polarized light, as discussed in Chapter 1. In this chapter we focus on one of these observations, which is the experiment done by Lee et al. [37], as shown in Figure 5.1. Here, the epoxy-based azopolymer square post is deformed in the presence of horizontally, vertically and circularly polarized light. It can be seen that deformations are directional: for linearly polarized light the post elongates in the direction of light polarization and for circularly polarized light the post deforms radially in the polarization plane.

The explanation of these deformations will be provided in this chapter using the orientation approach.[1]Because the deformations under homogeneous light illumination can be calculated analytically, we will use this system as a reference system to calibrate the material model. Later in the next chapters, using the

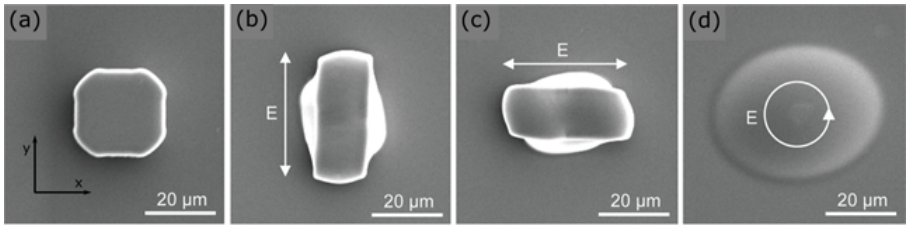

Figure 5.1: Deformations of a) the initial square post in the presence of homogeneous light intensity. Deformed post in the presence of b) vertically polarized light, c) horizontally polarized light and d) circularly polarized light. Modified and reproduced from Ref. [37].

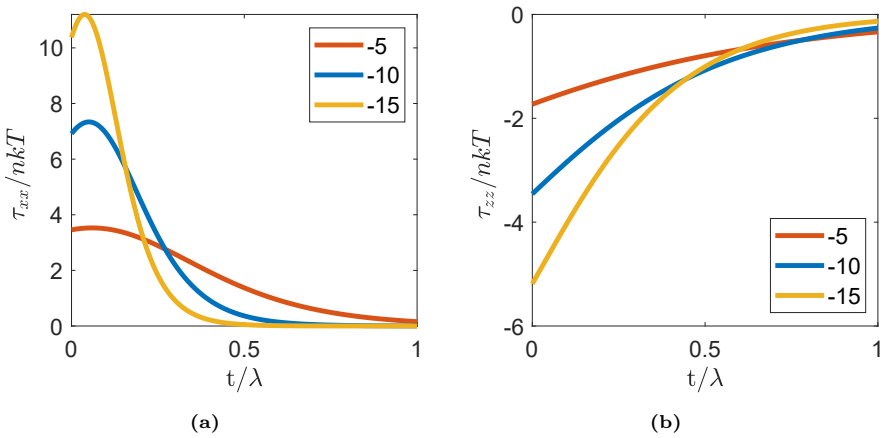

(a) **(b)**

Figure 5.2: The time dependent components of the light-induced stress tensor at different strengths of the reduced potential $V_r = -5, -10, -15$: a) τ_{xx} for horizontally and b) τ_{zz} for circularly polarized light.

same calibration, more complicated inscriptions can be modelled, for example surface relief gratings.

5.1 Light-induced stress tensor

The light-induced stress tensor for linearly and circularly polarized light is derived in Chapter 3 starting from initial isotropic state. For the light polarized in x direction, the τ_{xx} component of light-induced stress can be calculated using Equations (3.19) and (A.2). Additionally, for circularly polarized light, the τ_{zz} component of light-induced stress can be calculated using Equations (3.19) and (3.51). These components are presented in Figure 5.2 for different strengths of the reduced potential $V_r = -5, -10, -15$. It can be seen that for linearly polarized light τ_{xx} component of the stress tensor first experiences a jump at $t = 0$ and then decreases with time. On the other side, for circularly polarized light τ_{zz} component of the light-induced stress tensor is negative and its magnitude decreases with time. Further in this section, we will provide the analytical solutions for the plastic deformations developing under linearly and circularly polarized light.

5.1.1 Linearly polarized light

In the experiment discussed earlier in the current Chapter, see Figure 5.1, two kinds of linearly polarized light are used, horizontally and vertically polarized

[1]The results presented in this chapter are published in Yadav et al. [101]

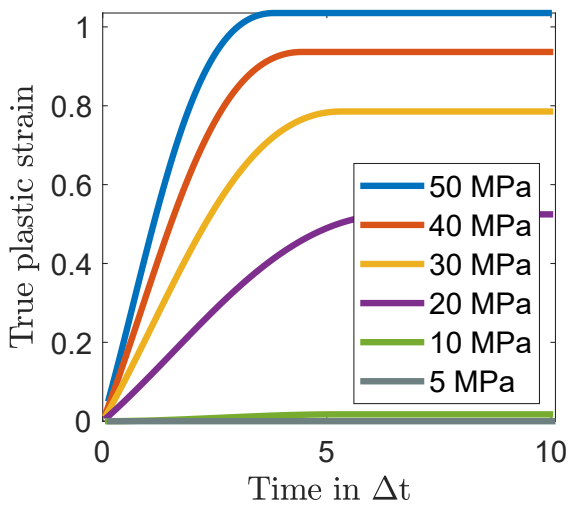

Figure 5.3: The time dependent true plastic strain for the linearly polarized light at different magnitudes of initial equivalent stress τ_{eq}. $\tau_{yield} = 10$ MPa, $\lambda = 50\Delta t$.

light. We assume that the light polarization for horizontally polarized light is in the x direction and for vertically polarized light it is in the y direction.

Horizontally polarized light:

For the light linearly polarized in the x-direction, the yy and zz components of the 2nd order orientation tensor $\langle \boldsymbol{uu} \rangle$ are equal and can be calculated from its xx component, as shown in Equation (3.33). As discussed in Chapter 3, the off-diagonal components of $\langle \boldsymbol{uu} \rangle$ are zero. Using the Giesekus equation (3.19), the stress tensor can be calculated and it can be shown that $\tau_{yy} = \tau_{zz} = -\tau_{xx}/2$. Note that the trace of the stress tensor is zero: $\tau_{xx} + \tau_{yy} + \tau_{zz} = 0$.
Hence, the stress tensor for light polarized in the x direction can be written as follows:

$$\boldsymbol{\tau} = \begin{bmatrix} \tau_{xx} & 0 & 0 \\ 0 & -\frac{\tau_{xx}}{2} & 0 \\ 0 & 0 & -\frac{\tau_{xx}}{2} \end{bmatrix} \tag{5.1}$$

Vertically polarized light:

For the light linearly polarized in the y direction, the xx and zz components of 2nd order orientation tensor $\langle \boldsymbol{uu} \rangle$ are equal. Similar to the light polarized in

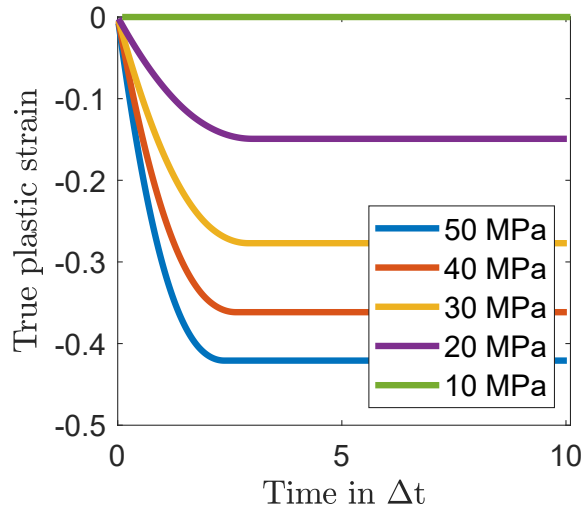

Figure 5.4: The time dependent true plastic strain for the circularly polarized light at different equivalent stress τ_{eq}. $\tau_{yield} = 10$ MPa, $\lambda = 50\Delta t$.

the x direction, the light-induced stress tensor can be calculated as follows:

$$\boldsymbol{\tau} = \begin{bmatrix} -\frac{\tau_{yy}}{2} & 0 & 0 \\ 0 & \tau_{yy} & 0 \\ 0 & 0 & -\frac{\tau_{yy}}{2} \end{bmatrix} \tag{5.2}$$

The plastic strain for viscoplastic materials can be calculated analytically using Equation (4.1) for different magnitudes of the equivalent stress τ_{eq}. For uniaxially deformed sample, τ_{eq} is equal to the magnitude of the tensile stress. In particular, for horizontally polarized light $\tau_{eq} =\mid \tau_{xx} - \tau_{yy} \mid = 3 \mid \tau_{xx} \mid /2$. For the constant applied stress, the plastic strain will linearly increase with time that makes the material to deform infinitely without stopping. On the other side, for azopolymers the light-induced stress is time dependent, see Figure 5.2(a). The analytically calculated true plastic strain ($\boldsymbol{\epsilon}_{pl} = \int \dot{\boldsymbol{\epsilon}}_{pl} dt$) is presented in Figure 5.3 for the following values of material parameters: yield stress $\tau_{yield} = 10$ MPa, $\gamma = (10\Delta t)^{-1}$ and the rotational time λ should be about $50\Delta t$, where Δt is the measure of time scale, ca. $10 - 60$ s. The true plastic strain is zero for the equivalent stresses less than or equal to the yield stress τ_{yield}. It is positive (= sample elongates) and increases with time with the slope proportional to the magnitude of initial equivalent stress. Later on, the true plastic strain tends to saturate.

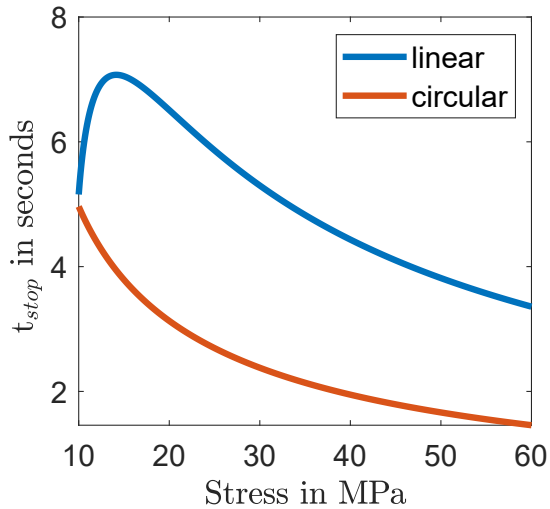

Figure 5.5: The dependence of stopping time on the initial equivalent stress when the azopolymer sample is illuminated with linearly (blue) and circularly (red) polarized light.

5.1.2 Circularly polarized light

For circularly polarized light propagating in the z-direction and the polarization vector rotating in the xy plane, the stress tensor can be written as follows:

$$\boldsymbol{\tau} = \begin{bmatrix} -\frac{\tau_{zz}}{2} & 0 & 0 \\ 0 & -\frac{\tau_{zz}}{2} & 0 \\ 0 & 0 & \tau_{zz} \end{bmatrix} \tag{5.3}$$

The equivalent stress for circularly polarized light is: $\tau_{eq} = 3 \mid \tau_{zz} \mid /2$. The analytically calculated true plastic strain is zero for the stresses less than the yield stress and it is negative (= sample contracts) for larger stresses, as shown in Figure 5.4. At short times, the magnitude of plastic strain increases linearly with the slope proportional to the magnitude of initial equivalent stress. At longer times, the true plastic strain tends to saturate, which means the sample stops to deform.

Stopping time

For linearly and circularly polarized light the equivalent stress depends on the magnitude of τ_{xx} and τ_{zz} components, respectively. As discussed before, these components of the light-induced stress tensor vanish with time, as shown in Figure 5.2. Correspondingly, the equivalent stress in the both cases decreases with time. The material stops to deform at the moment when the equivalent stress becomes equal to the yield stress (as described in the viscoplastic modeling part in Chapter 4). This time, at which the deformations stop, we call the stopping

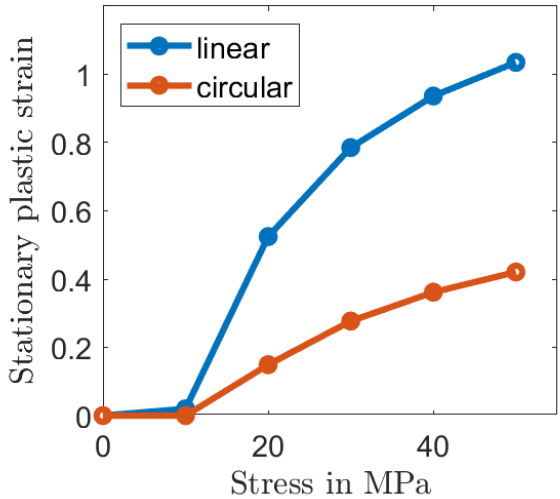

Figure 5.6: The dependence of stationary plastic strain on the initial equivalent stress when the azopolymer sample is illuminated with linearly (blue) and circularly (red) polarized light.

time t_{stop} and represent it in Figure 5.5.
The stopping time for linearly polarized light is larger than for circularly polarized light at the same equivalent stress. This is due to the fact that the magnitude of initial equivalent stress $|\tau_{eq}|= nkTV_r$ for the linear polarization and $|\tau_{eq}|= nkTV_r/2$ for the circular polarization. Thus, at the same equivalent stress, the value of reduced potential V_r is twice larger for the circular polarization. A larger V_r results in a faster drop of the light-induced stress, which reaches the value of yield stress at smaller t_{stop}.
It is clearly seen from Figure 5.5 that at the same initial equivalent stress the value of t_{stop} is considerably smaller for the circularly polarized light and hence the sample deformation is diminished. Further, the stationary plastic strain is compared for the both cases. It can be seen from Figure 5.6 that the stationary plastic strain for linearly polarized light is larger than for the circularly polarized light at the same equivalent stress. With this, it can be predicted that the sample will deform much more under linearly polarized light.

Fortunately, the directional photodeformations under homogeneous light illumination can be calculated analytically. However, it can not be done for the complex interference patterns. With this purpose, in the next section, we will optimize the ANSYS modeling in correspondence to the analytical results by calibrating the time step and the mesh size.

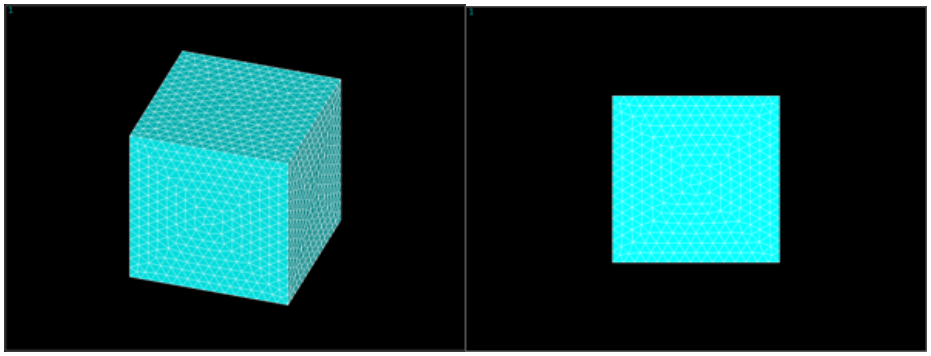

(a) (b)

Figure 5.7: ANSYS undeformed square post: (a) 3D view of 1/8 of the post and (b) top view.

5.2 Cuboid azopolymer sample

An azopolymer square post irradiated with linearly and circularly polarized light experiences mechanical deformation in the polarization and propagation direction, respectively, see Figure 5.1. Here, we simulate the deformations in a square post for both polarizations using the ANSYS software. The height of the post is taken the same as its length. Because of symmetry, it is enough to consider only the 1/8 of the original post, the 3D view of which is shown in Figure 5.7 (a). Symmetric boundary conditions are used here, which restrict the three connected faces of the cube sample to displace in the direction normal to the surface. The edge length of cubical sample in ANSYS is 10 μm. The parameters used in ANSYS modeling are Poisson's ratio= 0.49, yield stress τ_{yield} = 10 MPa, tangent modulus = 10^3 Pa, $\gamma = 0.1$ s^{-1}. The mesh size and the time step size are calibrated below.

Calibration

We compare the analytically calculated plastic strain with the plastic strain obtained in ANSYS for the square post under homogeneous intensity distribution. The time dependent plastic strains are presented in Figure 5.8 (a) for different time step sizes at the same mesh size, i.e. 0.5 μm. Very good fits with the analytical result are achieved for the time steps less than or equal to 0.1 μm. This step is valid for the whole range of applied stresses. Further, the mesh size is calibrated for the highest applied initial equivalent stress of 50 MPa and it can be seen from Figure 5.8 (b) that for the mesh sizes smaller than or equal to 1 μm, the plastic strains from ANSYS coincide with the analytical result. Therefore, the mesh size can be taken ≤ 1 and the time step size can be taken $\leq 0.1\Delta t$ for all the calculations in ANSYS.

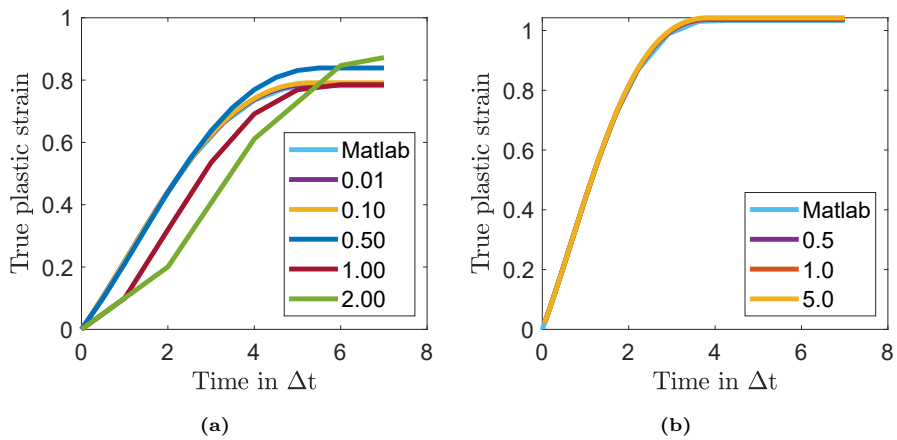

Figure 5.8: Plastic strain with respect to time a) for $\tau_{eq} = 30$ MPa with different time step sizes at 0.5 μm mesh size, b) for $\tau_{eq} = 50$ MPa with different mesh sizes at the time step $0.1\Delta t$.

5.2.1 Effect of linearly polarized light

The positive value of plastic strain means that the sample elongates along the light polarization. The magnitude of elongation can be calculated as:

$$l/l_0 = \exp(\epsilon) \approx \exp(\epsilon_{pl}) \tag{5.4}$$

Here, l_0 and l are the edge length of the square post in the absence and presence of illumination. As we discussed in Chapter 4, the elastic strain is considerably smaller than the accumulated plastic strain and can be neglected.
Figures 5.1 (b, c) and 5.9 show the end state of a plastically deformed post under linearly polarized light in the experiment and when simulated with ANSYS, respectively. The post is elongated more than twice of its original length along the light polarization till the moment $t_{stop} \approx 5\Delta t$ at $\tau_{eq} = 30$ MPa. The magnitude of elongation is comparable with that observed for the vertical and horizontal polarizations in the experiment, see Figure 5.1 (b, c).

5.2.2 Effect of circularly polarized light

Under circularly polarized light it was observed that there is no plastic deformation if the initial equivalent stress is less than or equal to $\tau_{yield} = 10$ MPa, see Figure 5.4. Above the yield stress, the plastic strain with negative values develops. This means that the sample contracts along the light propagation direction and expands in the plane perpendicular to it. The magnitude of expansion can be calculated as:

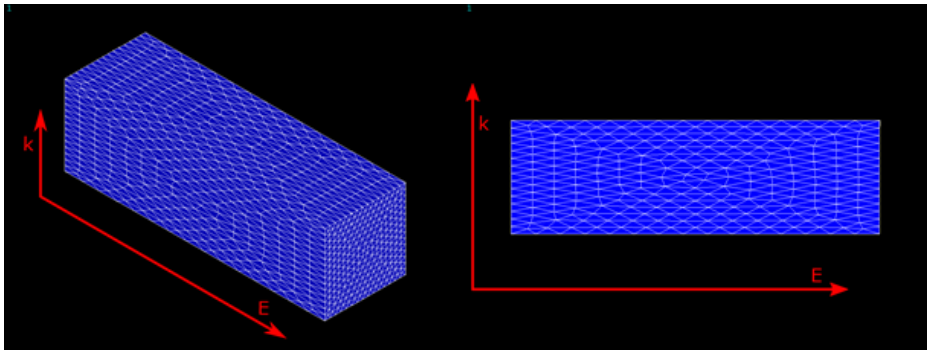

(a) **(b)**

Figure 5.9: Stationary deformation of 1/8 of the square post in the presence of linearly polarized light: (a) 3D view and (b) the top view shows the elongation along the light polarization $l/l_0 = 2.19$, $\tau_{eq} = 30$ MPa.

$$l/l_0 = \exp(\epsilon/2) \approx \exp(\epsilon_{pl}/2) \tag{5.5}$$

The end state of plastically deformed post is shown in Figure 5.10 for circularly polarized light. The theoretical prediction agrees with the experimental results by Lee et al. [37], as shown in Figure 5.1 (d) .

Conclusions

Comparing the deformed posts in Figures 5.1, 5.9 and 5.10, it can be concluded that the photo-induced deformations under linearly and circularly polarized light can be well explained using the proposed orientation approach. In accordance with the experiment, under linearly polarized light, the cube elongates in the direction of light polarization by forming a cuboid. On the other side, under circularly polarized light the post contracts in the direction of light propagation and expands in the polarization plane. The cross-section of simulated post maintains its square form under light irradiation, while the cross-section of real post transforms from a square to a circular form. Although the square has rounded edges, it should deform keeping its original form in the absence of surface tension. To understand the appearance of circular cross-section, it is important to note that the light intensity employed in the experimental study was rather high: $0.6W/cm^2$. This is much higher than the estimate of $0.1W/cm^2$, after which the photothermal effect starts to play an essential role [106]. Therefore, we expect that the temperature of the post irradiated with the circularly polarized light gradually increases with the exposure time. In the beginning of irradiation, the glassy azopolymer post deforms accordingly to the light-induced stresses caused by the reorientation of polymer backbones. However, at longer

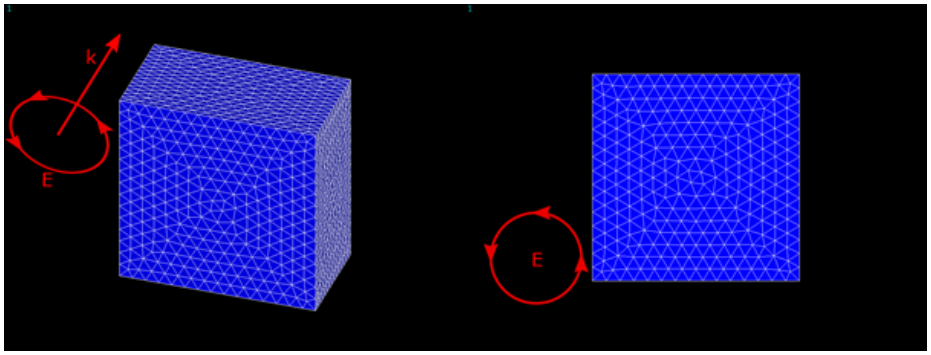

(a) **(b)**

Figure 5.10: Stationary deformation of 1/8 of the square post in the presence of circularly polarized light: (a) 3D view and (b) the top view shows the expansion perpendicular to the light propagation direction $l/l_0 = 1.23$, $\tau_{eq} = 50$ MPa.

exposure times, the post becomes heated above the glass transition temperature, where it starts to soften considerably and the surface tension forces come into play. This would explain why the cross-section attains a circular form after 5 min irradiation with the intensity of $0.6W/cm^2$. A similar softening effect of individual azopolymer pillars under a long laser exposure has been reported in Ref. [107]. Why the posts irradiated with the vertically and horizontally polarized light show the softening effects only at the short edges can be possibly explained by the following consideration. At the same light intensity, both the light-induced stress and the plastic strain are twice larger for the linear polarization than for the circular polarization. Hence, the conversion of light power into the mechanical power $P = \boldsymbol{\tau} \cdot \epsilon_{pl}$ should be approximately four times less effective for the circular polarization. As a result, much more energy is converted into heat and this could lead to pronounced softening observed for the irradiation with circularly polarized light. No softening effect has been observed for the same azopolymer irradiated with $10mW/cm^2$ [108].
In the next chapter, we focus on modeling the deformations under spatially dependent intensity interference patterns. For that, we use the ANSYS model which has been calibrated in the current chapter.

Chapter 6

Stripe patterns under Gaussian distributed light intensity

In this chapter, using the orientation approach, we give the theoretical interpretation of the experiment done by Ambrosio et al. [51]. This experiment shows that the surface deformations differ depending on the direction of movement of the laser beam with respect to the polarization direction, see Figure 6.1. When the laser beam is moved along the polarization direction, the formation of protrusions was observed. In the case when the laser beam is moved perpendicular to the polarization direction, the formation of grooves was observed.
The laser beam represents a light source with Gaussian distributed intensity. As we have discussed in the last chapters, the light-induced stress field is directly proportional to the light intensity and can be calculated using the orientation approach [101]. Implementing the Gaussian distributed stress field, the plastic deformations can be obtained using the ANSYS software and compared with the experimental results. Additionally, the effect of beam focusing on the strength of deformations is checked.[1]

6.1 Strongly focused beam

The laser beam has Gaussian distributed intensity which is maximum at the center of the beam and rapidly decreases away from the center:

$$I(x,y) = I_0 \exp\Big(-2\frac{(x-a)^2 + (y-b)^2}{w^2}\Big) \tag{6.1}$$

[1] The results presented in this chapter are published in Yadav et al. [103].

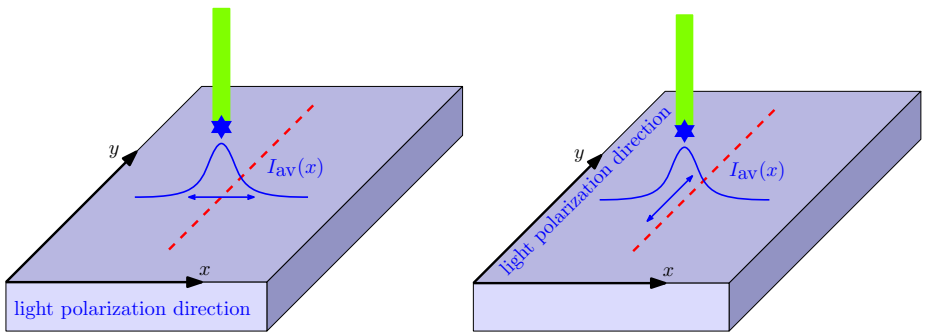

Figure 6.1: The laser beam is represented by the green stick moved in the y-direction (shown by the dotted red line). The formation of a) a groove and b) a protrusion is observed in the thin polymer films for light polarized in the x and y direction, respectively [109, 103].

Here, I_0 is the intensity at the beam center ($x = a$, $y = b$) and w is the beam radius at which the intensity falls to the $1/e^2$ of its maximal value I_0.
The total intensity for a particular laser beam is considered as constant, irrespective how strongly is the beam focused. The strength of beam focusing depends on the beam radius: the laser beam is more focused when the beam radius is smaller.

6.2 Light-induced stress field

The magnitude of effective potential depends on the light intensity, see Equation (2.39) from Chapter 2. Therefore, for Gaussian distributed light beam the magnitude of effective potential has spatial dependence which comes from the light intensity. With this effective potential, the corresponding light-induced stress tensor can be calculated using Equation (3.4).
In the experiment of Ambrosio et al. [51], the direction of light polarization was kept constant but the film was moved in different directions. In one case parallelly and in another case perpendicularly to the polarization direction. This is equivalent to moving the beam with different polarizations in the same direction, here along the y axis, as shown in Figures 6.1 (a) and 6.1 (b). With such an assignment, the stress tensor can be written in a simplified diagonal form which appears due to the axial symmetry of the system with respect to the polarization vector $\hat{\mathbf{E}}$ [56, 101].

For light polarized along x axis

The electric field vector $\hat{\mathbf{E}} = (1,0,0)$, its dyadic product and the corresponding stress tensor have the following form:

$$\hat{\mathbf{E}}\hat{\mathbf{E}} = \begin{bmatrix} 1 & 0 & 0 \\ 0 & 0 & 0 \\ 0 & 0 & 0 \end{bmatrix} \qquad \text{and} \qquad \boldsymbol{\tau} = \tau(x) \begin{bmatrix} 1 & 0 & 0 \\ 0 & -\frac{1}{2} & 0 \\ 0 & 0 & -\frac{1}{2} \end{bmatrix} \tag{6.2}$$

Here, $\tau(x)$ is the spatially dependent magnitude of the stress tensor.

For light polarized along y axis

The electric field vector $\hat{\mathbf{E}}$ (0,1,0), its dyadic product and the corresponding stress tensor are as follows:

$$\hat{\mathbf{E}}\hat{\mathbf{E}} = \begin{bmatrix} 0 & 0 & 0 \\ 0 & 1 & 0 \\ 0 & 0 & 0 \end{bmatrix} \qquad \text{and} \qquad \boldsymbol{\tau} = \tau(x) \begin{bmatrix} -\frac{1}{2} & 0 & 0 \\ 0 & 1 & 0 \\ 0 & 0 & -\frac{1}{2} \end{bmatrix} \tag{6.3}$$

For a fast movement in the y-direction, the intensity can be averaged over all possible y inside the laser spot which results in the following expression:

$$I_{av}(x) = CI_0 \exp\Big(-\frac{2(x-a)^2}{w^2}\Big) \tag{6.4}$$

Here, $C = \sqrt{\pi/2}\mathrm{erf}(\sqrt{2})/2 \approx 0.60$.

As explained in Chapter 3, the light-induced stress depends on various optical and material parameters, the intensity of light being one of them. Hence, the magnitude of the stress tensor in Equations (6.2) and (6.3), $\tau(x) \sim I_{av}$, will have the same x dependence as the average intensity of the beam:

$$\tau(x) = \tau_0 \exp\Big(-\frac{2(x-a)^2}{w^2}\Big) \tag{6.5}$$

Here, τ_0 is the magnitude of the stress tensor at the stripe center ($x = a$).
When the glassy azopolymer sample is put under light illumination for a longer time (in order of minutes), the stress tensor decays gradually with time due to a slow reorientation of backbone segments, as shown in Figure 5.2 from Chapter 5. However, for the case when the thin azopolymer films are moved very fast under the Gaussian beam, the exposure time for one spot on film is very short (in order of seconds). In particular, the inscription time for a 26μm long stripe was about 2 min 22 s [110]. Therefore, the deformations of a fast moving thin film are mostly caused by the light-induced stress generated at the very beginning of illumination. With this, we can assume that τ_0 is constant in time for the fast moving laser beam.

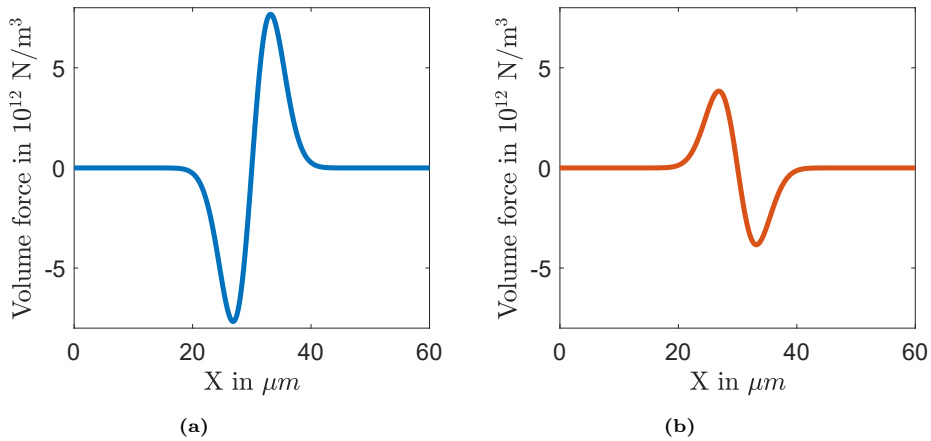

Figure 6.2: The x component of the volume force: (a) stretching for light polarized in x direction and (b) compressive for light polarized in y direction. $\tau_0 = 40$ MPa. The beam radius $w = 2\sqrt{10}\ \mu m$.

Volume Force and Traction

Using the orientation approach, we are able to predict the light-induced stress field in the azopolymer sample. However, in mechanical applications it is not possible to apply the forces to a solid body in the form of the stress tensor directly. They can be either applied to the interior of the body in the form of so called volume forces or to the surface of the body as surface traction [111]. Let us first consider the volume force formalism, as it easily explains why x and y polarized light beams induce different deformations. The external force per unit volume can be calculated from the stress tensor as:

$$\boldsymbol{f} = -\nabla \cdot \boldsymbol{\tau} \tag{6.6}$$

The k component is as follows:

$$f_k = -\sum_i \frac{d\tau_{ik}}{dx_i} \tag{6.7}$$

The stress components in the both cases have only x dependence, see Equations (6.2), (6.3) and (6.5). For the both polarization only the x component of the volume force has a non-zero value.
For the light polarized in x direction, the x component of the volume force can be written as:

$$f_{\mathrm{x}} = -\frac{d\tau}{dx} = 4\tau_0 \frac{x-a}{w^2} \exp\Big(-\frac{2(x-a)^2}{w^2}\Big) \tag{6.8}$$

For the light polarized in y direction, the x component of the volume force can be written as:

$$f_{\mathrm{x}} = \frac{1}{2}\frac{d\tau}{dx} = -2\tau_0 \frac{x-a}{w^2} \exp\Big(-\frac{2(x-a)^2}{w^2}\Big) \tag{6.9}$$

The magnitude of volume force for light polarized in x direction is twice the magnitude of the volume force for light polarized in y direction. Hence, we can expect that the magnitude of deformations caused by the light polarized in x direction will be larger than the deformations caused by the light polarized in y direction. The opposite sign of the volume force in Equations (6.8) and (6.9) predicts that the deformations will be in opposite direction for two different polarization. As can be seen from Figure 6.2 (a), x polarized light produces the stretching force, as it is positive at $x > a = 30$ μm and negative at $x < a$. Contrary, y polarized light results in the compressive force along the x direction, see Figure 6.2 (b).
Interestingly, the formalism of volume force predicts that no effect should be observed for the light polarized at a particular angle to the moving direction y. This angle can be found by considering the light-induced stress tensor in the principle axes and then rotating it into the laboratory coordinate system. The volume force for an arbitrary angle φ between the light polarization and the x axis is:

$$f_{\mathrm{x}} = -\frac{1}{2}\frac{d\tau}{dx}\Big(3\cos^2\varphi - 1\Big) \tag{6.10}$$

Hence, the force becomes equal to zero at $\varphi = 54.7°$, i.e. at 35.3° to the moving direction.

6.3 Modeling conditions

ANSYS modeling

As we discussed in Chapters 4 and 5, we use the Perzyna option in ANSYS, represented by Equation (4.5), to calculate the light-induced plastic deformations. All material properties are same as used in Chapter 5 for modeling the directional photodeformations under homogeneous light intensity.
At first we put a cubic sample, which has the edge of 30μm, under Gaussian distributed light beam. The cube is finely meshed in ANSYS with the mesh size of 0.1μm, which is in the calibrated range determined in Chapter 5. The most important part of modeling in ANSYS is setting up adequate boundary conditions as they define the final stress field. The following boundary conditions are chosen:

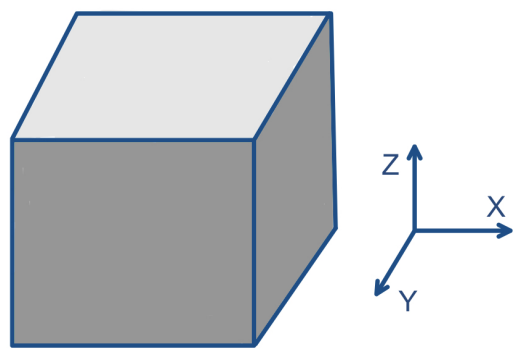

Figure 6.3: The surface represented with the light gray colour is free to move in all three directions and the all four side surfaces represented with dark grey color are restricted to move in the normal direction.

- The bottom face of the sample is restricted from moving in all three directions similar to the experiments, where the azopolymer sample is "glued" to the substrate surface due to a strong adhesion [37, 52].
- The upper surface is free to move in all three directions.
- All other sides are restricted from moving in the normal direction, see Figure 6.3.

Application of stress field

It can be proved that the stretching volume force (6.8) applied to the elastic solid at previously mentioned boundary conditions induces the same deformation field as the traction force acting normally on the upper sample surface in negative direction (inwardly):

$$t_z(x) = -\tau_{max} \exp(-\frac{2(x-a)^2}{w^2}) \tag{6.11}$$

with $\tau_{max} = \tau_0$. Similarly, the contractive volume force (6.9) is equivalent to the traction force acting in positive direction (outwardly):

$$t_z(x) = \tau_{max} \exp(-\frac{2(x-a)^2}{w^2}) \tag{6.12}$$

with $\tau_{max} = \tau_0/2$.
In both cases, to test the strength of the effect, we apply different maximal traction τ_{max} at the stripe center, ranging from 40 MPa to 80 MPa. Figure 6.5 presents exemplary how the azopolymer surface will deform after 5 s in the

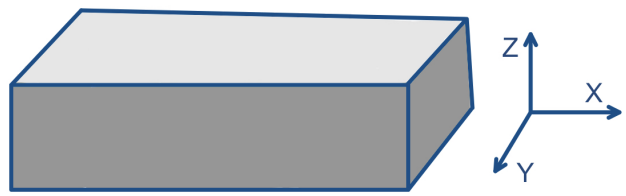

Figure 6.4: The top surface represented with the light gray colour is free to move in all three directions and the all four side surfaces represented with dark grey color are restricted to move in the normal direction.

presence of light polarized in the x direction at $\tau_{max} = 50$ MPa and the beam radius $w = 2\sqrt{10}$ μm. In accordance with the experiment of Ambrosio et al. [51], the deformed surface looks like a stripe-like well with uplifted ends. Figure 6.9 shows an example of the deformed surface in the presence of light polarized in the y direction at the same conditions. Again, in accordance with the experiment, a stripe-like protrusion can be observed. Comparing modeling results with the depth 0.2 μm and the height of stripes 0.05 μm inscribed experimentally [51], it is found that traction forces with τ_{max} above 50 MPa considerably overpredict the strength of the effect. The surface deformations are far above 10 μm and do not disappear at the sample boundaries in the x-direction.
Therefore, in an attempt to reproduce the experiment of Ambrosio et al. [51] not only qualitatively but also quantitatively, we chose another sample ($0 \leq x \leq 60\mu$ m, $0 \leq y \leq 15\mu$m, $0 \leq z \leq 15\mu$m), which is twice as long in the x-direction and twice as short in two other directions. The latter adjustment is made to keep the computational effort in reasonable limits. The boundary conditions are the same as for the first sample, see Figure 6.4.

6.4 Modeling results

The stress tensor corresponding to light polarized in x and y direction is represented by Equations (6.2) and (6.3). The traction force is applied to the sample ($0 \leq x \leq 60\mu$ m, $0 \leq y \leq 15\mu$m, $0 \leq z \leq 15\mu$m) using Equation (6.11) and (6.12) for light polarized in x and y direction, respectively. The applied traction force is maximum at the centre of the beam. Next, we discuss the modeling results corresponding to both polarizations.

Light polarized in x direction

In this case, the formation of grooves is observed at the centre of the illuminated sample $x = 30$ μm due to pushing the material away from the center. The material which is pushed away builds in small hills at the both sides of the groove. To check the effect of the intensity of light, the traction forces corresponding to different light-induced stresses are applied. The maximal stress τ_{max} rang-

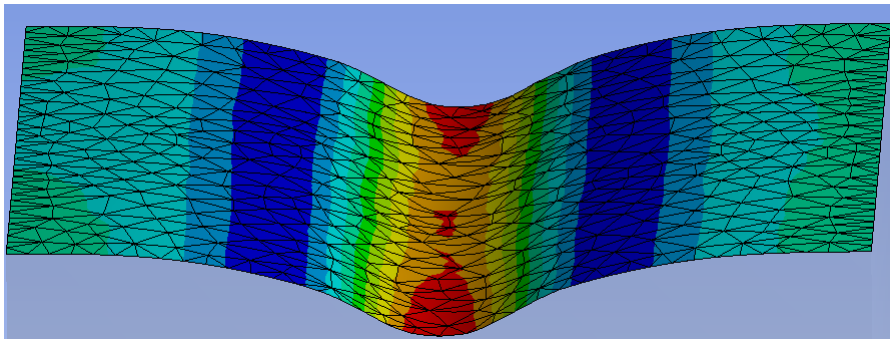

Figure 6.5: The deformations for the upper surface of the material in the presence of x polarized light. $\tau_{max} = 50$ MPa. The film dimensions are $0 \leq x \leq 60$ μm, $0 \leq y \leq 15$ μm, $0 \leq z \leq 15$ μm and the beam radius $w = 2\sqrt{10}$ μm.

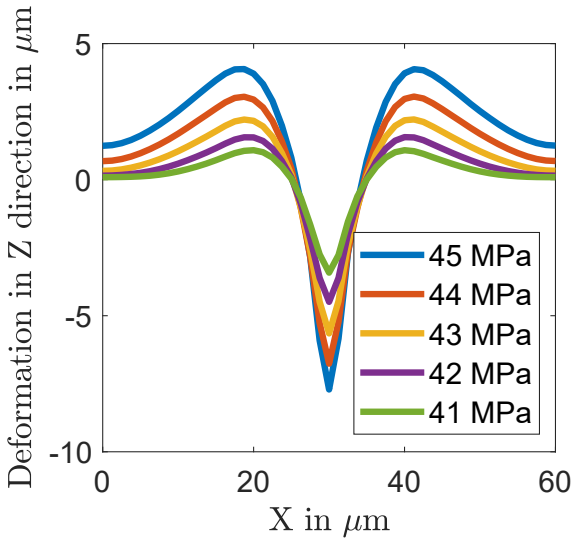

Figure 6.6: The deformations in z direction for light polarized in x direction.The film dimensions are $0 \leq x \leq 60$ μm, $0 \leq y \leq 15$ μm, $0 \leq z \leq 15$ μm and the beam radius $w = 2\sqrt{10}$ μm.

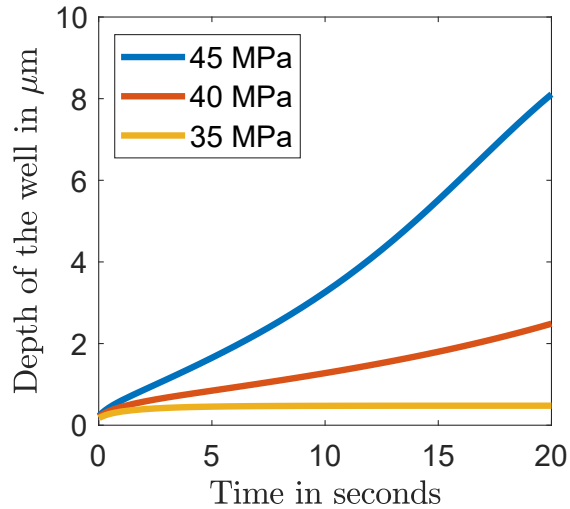

Figure 6.7: Time-dependent deformations in z direction for light polarized in the x direction. Value of the maximum traction τ_{max} is shown in the legend. The film dimensions are $0 \leq x \leq 60$ μm, $0 \leq y \leq 15$ μm, $0 \leq z \leq 15$ μm and the beam radius $w = 2\sqrt{10}$ μm.

ing from 41 MPa to 45 MPa gives an effect comparable to the experimental observations [51]. The depth of the grooves increases with magnitude of the maximal stress, see Figure 6.6. Also, it is observed that the depth of the well for a particular light-induced stress increases with the time, see Figure 6.7.

To study the effect of beam focusing on the deformations, we select the beams with different radii w but having the same total intensity I_{tot}, obtained by integration of I_{av} in Equation (6.4):

$$I_{tot} = \int C I_0 \exp\Big(- \frac{2(x-a)^2}{w^2} \Big) dx = \frac{1}{2} \pi I_0 w^2 \tag{6.13}$$

It can be seen that the total intensity I_{tot} is directly proportional to the square of beam radius w^2. Usually, the source of laser light has a constant total intensity (power) I_{tot}. For example, in the experiment of Ambrosio et al. [51], the power of the laser used is 12 μW. Focusing a beam to the spots with decreasing radius can lead to increase of the intensity at the center of beam by orders of magnitude.

Figure 6.8 illustrates a possibility to manipulate the strength of the effect by changing the radius w of the light polarized in the x direction. The maximal traction (at $x = 30$ μm) is equal to 40 MPa at $w = 2\sqrt{10}$ μm and it is adjusted for other beam radii in such a way that the total intensity transmitted by the Gaussian beam stayed constant. It can be seen from Figure 6.8 that the depth of the groove and height of accompanying protrusions are very sensitive to the small adjustments in the size of the laser spot. In particular, weaker focusing

results in a quick disappearance of the surface modulation, which can be explained by the drop of light-induced stress below the yield stress in the most part of the illuminated area.

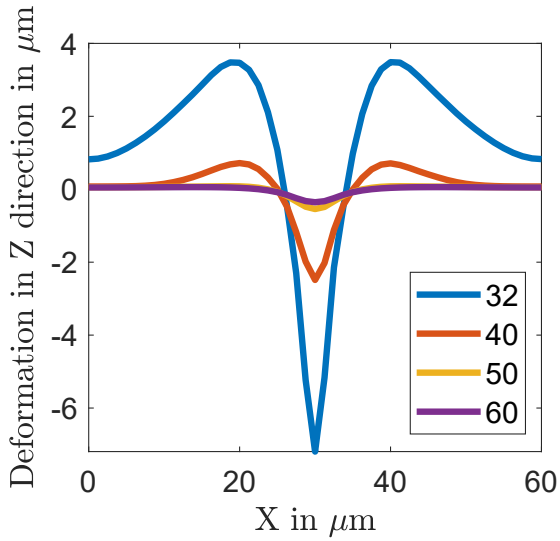

Figure 6.8: The deformations in z direction for the light polarized in x direction at different values of squared beam radius w^2, shown in the legend. The film dimensions are $0 \leq x \leq 60$ μm, $0 \leq y \leq 15$ μm, $0 \leq z \leq 15$ μm.

Light polarized in y direction

The volume force for the light polarized in the y direction is half of the volume force appearing under the light polarized in the x direction, compare Equations (6.8) and (6.9). Thus, we apply twice smaller maximal stresses τ_{max}, when the beam is moved in the direction perpendicular to the light polarization. In this case, formation of the protrusions is observed at the center of the illuminated area $x = 30$ μm. At the both sides to the protrusions, shallow grooves are formed. The deformed upper surface of the sample is represented in Figure 6.9. The height of the protrusion increases with the magnitude of light-induced stress, see Figure 6.10. Additionally, we study the evolution of the protrusion height with time for a beam radius $w = 2\sqrt{10}$ μm, see Figure 6.8. The height of protrusions slightly increases with time and it reaches saturation at longer times.

Conclusions

We can conclude that the formation of protrusions and grooves caused by the laser moving parallelly and perpendicularly to the polarization direction is well

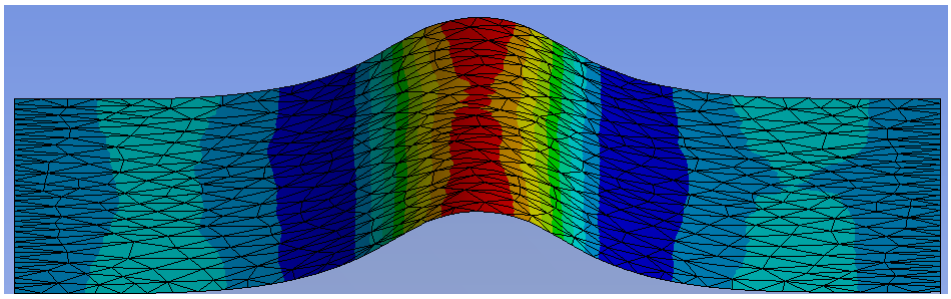

Figure 6.9: The deformations for the upper surface of the material in the presence of y polarized light. $\tau_{max} = 50$ MPa. The film dimensions are $0 \leq x \leq 60$ μm, $0 \leq y \leq 15$ μm, $0 \leq z \leq 15$ μm and the beam radius $w = 2\sqrt{10}$ μm.

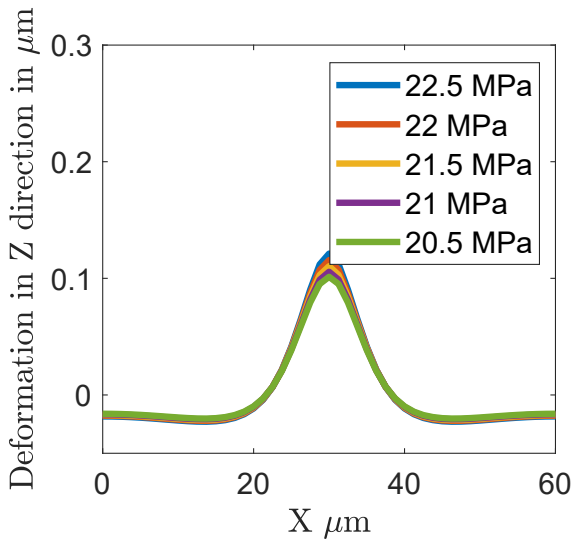

Figure 6.10: The deformations in z direction for light polarized in y direction.The film dimensions are $0 \leq x \leq 60$ μm, $0 \leq y \leq 15$ μm, $0 \leq z \leq 15$ μm and the beam radius $w = 2\sqrt{10}$ μm.

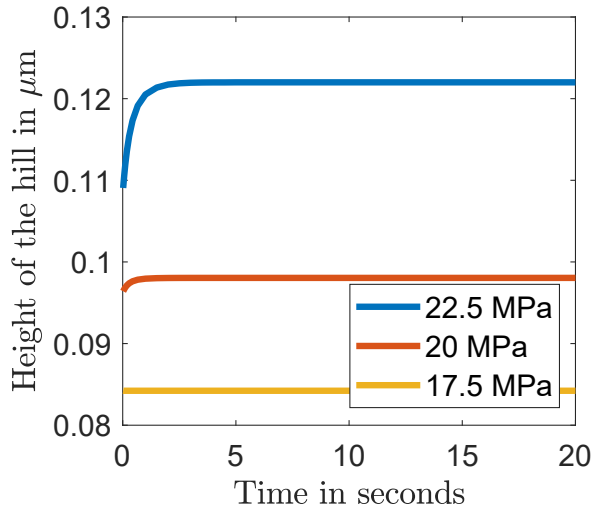

Figure 6.11: Time-dependent deformations in z direction for light polarized in the y direction. Value of the maximum traction τ_{max} is shown in the legend. The film dimensions are $0 \leq x \leq 60$ μm, $0 \leq y \leq 15$ μm, $0 \leq z \leq 15$ μm and the beam radius $w = 2\sqrt{10}$ μm.

explained using the proposed orientation approach. Additionally, it can be understood, why the magnitude of deformations, when the laser is moved in the polarization direction, is much smaller than the magnitude of deformations, when it is moved perpendicularly to the polarization direction. This is because the traction force produced in the first case is only half of the traction force produced in the second case.
For larger traction forces the difference between light-induced stress and the yield stress is higher, which corresponds to profound plastic deformations for the larger area on the illuminated film, see Equation (4.5) and Figure 6.12.

In the next chapter, we focus on modeling the inscription of surface relief gratings under spatially dependent light interference patterns. The samples are illuminated by a particular pattern till saturation of plastic deformations. Thus, the light-induced stress has time dependence and an external subroutine will be used to implement it.

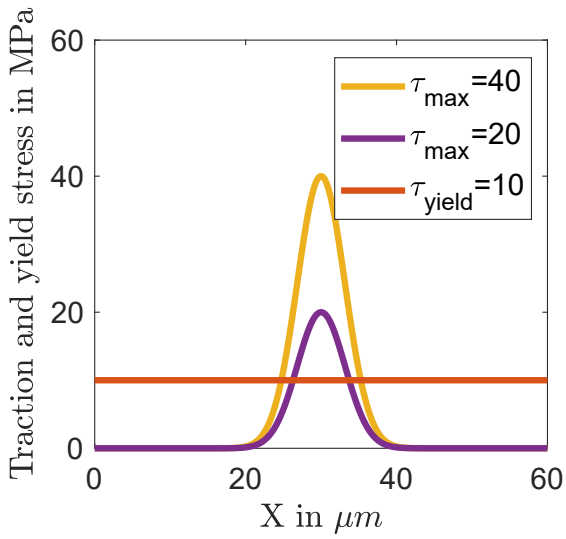

Figure 6.12: The film area in which the stresses exceed the yield stress rapidly shrinks with decrease of $\boldsymbol{\tau}_{max}$. This example is calculated for the beam radius $w = 2\sqrt{10}\mu$m [103].

Chapter 7

Complex photodeformations under intensity interference patterns

This chapter is dedicated to the complex structuring of azopolymer samples under intensity interference patterns. Since the discovery of surface relief gratings made by Tripathy et al. [41] and Natansohn et al. [40], there is no convincing theoretical explanation for the formation of these gratings, as we discussed in Chapter 2. In this chapter, we will prove that the orientation approach can give appropriate explanation for the photodeformations in azopolymers under light interference patterns. In particular, we will explain the following phenomena observed in the group of Santer et al. [52, 102]:

- Directional deformation of azopolymeric spherical colloid under linearly polarized light, as shown in Figure 7,
- Formation of a necklace structure with beads and of a wave-like structure when elongated colloid is irradiated with PP and SS interference patterns, see Figure 7.2,
- Restructuring of the gap edges in a scratched azopolymer film during irradiation with the RL and LR polarization patterns, see Figure 7.3.

In Chapter 6, we have described and explained the photodeformations under moving laser beam that has spatially varying intensity. In this current chapter, we reproduce the experiments in which the sample is irradiated for long time. Thus, the light-induced stress for such cases must have not only the spatial but also the time dependence, as it is discussed in Chapter 3. Next, we focus on the viscoplastic finite element modeling of the three phenomena mentioned above.[1]

[1] The results presented in this chapter are published in Loebner and Yadav et al. [102]

Figure 7.1: AFM micrograph of the initial and elongated colloid in the presence of linearly polarized light. The light-induced elongation ratios is about 5. Modified and reproduced from Ref. [52].

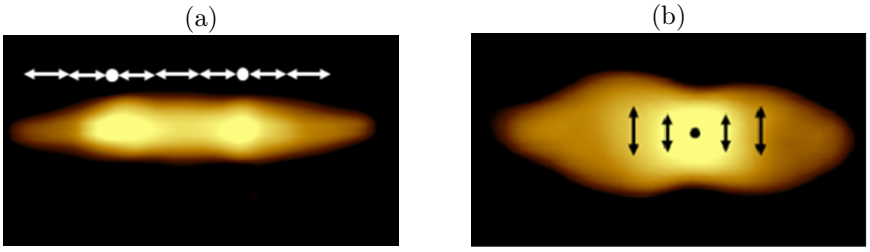

Figure 7.2: AFM micrograph of the SRG inscribed in colloidal particles using a) PP interference pattern and b) SS interference pattern. The arrows show the polarization direction and their length is related to the light intensity. Modified and reproduced from Ref. [102].

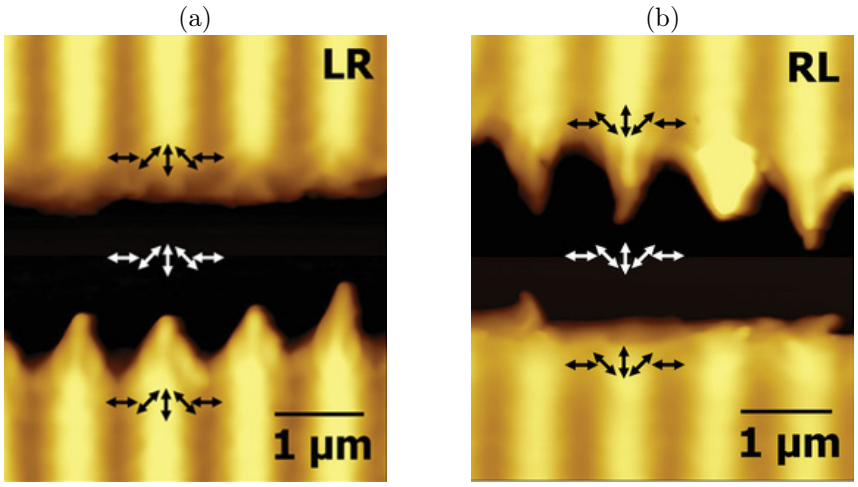

Figure 7.3: AFM micrographs of the gap edges structured during irradiation with (a) RL and (b) LR polarization pattern. White and black arrows show the distribution of the electrical field vectors. Modified and reproduced from Ref. [102].

7.1 Formation of ellipsoidal colloid and effect of spatially varying light intensity

This section of the thesis is based on the experiments performed at the chair of Prof. Santer, University of Potsdam. In particular, the photodeformations in the spherical colloid consisting of azobenzene containing polymer (PMMA-co-DRIA) are studied. The diameter of azopolymer colloid used in the experiment is between 0.1-1 μm. Firstly, the colloid is put under linearly polarized light. It deforms in the direction of the light polarization by forming an elongated spheroid, see Figure 7.1. For large colloids the elongation ratios can be as high as 5. The opto-mechanical stress needed for such large deformations is estimated to be of the order of 100 MPa [52].
Secondly, the same elongated colloid is irradiated with SS and PP interference patterns. Formation of necklace structure and of wave-like structure is observed on the elongated spheroid, as shown in Figure 7.2, when irradiated with PP and SS interference pattern, respectively. In the experiment, it is observed that the behaviour of the colloid under these interference patterns is different: the movement of the material is in the opposite direction for a particular point in the sample. For the SS polarized light there is a hill formation at the maximum intensity and a well formation at the minimum intensity, while in the case of PP irradiation a well forms at the maximum intensity and a hill forms at the minimum intensity, as seen in Figure 7.2.
We start our modeling with initial spherical colloid of 1μm diameter under linearly polarized light. For this purpose, the orientation approach is used to predict the light-induced stress in the spherical colloid.

7.1.1 Spherical azopolymer colloid in the presence of linearly polarized light

We assume that the electric field vector of linearly polarized light is in the x-direction. As shown in Chapter 5, the light-induced stress arising due to reorientation of polymer backbones can be written as follows:

$$\tau = \tau_{xx} \begin{bmatrix} 1 & 0 & 0 \\ 0 & -\frac{1}{2} & 0 \\ 0 & 0 & -\frac{1}{2} \end{bmatrix} \tag{7.1}$$

Here, τ_{xx} is the maximal normal stress acting in the x direction. We remind that τ_{xx} can be calculated with the help of Geisekus equation (3.19):

$$\tau_{xx} = 3nkT \frac{\partial}{\partial t_\lambda} \langle u_x^2 \rangle \tag{7.2}$$

where the derivation of time dependent $\langle u_x^2 \rangle$ is described in Chapter 3.
To calculate the directional deformations corresponding to the light-induced stress, we use the finite element software ANSYS. The direct implementation

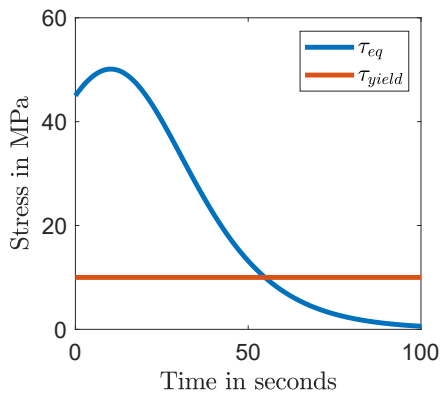

(a) **(b)**

Figure 7.4: a) Time evolution of equivalent stress corresponding to $\tau_{xx,0} = 30$ MPa. b) Dependence of stopping time on the initial applied stress.

of the spatially and time-dependent stresses is not trivial in ANSYS. Thus, the stresses are applied with the help of Userthstrain subroutine, described in detail in section 4.2. The modeling parameters corresponding to the ANSYS calculations are given below.

Modeling parameters

The glassy azopolymer (PMMA-co-DRIA) is characterized by the same material model used previously in Chapters 5 and 6 [101, 103]: the Young's modulus of 1 GPa, Poisson ratio of 0.49 (quasi incompressible material) and the yield stress of 10 MPa. To reduce the computational time, we choose $\gamma = 0.01s^{-1}$ and $\lambda = 1000s$, which provides $C_\eta = 0.33$ MPa, quite close to the previous estimate $C_\eta = 0.68$ MPa for the homogeneous irradiation, see Section 3.2. The reduced potential strength V_r defines the magnitude of light-induced stress $\tau_{xx,0}$ in the beginning of the irradiation:

$$\tau_{xx,0} = -\frac{2}{3} nkTV_r \tag{7.3}$$

The strength of the effective orientation potential depends on a number of material and optical parameters, see Equation (2.39). Hence, there is no straightforward way to predict V_r from the light intensity used in this experiment, instead different stress are probed in the modeling to achieve similar elongation of a colloid. We applied $\tau_{xx,0} = 15, 20, 25$ and 30 MPa which corresponds to $V_r = -21.7, -28.9, -36.2, -43.4$. Here, we remind that the light-induced stress slightly increases in the beginning of illumination and then gradually diminishes to 0, as shown in Figure 7.4 (a). The plastic deformations develop only when

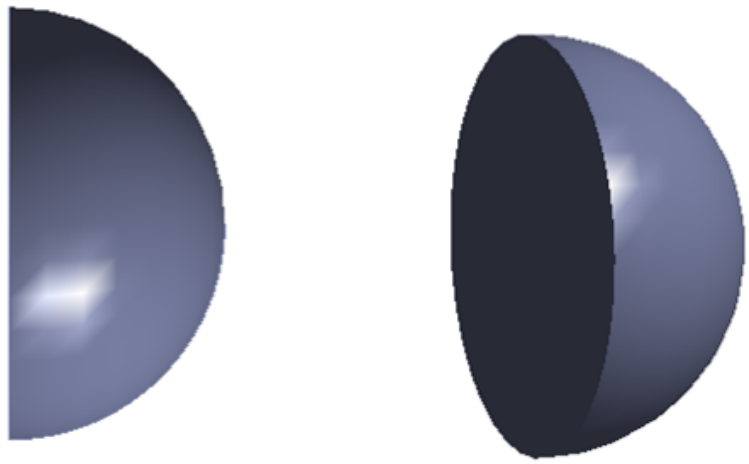

(a) **(b)**

Figure 7.5: Initial half of the sphere with diameter 1μm: (a) top view (b) 3D view.

the light-induced stress is greater than the yield stress. The time, at which the light-induced stress decreases to the yield stress and the plastic deformations saturate, is defined as the stopping time t_{stop}. As shown in Figure 7.4, the stopping time is not a monotonic function of $\tau_{xx,0}$. At smaller τ_{xx}, the stopping time t_{stop} rapidly increases to its maximum value and then slowly decreases at larger $\tau_{xx,0}$. Because the stopping time is different for different $\tau_{xx,0}$, we choose to simulate for a fixed time which is 50 seconds. The simulation time is somewhat smaller than the stopping time for all applied stresses. Thus, the deformations do not reach saturation during the simulation time, which is similar to the experimental situation [52].

The initial diameter of spherical colloid is chosen to be 1μm and only a half of it is simulated to suppress translation and rotation of the sample, see Figure 7.5. The following boundary conditions are used in the ANSYS modeling:

- The curved surface is free to move in all three directions,
- The symmetry plane is restricted to move in the normal direction,
- The center of the symmetry plane is pinned by restricting it to move in all three directions.

Under homogeneous irradiation, the colloid elongates along the light polarization, see Figure 7.6 and Table 7.1. The length of the half-sphere gradually increases with time reaching 2.08 and 2.76 μm after 50 s of radiation at $\tau_{xx,0} = 25$ and 30 MPa, respectively. The radius of cross-section decreases with time but

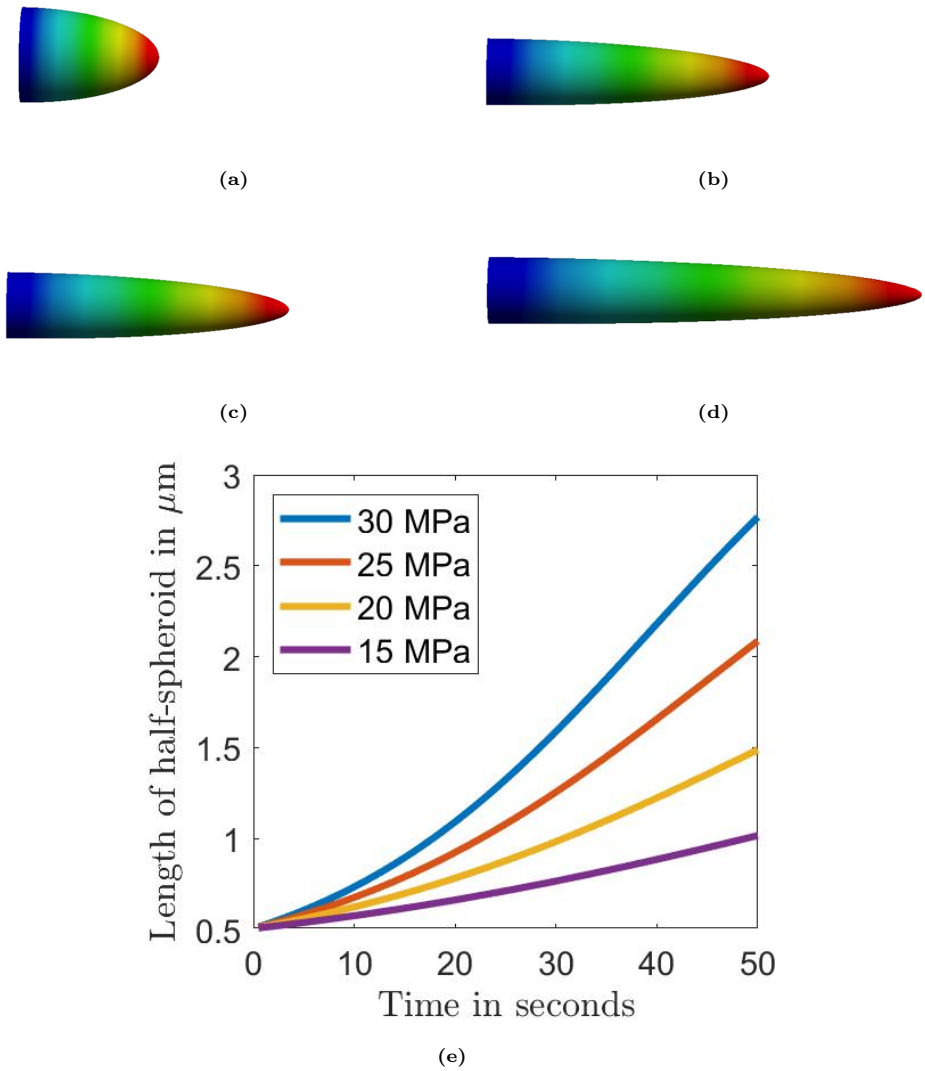

Figure 7.6: The deformed half-spheroid after 50 s of irradiation for $\tau_{xx,0}$ equal to a) 15 MPa, b) 20 MPa, c) 25 MPa and d) 30 MPa is shown here. e) The time dependence of length of the half-spheroid at different $\tau_{xx,0}$.

$\tau_{xx,0}$ (MPa)	radius (μm)	length (μm)	$\langle u_x^2 \rangle$	$\langle u_y^2 \rangle$	volume (μm^3)	S
15	0.34	1.01	0.58	0.21	0.48	0.37
20	0.28	1.48	0.66	0.17	0.48	0.49
25	0.24	2.08	0.74	0.13	0.50	0.61
30	0.21	2.76	0.80	0.10	0.50	0.70

Table 7.1: Light-induced changes in the half-spheroid corresponding to the different initial applied stresses $\tau_{xx,0}$ after 50 s of irradiation.

the volume stays unchanged.

To measure the magnitude of elongation in the direction of light polarization, the elongation ratio is calculated which is as follows:

$$e_l = l_f / l_i \tag{7.4}$$

Here, l_i and l_f are the initial and final length of the half-spheroid.
The elongation ratio for $\tau_{xx,0} = 25$ and 30 MPa is 4.2 and 5.5, which is comparable with that observed in the experiment. The polymer chains in the stretched colloid become highly oriented along the direction of light polarization at large stresses, for example $\langle u_x^2 \rangle = 0.74$ for $\tau_{xx,0} = 25$ MPa and $\langle u_x^2 \rangle = 0.80$ for $\tau_{xx,0} = 30$ MPa. The scalar order parameter $S = [3\langle u_x^2 \rangle - 1]/2$ for the nematic director along the x axis changes from 0 for isotropic initial state to 0.6 - 0.7 for highly oriented state, see Table 7.1. For smaller stresses the orientation and elongation effects are accordingly smaller.
Further, the same elongated colloid is irradiated with spatially varying intensity, as described in the next section.

7.1.2 Light-induced stress for spatially varying intensity

In accordance with the experiment [102], we applied linearly polarized light with sinusoidally varying intensity to the elongated colloids:

$$I(x) = 2I_0 \cos^2 \pi x / D \tag{7.5}$$

Here, I_0 is the total intensity of the laser and D is the optical period of grating. The factor 2 ensures that the light intensity, averaged over the grating period, is equal to the intensity I_0 of the laser. The intensity of light is maximum at $x = 0$, where it equals to $2I_0$.

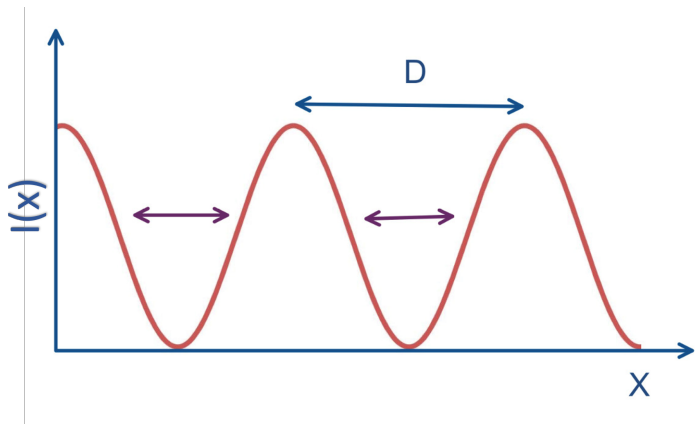

Figure 7.7: The variation of the light intensity with optical period D and light polarization direction in x direction for PP interference pattern is represented by the blue curve.

PP interference pattern

In the PP interference pattern, the light is polarized in the x direction and hence has the same polarization as the light used to irradiate the initial colloid. The initial orientation state for this case is the final orientation state which is represented in Table 7.1 for different $\tau_{xx,0}$. Due to the orientation symmetry around the x-axis (i.e. $\langle u_y^2 \rangle = \langle u_z^2 \rangle$), the induced stress field is also uniaxially symmetric (i.e. $\tau_{yy} = \tau_{zz}$). The spatially dependent intensity $I(x)$, as shown in Figure 7.7, induces spatially dependent reduced potential:

$$V_r(x) = 2V_r \cos^2 \pi x/D \tag{7.6}$$

The initial magnitude of τ_{xx} can be calculated using Equations (7.3) and (7.6) as follows:

$$\tau_{xx,0} = -\frac{4}{3} nkTV_r \cos^2 \pi x/D \tag{7.7}$$

The time evolution of τ_{xx} is calculated using Equations (3.24) and (7.2) with an initial value of $\langle u_x^2 \rangle$ which corresponds to the orientation of backbone segments at the end of the homogeneous irradiation, see Table 7.1.

ANSYS software is used to calculate the plastic deformations in the elongated azopolymer colloid. Boundary conditions, similar to those used for the initial half-sphere, are applied. The spatially distributed light-induced stresses are again applied with the help of Userthstrain subroutine, described in section 4.2. In the experiment, the irradiation time for interference patterns is 3-5 times less than for the homogeneous illumination used to elongate the initial sphere [52]. Thus, the light-induced stress is applied for 10 seconds which is 5 times shorter than the time used to elongate the half-sphere.

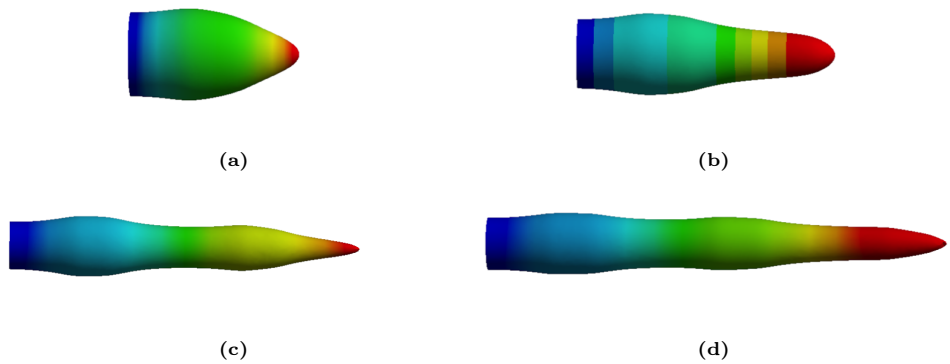

Figure 7.8: The deformed half-spheroid after 10 s of irradiation for initial $\tau_{xx,0}$ a) 15 MPa, b) 20 MPa, c) 25 MPa and d) 30 MPa is shown here.

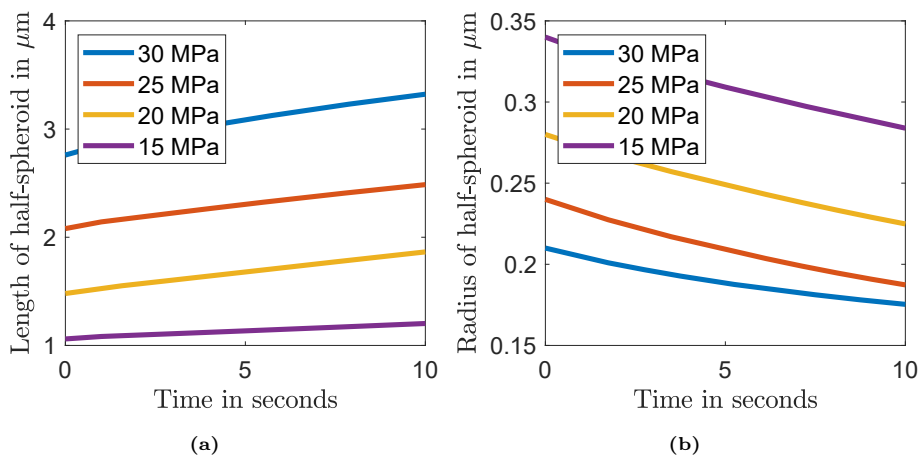

Figure 7.9: Dependence of a) length and b) radius of half-spheroid on the initial value of $\tau_{xx,0}$ under the PP interference pattern.

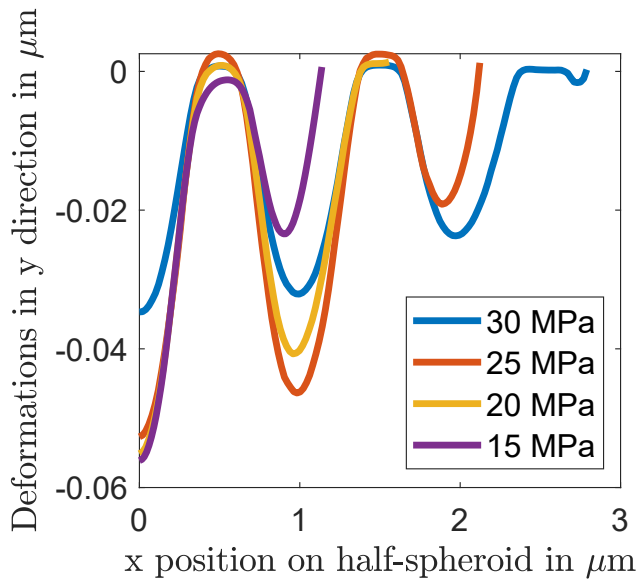

Figure 7.10: The final deformations in y direction at different $\tau_{xx,0}$ under the PP interference pattern.

Under the PP interference pattern, the elongated colloid develops a modulated cross-section, which is symmetric around x-axis, see Figure 7.8 (a) - (d). Formation of a well at the maximum intensity and a hill at the minimum intensity of the light interference pattern can be observed, as shown in Figure 7.8 (a) - (d). At the sample positions with larger light intensities, the difference between light-induced stress and the yield stress is higher, which explains more profound plastic deformations. As the light is polarized in the x direction, it induces further elongation of the colloid along this direction. Therefore, the length of the half-spheroid increases slightly with the time, see Figure 7.9 (a). Additionally, the radius of cross-section at $x = 0$ is decreased with the time for all applied stresses, see Figure 7.9 (b). In the experiment, this further stretching in the polarization direction is hindered due to the strong adhesion to the substrate. The elongation of the half-spheroid and the intensity modulation are working against each other which results in a non-monotonic dependence of plastic deformation in y direction on initially applied stress $\tau_{xx,0}$ at the same x position, as shown in Figure 7.10.

In Figure 7.11, the directional deformations in the y direction are compared for two different irradiation times. At intensity minima, there are nearly no deformations after 5 s and only small deformations develop after 10 s due to material transport from intensity maxima, see Figure 7.11. At positions with maximum intensity, the plastic deformation after 10 s of irradiation is less than the twice of deformation after 5 s. This is explained by the fact that the rate of deformation is decreasing with irradiation time.

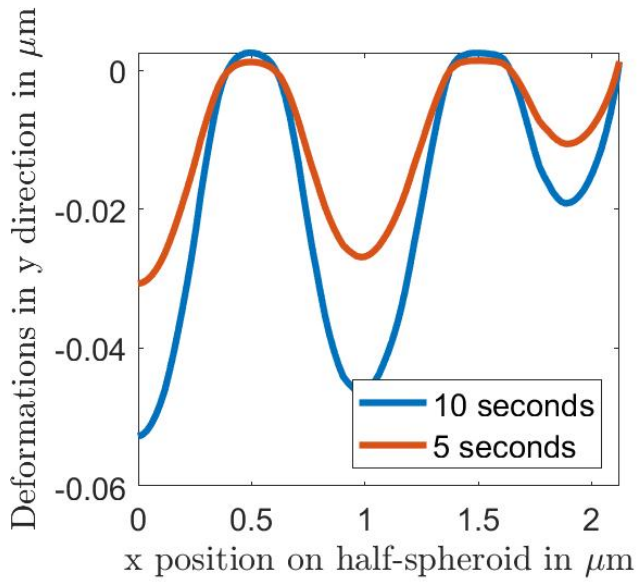

Figure 7.11: Directional deformation in y direction under the PP interference pattern after 5 s (red line) and 10 s (blue line) of irradiation time, at $\tau_{xx,0} = 25$ MPa.

Further, we study how the optical period affects the deformation in the half-spheroid under the PP interference pattern. The selected optical periods for this study are $D = 0.8, 1.0$ and 1.2 μm at applied stress $\tau_{xx,0} = 25$ MPa. The value of the optical period prescribes the position of the grating maxima and minima. As the length of the optical period increases, the maximum directional deformations in the y direction decrease, see Figure 7.12 (a). Additionally, the length of the half-spheroid slightly differs for different optical periods, see Figure 7.12 (b). This is due to the two effects compensating each other, which are elongation of the colloid and surface modulation.

SS interference pattern

In the SS interference pattern, the light is polarized along the y direction, as shown in Figure 7.13, and hence is perpendicular to the polarization of the light used to irradiate the initial half-spherical colloid. The initial orientation state is the final orientation state which is represented in Table 7.1 for different $\tau_{xx,0}$. It can be seen that the orientation state is asymmetric around the polarization direction y. Thus, time dependent components of the orientation tensor are calculated using the closure approximations, as explained in Section 3.4.2. The time evolution of the different components of the orientation tensor is shown exemplary in Figure 3.4. Additionally, the stress tensor is calculated using the Giesekus equation (3.19). The stress fields are not symmetric around the x axis, thus all diagonal components of the stress tensor are different.

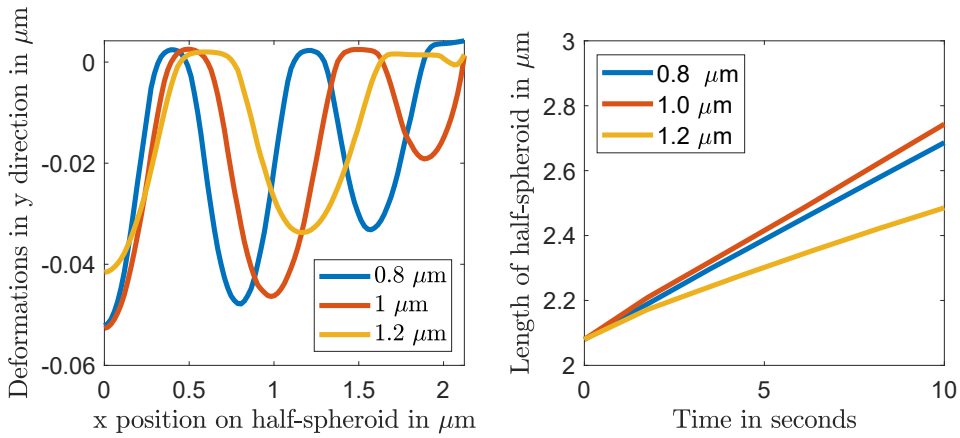

(a) **(b)**

Figure 7.12: a) The deformations in y direction and b) length of half spheroid dependence on the optical period at initial maximal stress $\tau_{xx,0} = 25$ MPa.

$$\boldsymbol{\tau} = \begin{bmatrix} \tau_{xx} & 0 & 0 \\ 0 & \tau_{yy} & 0 \\ 0 & 0 & \tau_{zz} \end{bmatrix} \tag{7.8}$$

The stress tensor components τ_{xx}, τ_{yy} and τ_{zz} are calculated using Equations (3.53), (3.54), (3.55) and (3.19) with the initial values of orientation tensor components, which correspond to the orientation of backbone segments at the end of the homogeneous irradiation, see Table 7.1.
The scalar rate of plastic strain $\dot{\epsilon}_{pl}$ is calculated in the ANSYS software using the Perzyna option (4.5), which contains the equivalent stress τ_{eq} as a parameter. Its value for the diagonal stress tensor, represented by Equation (7.8), can be written as follows:

$$\tau_{eq} = \sqrt{(\frac{3}{2}(\tau_{xx}^2 + \tau_{yy}^2 + \tau_{zz}^2))} \tag{7.9}$$

The rate of plastic strain tensor is defined as:

$$\dot{\boldsymbol{\epsilon}}_{pl} = \frac{3\dot{\epsilon}_{pl}}{2\tau_{eq}}\boldsymbol{\tau} \tag{7.10}$$

The light-induced stresses can be applied with the help of Userthstrain subroutine and the above equation for the true plastic strain, as described in Section 4.2. Similar boundary conditions to those used for the initial half-spherical colloid are applied.
Under the SS interference pattern, the elongated colloids develop a modulated cross-section, which is not anymore symmetric around the axis x, because

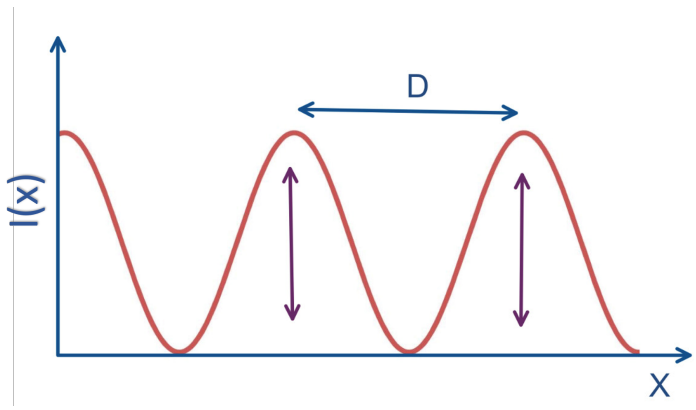

Figure 7.13: The variation of the light intensity with optical period D and light polarized in y direction for the SS interference pattern is represented by the blue curve.

$\tau_{zz} < \tau_{yy}$. The elongated colloid with asymmetric cross-section is presented in Figure 7.14 for an optical period of $D = 1$ μm. Formation of a hill at the maximum intensity and a well at the minimum intensity of the light interference pattern can be observed, as shown in Figure 7.14. At $x = 0$, the z radius of the half-spheroid decreases with time and the y radius increases with time, as can be seen in Figure 7.15 (a) and (b). Additionally, the length of the half-spheroid slightly decreases with the time, see Figure 7.15 (c). This is hindered in the experiments because of the adhesion of the sample to the substrate. The intensity modulation and the contraction of the half-spheroid along the x and z direction are favouring the directional deformation in the y direction. Thus, larger plastic deformations in y direction are observed for higher initially applied stress $\tau_{xx,0}$, see Figure 7.16. Additionally, the directional deformations in the y direction are compared for two different irradiation times, see Figure 7.17. At intensity minima, the same slight deformations are observed after 5 and 10 s, see Figure 7.17. At intensity maxima, the plastic deformation after 10 s of irradiation is two and a half times larger than the deformation after 5 s. Although the rate of plastic deformation decreases with time, the effect of sample contraction overrules this rate effect. Further, we study how the optical period affects the deformation in the half-spheroid for $\tau_{xx,0} = 25$ MPa under the SS interference pattern. As the length of the optical period D increases from 0.8 to 1.2 μm, the maximum directional deformations in the y direction noticeably increase, as seen in Figure 7.18.

7.2 Surface relief gratings

Surface relief gratings have been studied and used in different applications by many groups [41, 49, 50]. Nevertheless, it is a phenomenon which is not explained well till now. There are mainly two kind of surface relief gratings:

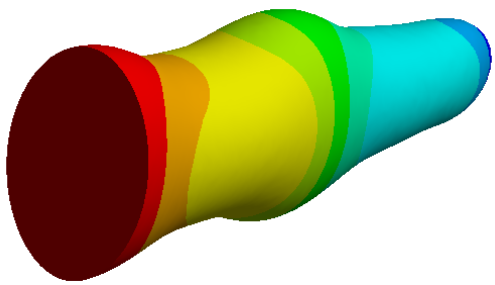

Figure 7.14: 3D view of wave-like structure developed after 10 s irradiation with the SS interference pattern at $\tau_{xx,0} = 25$ MPa.

one is formed when azopolymer films are irradiated with intensity interference patterns, another can be formed with polarization interference patterns. In intensity interference patterns the intensity of light has spatial dependence and polarization is fixed in one direction but for polarization interference patterns the intensity is constant and only the polarization varies in space, for more detail see Section 2.3.3. Specially the inscription of surface relief gratings under polarization interference patterns is hard to explain and most theories do not consider this case. Recently to understand such inscriptions a special experiment was conducted at the University of Potsdam. First, a thin polymer film (500 nm) is scratched by the AFM tip to form a micrometer wide gap. Afterwards, the film is exposed to irradiation with either RL or LR polarization interference patterns. It is clearly visible that formation of the surface relief gratings takes place together with the protrusion of the polymer material into the gap only at the positions where $\boldsymbol{E}$ vectors converge, as shown in Figure 7.3.

Below, we focus on modeling and interpretation of this particular experiment. To depict the experimental setup, we choose two coordinate systems in the finite element software ANSYS, which are the element coordinate system (ECS) and the global coordinate system (GCS). The ECS can be rotated with respect to the GCS and thus can be used to implement a spatially dependent polarization pattern. In particular we apply the following rotation θ_{xy} of the ECS with respect to the GCS:

- a) for the pattern RL: $\theta_{xy} = (X/D + 0.5)\pi$
- b) for the pattern LR: $\theta_{xy} = (-X/D + 0.5)\pi$

Here, X is the position of the element center in the GCS and D is the period of

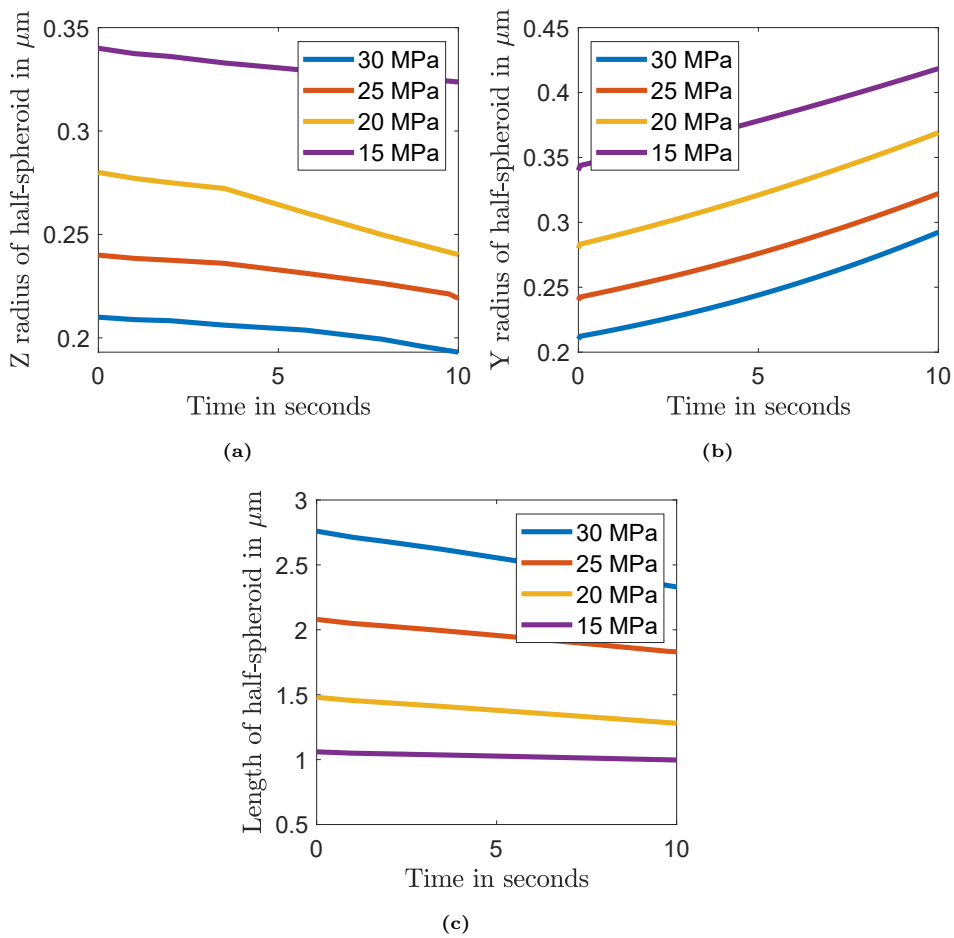

Figure 7.15: Time dependence of half-spheroid sizes for different $\tau_{xx,0}$ under the SS interference pattern: a) radius in the z direction, b) radius in the y direction and c) length of the half-spheroid.

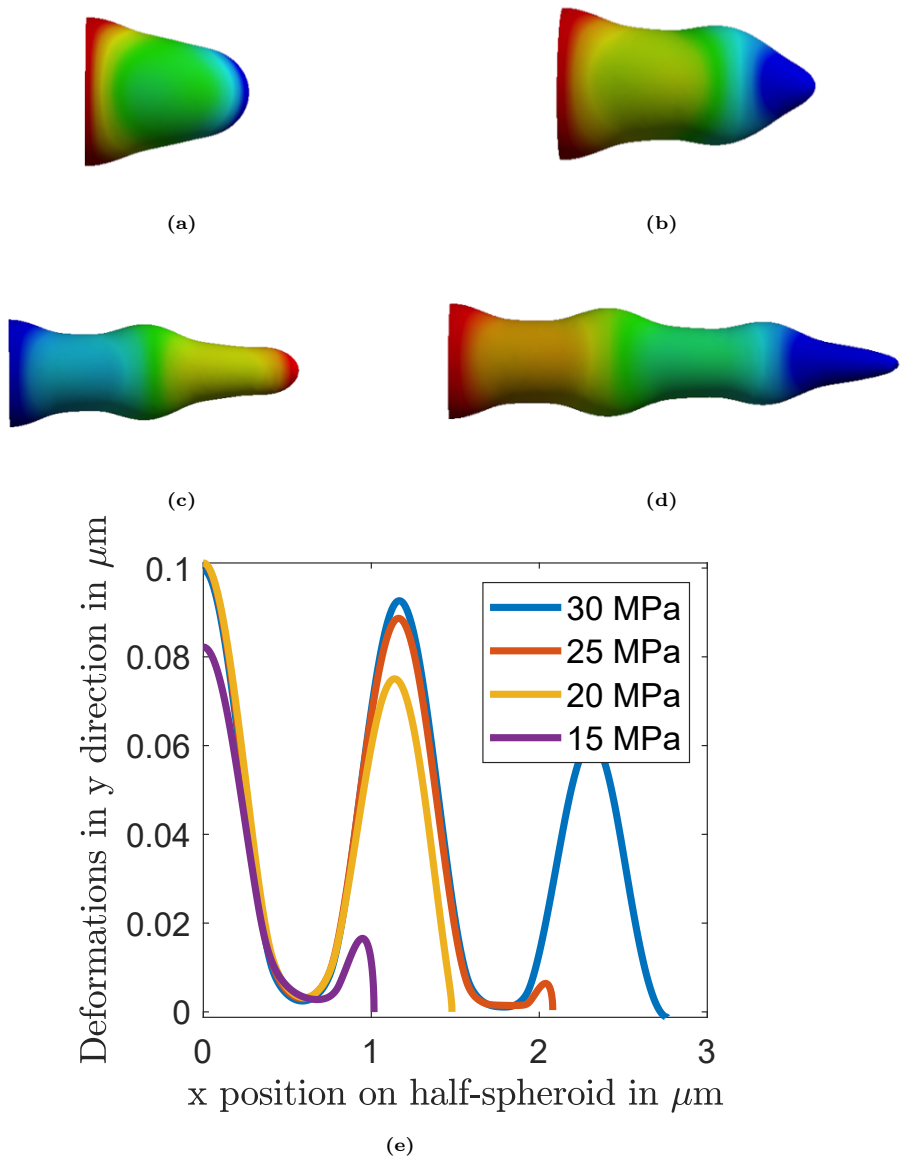

Figure 7.16: The deformed half-spheroid after 50 seconds of irradiation for initial $\tau_{xx,0}$ a) 15 MPa b) 20 MPa c) 25 MPa d) 30 MPa is shown here. e) The final deformations in y direction depending on initial $\tau_{xx,0}$ under the SS interference pattern.

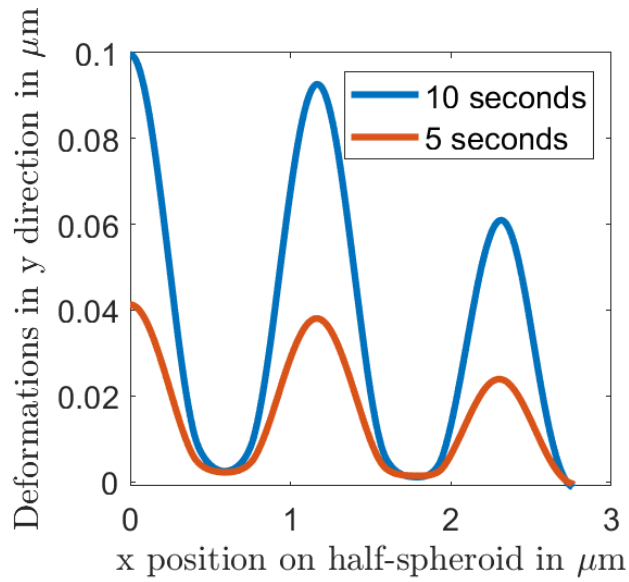

Figure 7.17: Directional deformation in y direction at 5 s and at 10 s of irradiation, $\tau_{xx,0} =$ 25 MPa.

optical grating.

Boundary Conditions

The following boundary conditions are used:

- The sample is "glued" to the substrate in the experiment, to mimic this effect the bottom surface is restricted to move in all three directions,
- The left and right side surfaces (represented with dark gray color, see Figure 7.19) of the sample are restricted to move in the normal directions,
- Three other surfaces (represented with light gray color, see Figure 7.19) are free to move in all directions.

The sample is meshed with 1 μm size mesh. The magnitude of light-induced stress at the beginning of irradiation is chosen to be 25 MPa in each element. The light-induced stress is applied in terms of total strain using the Userth-strain subroutine, as discussed in Chapter 4. Again, the Perzyna option is used to model the plastic deformation induced in azopolymer sample during 80 s of irradiation time.

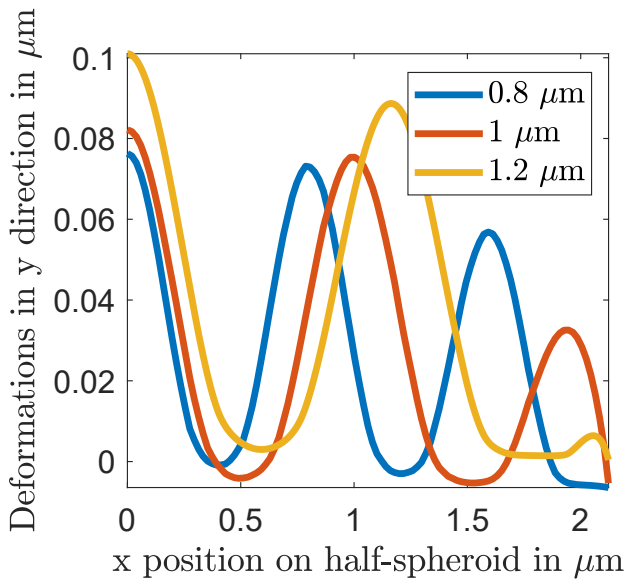

Figure 7.18: Directional deformation at the initial value of $\tau_{xx,0} = 25$ MPa under the SS interference pattern for different optical periods D.

Modeling parameters

The viscoplastic modeling predicts exactly the same effect as observed in the experiment: the azopolymer protrudes into the gap only at the positions where the red vectors of light polarization converge, compare Figure 7.20 with Figure 7.3. Similar to the experiment, the light-induced deformations are mirrored when changing from the RL to LR interference pattern, see Figure 7.3. Such anisotropic effect in the modeling is caused by the fact that during the rotation of the ECS various elements of the sample stretch in different directions, as shown on Figure 7.20 by red arrows. These arrows prescribe the direction of light polarization which defines the main axis of light-induced stress. Therefore, the azopolymer stretches horizontally, when the red arrows coincide with the x direction of the GCS. This gives rise to the valleys in azopolymer film. The material stretches vertically, when the red arrows are perpendicular to the x direction of the GCS, which gives rise to protrusions. In other words, the constant light-induced stress applied in different directions affects the stretching of an azopolymer film in different ways. This is a reason for the strong anisotropy between the RL and LR patterns.

The modeled structures after 80 seconds of irradiation (Figure 7.20) bear a striking resemblance to the AFM micrographs (Figure 7.3):

- formation of protrusions is observed at the film edge where the electric field vectors converge,
- only slight modulations are observed at the other edge where the electric

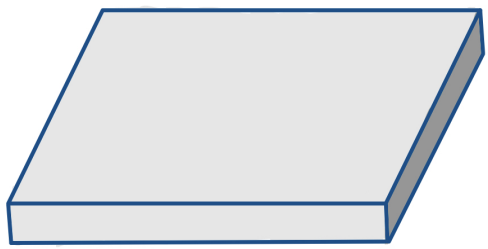

Figure 7.19: The surfaces represented with the light gray colour are free to move in all three directions, the two side surfaces represented with dark grey color are restricted to move in the normal direction and the bottom surface is restricted to move in all three direction.

field vectors diverge,

- surface relief gratings are formed far away from the edges in the film body.

Additionally, the viscoplastic modeling allows to follow in time gradual elongation of the sample along the y axis together with the growth of surface relief along the z axis, as shown in Figure 7.21. The deformations weaken upon decrease of the rotational time λ of backbone segments, see Figure 7.21. This indicates that azopolymers built from longer rigid segments should exhibit more pronounced topographical changes.

Conclusion

We can conclude that the photo-induced deformations in stretched oriented colloids as well as at the edges of the scratch in isotropic polymer films are reproduced and well explained using viscoplastic modeling of the azopolymer samples based on the orientation approach. In particular, it can be seen that formation of beads and wave-like structure is formed when elongated colloid is illuminated with PP and SS interference patterns. It can be understood that the deformations in the y direction are larger for the SS interference pattern than the photodeformations induced under the PP interference pattern due to the contraction of the colloid under SS and elongation under PP irradiation. Further, the photodeformations under RL and LR interference patterns are calculated and, when compared with the experimental results, they perfectly coincide with the observed deformations as discussed above. Thus, combined experimental and modeling study delivers a decisive proof that the orientation mechanism of polymer backbones is behind inscription of topographical structures in azobenzene containing polymer films.

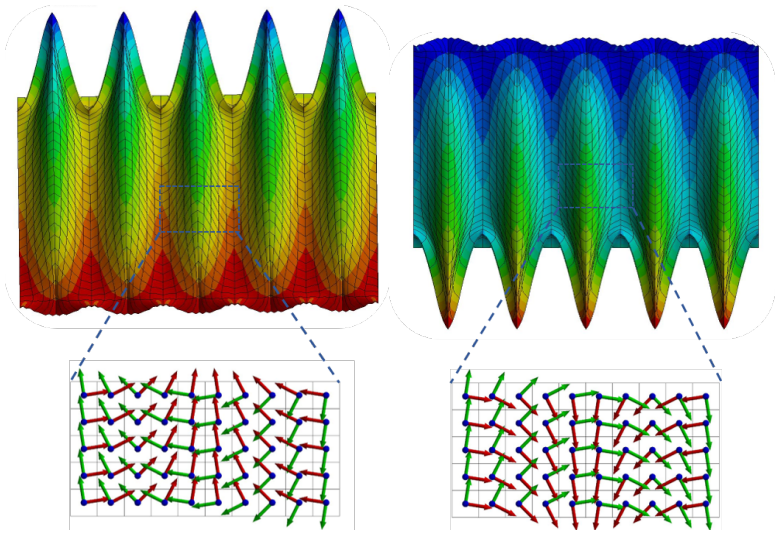

(a) **(b)**

Figure 7.20: Plastically deformed azopolymer films at $\tau_{xx,0} = 25$ MPa after 80 s irradiation with (a) the RL pattern and (b) LR pattern. Insert shows the rotation of ECS along the period of the optical grating. The light polarization is represented by red arrows.

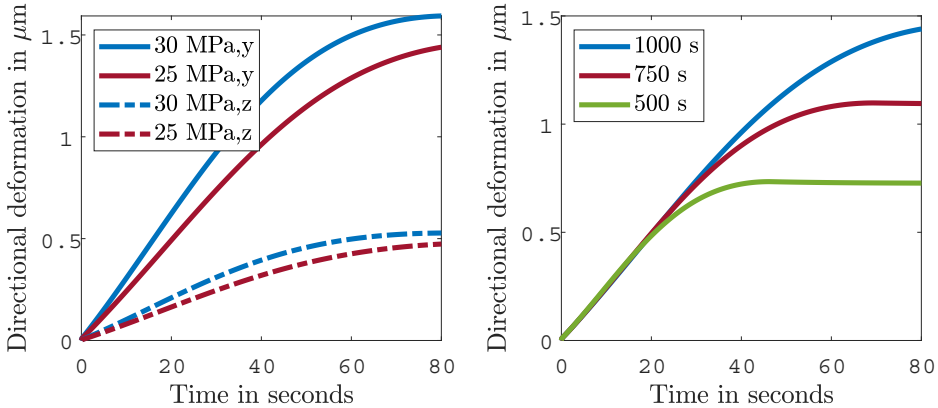

(a) **(b)**

Figure 7.21: (a) Under the RL pattern the azopolymer gradually protrudes along the axis y and builds a surface relief along the axis z; $\lambda = 1000$ s (b) The growth of protrusion reduces with the decrease of rotational time λ of backbone segments; $\tau_{xx,0} = 25$ MPa.

Chapter 8

Summary and outlook

8.1 Summary

In this thesis, a study is presented for photoinduced deformations in azobenzene containing side-chain polymers under different light irradiation patterns. In particular, the photodeformations are investigated under homogeneous irradiation with linearly and circularly polarized light, and under inhomogeneous irradiation with PP, SS, RL and LR interference patterns. During irradiation with light of appropriate wavelength the electro-magnetic energy is converted by isomerizing azobenzene chromophores into mechanical work that causes the deformations in the photosensitive material. It is proposed to explain these mechanical deformations using the orientation approach, which takes into account the reorientation of the chromophores in the direction perpendicular to the light polarization. In side-chain azopolymers, this should result in reorientation of backbone segments along the light polarization. The orientational hypothesis is tested by modeling the photoinduced deformations: analytically in case of homogeneous irradiation and using finite element modeling software ANSYS for complex irradiation patterns.

The effective orientation potential for the circularly polarized light is derived for the first time based on the angular hole burning effect. In analogy to the linearly polarized light, to simplify the kinetics of trans-cis isomerization under circularly polarized light, an effective orientation potential is introduced. This potential is shown to be minimum along the propagation direction and maximum in the polarization plane. Therefore, the effective potential for circularly polarized light induces the reorientation of the azobenzene chromophores along the propagation direction. Due to the rigid attachment of the chromophores with the main chain, the backbone segments in side-chain azopolymers should reorient into the polarization plane. The effective orientation potential acting on azobenzenes is recalculated to the orientation potential acting on backbone segments by taking the architecture of azopolymers into

account.

Based on the orientation approach, a new formalism is developed to describe the time evolution of light-induced stresses. The side-chain azopolymers are modeled as an ensemble of rigid Kuhn segments in the presence of an external orientation potential. Average orientation state of the ensemble of rigid backbone segments is described by the 2nd and 4th order orientation tensors. The components of 4th order orientation tensor are calculated using suitable closure approximations, which are developed for uniaxial and biaxial orientation order. The reorientation of backbone segments is accompanied by appearance of light-induced stress. It can be expressed as a contraction of the orientation tensors with the dyadic product of unit vector describing either light polarization or light propagation direction. Finally, it is shown that the total stress tensor is directly proportional to the rate of change of 2nd order orientation tensor.

Viscoplastic modeling is developed in the framework of finite element software ANSYS to predict the photoinduced deformations. For this purpose, the viscoplastic Perzyna model is chosen to calculate the photodeformations above the yield stress. Below the yield stress, negligible elastic deformations are predicted due to very large Young's modulus. The values of yield stress and Young's modulus for glassy azopolymers are taken from mechanical experiments and assumed to be unaltered by the presence of light. Additionally, a technical tool is developed, together with the firm CADFEM, to implement spatially and time varying stress fields using an external subroutine Userthstrain.

The computational time is down-scaled by properly adjusting the modeling parameters to attain the experimental time scale. A relation between the viscosity of plastic flow η and the rotational time λ of the rigid segments is established. The viscosity of the plastic flow in azopolymer materials is estimated to be of the order of 1 GPa s. In viscoplastic modeling in ANSYS, the viscosity is represented in terms of the viscosity parameter γ and the yield stress τ_{yield}. Time scale used in the experiments is of the order of hours, which is computationally expensive in ANSYS. Thus, to scale down the computational time, the viscosity parameter γ and the rotational time λ are adjusted.

Experimental results under homogeneous light intensity are well explained using the orientation approach. The plastic deformations are calculated using the viscoplastic modeling and are compared with the experimental results observed in an epoxy-based side-chain azopolymer [37]. In accordance with the experiment, the square post deforms vertically and horizontally for the vertical and horizontal linear polarization, respectively. Under the circularly polarized light, the square post deforms radially by contracting in the propagation direction. The magnitude of light-induced stress, predicted by the orientation approach for circular polarization is half of stress predicted for linear polar-

ization, which explains the more than twice smaller photodeformations in the presence of circularly polarized light.

Experimentally inscribed shapes under spatially dependent intensity and polarization patterns are well reproduced using the orientation approach. In this thesis multiple experiments, in which spatially dependent light intensity is used, are discussed and explained using the orientation approach. In one series of experiments, the strongly focused laser beam inscribes grooves and elongated hills on the azopolymer surface when moved fast in the direction perpendicular and parallel to light polarization, respectively. The light-induced stresses, in this case, are assumed to be constant due to the very short exposure time for one spot on the azopolymer surface. The depth of grooves and height of hills, predicted by the viscoplastic modeling, are compared with the experimental observations, and a good agreement is established. In another series of experiments, the deformations in the elongated oriented colloids under PP and SS intensity interference patterns are modeled and it is found that the formation of beads and wave-like structures are in accordance with the experiment. At last, the formation of peculiar structures at the edges of thin azopolymer film under RL and LR polarization interference patterns are modeled and exactly reproduced. Hence, the orientation approach correctly predicts local variations of the main axis of light-induced stress in each interference pattern for both initially isotropic and highly oriented materials.

The orientation approach, used in this thesis, is proved to be the most promising approach and only one which takes the architecture of the side-chain azopolymers explicitly into account. It builds an understanding of the role of light polarization in realignment of the main chain due to reorientation of the azobenzene chromophores. With this thesis, it is suggested that the orientation approach implements a self-sufficient and convincing mechanism to describe photoinduced deformations in azopolymer materials that in principle does not require auxiliary assumptions, like photosoftening or photofluidization.

8.2 Outlook

Further, viscoplastic material modeling based on the orientation approach can be used to describe surface deformations induced by complex light interference patterns. The origin of the spiral surface reliefs and the wavefront sensitivity of photodeformations, as described in Refs [18] and [57], represents a very challenging problem for the orientation approach. Here, the orientation potential for helically phased beams is needed to be calculated using the angular hole burning effect. Also, it should be checked, whether the stress tensors obtained in this thesis are able to reproduce the interference term between longitudinal and lateral components of the electric field responsible for the spiral deformations [92]. It would be interesting to model light-induced reversible inscription of photosensitive polymer films, in particular the erasure of surface relief grat-

ings by illuminating azopolymer films with successive interference patterns [44]. Also, it would be fascinating to investigate the formation of two dimensional gratings on the surface of azopolymer films, when first irradiated with interference pattern and later irradiated with the same interference pattern rotated by 90^0 [112]. For these two experiments, it is important to develop a procedure in ANSYS, which can implement light-induced stress fields corresponding to the time and spatial variation of successive interference patterns.

List of Publications

Journal papers

J1 Bharti Yadav, Jan Domurath, Kwangjin Kim, Seungwoo Lee and Marina Saphiannikova. "Orientation approach to directional photodeformations in glassy side-chain azopolymers". In: *The Journal of Physical Chemistry B* **2019**, 123, 3337-3347. DOI: 10.1021/acs.jpcb.9b00614.

J2 Bharti Yadav, Jan Domurath and Marina Saphiannikova. "Modeling of stripe patterns in photosensitive azopolymers". In: *Polymers* **2020**, 12, 735. DOI: 10.3390/polym12040735.

J3 Sarah Loebner, Bharti Yadav, Nimo Lomadze, Nina Tverdokhleb, Hendrik Donner, Marina Saphiannikova and Svetlana Santer. "Local direction of optomechanical stress in azobenzene containing polymers during surface relief grating formation". In: *Macromolecular Materials and Engineering* **2022**, 307, 2100990. DOI: 10.1002/mame.202100990.

Presentations

P1 Marina Saphiannikova, Olga Guskova, Markus Koch, Petrova, T., Vladimir Toshchevikov, Bharti Yadav. "Modeling directional photodeformations in azobenzene polymers". In: *14th Mediterranean Workshop and Topical Meeting Novel Optical Materials and Applications.* Cetraro, IT, 02.06.2019 - 08.06.2019

P2 Bharti Yadav, Domurath, Jan Domurath, Marina Saphiannikova. "Modelling of light-induced deformationsin side-chain azopolymers". In: *Frühjahrstagung der Deutschen Physikalischen Gesellschaft 2019.* Regensburg, DE, 31.03.2019 - 05.04.2019

P3 Bharti Yadav, Jan Domurath, Marina Saphiannikova. "Orientation approach to directional photodeformations in glassy side-Chain azopolymers". In: *15th International Saint Petersburg Conference of Young Scientists.* Saint Petersburg, 28.10.2019 - 31.10.2019

P4 Marina Saphiannikova, Olga Guskova, Markus Koch, Vladimir Toshchevikov, Bharti Yadav. "Versatile photomechanical response of azobenzene polymers". In: *13th IPF Colloquium-Smart Polymer Systems.* Dresden, 22.11.2018

Poster

Po1 Bharti Yadav, Jan Domurath, Marina Saphiannikova. "Modelling of light-induced deformations in side-chain azopolymers". In: *13th IPF Colloquium-Smart Polymer Systems.* Dresden, 22.11.2018

Po2 Bharti Yadav, Vladimir Toshchevikov, Seungwoo Lee, Marina Saphiannikova. "Prediction of light induced mechanical stress in side chain azopolymers". In: *3rd International Conference on Photoalignment and Photopatterning in Soft Materials.* Tampere, FI, 11.06.2018 - 14.06.2018

Proceedings

Pr1 Olga Guskova, Markus Koch, Savchenko, V., Bharti Yadav, Marina Saphiannikova. "Light-induced order-disorder transitions in azobenzene-containing systems in solution and solid state". In: *Jahresbericht 2020 - Leibniz-Institut für Polymerforschung Dresden.* S.86-87

Pr2 Jan Domurath, Bharti Yadav, Marina Saphiannikova. "Predicting mechanical stress in fi eld-responsive polymers with an evolving microscopic order". In: *Jahresbericht 2019 - Leibniz-Institut für Polymerforschung Dresden.* - S. 92-93

Appendix A

Time dependent components of the stress tensor

A.1 Calculations of stress tensor components

τ_{xx} can be calculated with the help of Geisekus equation (3.19):

$$\tau_{xx} = 3nkT\frac{\partial}{\partial t_\lambda}\langle u_x^2\rangle \tag{A.1}$$

The x component of the orientation tensor for linearly polarized light in x direction is as follows:

$$\langle u_x^2\rangle(t) = \frac{u_1 - u_2\frac{u_0-u_1}{u_0-u_1}e^{a(u_1-u_2)t}}{1-\frac{u_0-u_1}{u_0-u_1}e^{a(u_1-u_2)t}} \tag{A.2}$$

Here, $u_0 = \langle u_x^2\rangle(0)$ is the initial value in the absence of light and

$$u_{1,2} = \frac{1}{2} + \frac{1}{2V_r} \pm \frac{1}{2}\sqrt{(1+\frac{1}{V_r})^2 - \frac{4}{3V_r}} \tag{A.3}$$

The derivative of the orientation tensor component can be written as follows:

$$\frac{\partial\langle u_x^2\rangle(t)}{\partial t_\lambda} = \frac{V_r(u_1-u_2)^2\frac{u_0-u_1}{u_0-u_1}e^{a(u_1-u_2)t}}{(1-\frac{u_0-u_1}{u_0-u_1}e^{a(u_1-u_2)t})^2} \tag{A.4}$$

Using equation (A.1) and (A.4), time evolution of τ_{xx} component of the stress tensor can be expressed as follows:

$$\tau_{xx} = 3nkT\frac{V_r(u_1-u_2)^2\frac{u_0-u_1}{u_0-u_1}e^{a(u_1-u_2)t}}{(1-\frac{u_0-u_1}{u_0-u_1}e^{a(u_1-u_2)t})^2}\rangle \tag{A.5}$$

Similarly the time evolution of the stress tensor components can be calculated. In case of light polarized along x direction, the $\tau_{yy} = \tau_{zz} = -1/2\tau_{xx}$.

$$\tau_{yy} = \tau_{zz} = -\frac{3nkT}{2}\frac{V_r(u_1 - u_2)^2 \frac{u_0-u_1}{u_0-u_1} e^{a(u_1-u_2)t}}{(1 - \frac{u_0-u_1}{u_0-u_1} e^{a(u_1-u_2)t})^2}\rangle \tag{A.6}$$

Appendix B

APDL commands and subroutine computational codes

B.1 Mechanical APDL code for implementation of homogeneous stress

```
!   looking at the time dependent solution for the case when external
!   stress is applied on one of the face of the cube.
/clear
/PREP7 ! Enter the Preprocessor
block,0,10,0,10,0,10
*ask,t_ini,initial time of the calculation
*ask,t_inc, time increment in the calcultaion
*ask,n,no of time steps for which the clculation will be done.

t_fin=t_inc*n! final time of the calculations.
/PNUM,AREA,1
ET,1,285! Define Plane285 as element #1
mp,ex,1,1e9
mp,PRXY,1,0.49
tb,biso,1!table creation to define yield stress.
tbdata,1,1e7,1e3! data for yield stress, and tangent modulus
tb,rate,1,,,PEIRCE! model
tbdata,1,1,0.1
!   m and gamma (which is a function of viscosity of the material.)
ESIZE,0.7
VMESH,ALL
FINISH
```

```
sigma=-5e7
sigx=2*sigma/3!effective stress on the material
x0=1/3
k=1.383*1e-23
Tem=300
n1=2.5*1e26
lamda=50
vr=3*sigx/(2*n1*k*tem)
x1=(1/2)+(1/(2*vr))+(1/2)*sqrt((((1+(1/vr))*(1+(1/vr)))-(4/(3*vr))))
x2=(1/2)+(1/(2*vr))-(1/2)*sqrt((((1+(1/vr))*(1+(1/vr)))-(4/(3*vr))))
xd=(x0-x1)/(x0-x2)
xdd=x1-x2
*DO,t2,t_ini,t_fin,t_inc    !*do,par,ival,fval,inc--- par
!   defines the parameter to  be changed in all of the calculations,
!   ival- initial value of the parameter, fval - final value to the parameter,
    inc gives the increamennt in the paramenter
/SOLU
NLGEOM,ON
y=xd*exp((vr*xdd*t2)/(lamda))
y1=1.5*3*n1*k*tem*vr*(xdd*xdd)*y/((1-y)*(1-y))!returning to the
!   equivalent sress
SFA,6,,PRES,-y1
!   time at the end of the step.
t2=t2+t_inc
nropt,auto
Time,t2
DA,3,SYMM,Uy,0
DA,2,SYMM,Uz,0
DA,5,SYMM,UX,0
ANTYPE,static
solve
*Enddo
Finish
/post26
```

B.2 Mechanical APDL code used in workbench

```
/com,'Defintion of material data'
!   Assignment of the material's properties
Youngs_modulus = arg1
Poisson_ratio = arg2
Yield_stress = arg3
Tangent_modulus = arg4
```

```
gamma = arg5
gammain= 1 / gamma  !gamma inverse
Shear_modulus = Youngs_modulus / (2.0*(1.0+Poisson_ratio))
!   Clear all hitherto associated material data

mpdele,all,matid
tbdele,all,matid

!   Definition of the linear elastic properties

MP,EX,matid,Youngs_modulus
MP,NUXY,matid,Poisson_ratio

!   Activation of userthstrain

tb,cte,matid,,,user
tbdata,1,Shear_modulus,gamma,Yield_stress

!   Plasticity

tb,biso,matid
tbdata,1,Yield_stress,Tangent_modulus

!   inclusion of prezyna model

tb,rate,1,,,PEIRCE! model
tbdata,1,1,gammain

!   m and gamma (which is a function of viscosity of the material.)

!   Activation of state variables

tb,state,matid,,3
Material_ID = matid     ! for subsequent APDL-snippets
```

B.3 Definition of initial state variables

```
!   Commands inserted into this file will be executed just prior
to the ANSYS SOLVE command.
!   These commands may supersede command settings set by Workbench.

!   Active UNIT system in Workbench when this object was created:
Metric (um, kg, uN, s, V, mA)
!   NOTE:  Any data that requires units (such as mass) is assumed
```

```
to be in the consistent solver unit system.
!   See Solving Units in the help system for more information.

esel,s,mat,,Material_ID            ! Select all elements with material ID
inistate,set,mat,0                 ! disable material-based definition
inistate,set,node,0                ! disable node-based definition
inistate,set,dtyp,svar             ! type = state variables

!   Request element count and first element ID

*get,Element_count,elem,0,count  ! get number of elements
*get,ID,elem,0,num,min           ! get ID of the first element

!   Loop over all elements

*do,i,1,Element_count,1
dp = 1.17
delta = (3.14*(centry(ID))/dp)
fy = (cos(delta))*(cos(delta))
value =100*fy
!   value is assigned to all IP of the element
inistate,define,ID,all,,,0,value,0

ID = ELNEXT(ID)       ! request next id
*enddo

ALLSEL
```

B.4 Userthstrain subroutine

```
*     State variables:

*     ustatev(1) = time  (coded via the temperature for dll)
*     ustatev(2) = sigma_xx_light
*     ustatev(3) = plastic strain
*     ustatev(4) = time dependent stress

*     Properties:

*     propv(1) = shear modulus
*     propv(2) = time constant for the light-induced contribution
*     propv(3) = yield stress
*.....................................................................
```

```
      subroutine userthstrain (nprop,propv,ncomp,epth)

      implicit none
*.....................................................................
*     Declaration of global parameters

      integer           nprop, ncomp
      double precision propv(nprop),epth(ncomp)
*.....................................................................
*     Declaration of local parameters

      integer elemId,matipt,i,nstatev,ldstep
      double precision time,ustatev(3),dt,condition,elastic
      double precision Tem,n1,lamda,vr,x1,x2,xd,xdd
      double precision sigx,x0,k,n,y,y1,sigma,y2,vr1,y3,tp,x11,x22,vr11
      double precision vr111,x33,xd1,xd2,stress
*.....................................................................
*     Declaration of external functions

      external get_ElmInfo,put_ElmData,get_ElmData
*.....................................................................
*     Request element information

      call get_ElmInfo('ELEMID  ',elemId)
      call get_ElmInfo('MATIPT  ',matipt)
      call get_ElmInfo('NSVAR   ',nstatev)
      call get_ElmInfo('LDSTEP  ',ldstep)

      call get_ElmData('TEMP',elemId,matipt,i,time)
      call get_ElmData('SVAR', elemId, matipt, nstatev, ustatev)

      dt = time - ustatev(1)
      sigma=ustatev(2)
      sigx=1d6*ustatev(2)
      x0=0.33d0
      k=1.383*1d-23
      tp=300.0d0
      n1=2.5*1d26
      lamda=250.0d0
      vr=-3*sigx/(2*n1*k*tp)
      vr1=(4/(3*vr))
      vr11=(1+(1/vr))*(1+(1/vr))
      vr111=vr11-vr1
      x11=0.5d0+(1/(2*vr))
      x22=sqrt(vr111)
      x33=0.5d0*x22
```

```
      x1=x11+x33
      x2=x11-x33
      xd1=(x0-x1)
      xd2= (x0-x2)
      xd=xd1/xd2
      xdd=x1-x2
      y=xd*exp((vr*xdd*(ustatev(1)+dt))/(lamda))
      y2=y/((1-y)*(1-y))
      y3= n1*k*tp*vr

      y1=4.5d0*y3*(xdd*xdd)*y2

*stress in the units of Mpa
      stress = y1*1d-6
      condition = propv(3)

*     elastic and plstic strain
*in the case when stress is less then yield stress the plastic strain will
same as the maximum strain
      if(stress .le. condition) then
      ustatev(3) = ustatev(3)
      else
      ustatev(3) = ustatev(3)+dt*(stress/(propv(3))-1.d0)
     +           / propv(2)
      end if

*     ustatev(4) = propv(3)/(2.d0*propv(1))

      elastic = propv(3)/(3.d0*propv(1))
*       elastic = 0.d0


*     Dummy output

      if(ldstep.eq.-1) then
        write(*,*) 'Dummy'
      end if


* only for biso

      epth(1) = -ustatev(3)/(2.d0) - elastic/2.d0
      epth(2) = ustatev(3)/(1.d0) + elastic
      epth(3) =  -ustatev(3)/(2.d0) - elastic/2.d0

*     Store state variables
```

```
*line no 127 next line
      ustatev(1) = time
      call put_ElmData ('SVAR', elemId, matipt, nstatev, ustatev)
      write(*,*) y1,ustatev(3)
      end
*.....................................................................
```

Bibliography

[1] Y. Yu, M. Nakano, and T. Ikeda. "Directed bending of a polymer film by light". In: *Nature* 425 (2003), p. 145. DOI: 10.1038/425145a.

[2] K. Ichimura, SK. Oh, and M. Nakagawa. "Light-driven motion of liquids on a photoresponsive surface." In: *Science.* (2000), pp. 1624–1626. DOI: 10.1126/science.288.5471.1624.

[3] W. C. Xu, S. Sun, and S. Wu. "Photoinduced Reversible Solid-to-Liquid Transitions for Photoswitchable Materials". In: *Angewandte Chemie International Edition* 58.29 (2019), pp. 9712–9740. DOI: 10.1002/anie.201814441.

[4] B. Yang et al. "Athermal and soft multi-nanopatterning of azopolymers: phototunable mechanical properties". In: *Angewandte Chemie International Edition* 59.10 (2020), pp. 4035–4042. DOI: 10.1002/anie.201914201.

[5] D. Bléger and S. Hecht. "Visible-light-activated molecular switches". In: *Angewandte Chemie International Edition* 54.39 (2015), pp. 11338–11349. DOI: 10.1002/anie.201500628.

[6] D. Bléger. "Orchestrating molecular motion with light-from single macromolecules to materials". In: *Macromolecular Chemistry and Physics* 217.2 (2016), pp. 189–198. DOI: 10.1002/macp.201500330.

[7] M. Irie et al. "Photochromism of diarylethene molecules and crystals: memories, switches, and actuators". In: *Chemical Reviews* 114.24 (2014), pp. 12174–12277. DOI: 10.1021/cr500249p.

[8] G. Ragazzon et al. "Light-powered autonomous and directional molecular motion of a dissipative self-assembling system". In: *Nature Nanotechnology* 10 (2015), pp. 70–75. DOI: 10.1038/nnano.2014.260.

[9] E. Merino and M. Ribagorda. "Control over molecular motion using the cis–trans photoisomerization of the azo group". In: *Beilstein Journal of Organic Chemistry* 8 (2012), pp. 1071–1090. ISSN: 1860-5397. DOI: 10.3762/bjoc.8.119.

[10] M. Hepel and C.J. Zhong. "Functional nanoparticles for bioanalysis, nanomedicine, and bioelectronic devices". In: *ACS Symposium Series* v. 2 (2013).

[11] M. Naito et al. *Nanoparticle Technology Handbook*. Elsevier Science, 2007. ISBN: 9780080558028.

[12] V. G. Chigrinov, V. M. Kozenkov, and H. Kwok. *Photoalignment of liquid crystalline materials*. John Wiley & Sons, Ltd, 2008. DOI: 10.1002/9780470751800.

[13] N. Tabiryan et al. "Superlens in the skies: liquid-crystal-polymer technology for telescopes". In: *SPIE Newsroom* (2016). DOI: 10.1117/2.1201601.006317.

[14] A. Ryabchun and A. Bobrovsky. "Photocontrollable Deformations of Polymer Particles in Elastic Matrix". In: *Advanced Optical Materials* 7.24 (2019), p. 1901486. DOI: 10.1002/adom.201901486.

[15] F. Lancia et al. "Mechanical adaptability of artificial muscles from nanoscale molecular action". In: *Nature Communications* 10 (2019), p. 4819. DOI: 10.1038/s41467-019-12786-2.

[16] S.L. Oscurato et al. "Large-scale multiplexed azopolymer gratings with engineered diffraction behavior". In: *Advanced Materials Interfaces* 8.21 (2021), p. 2101375. DOI: 10.1002/admi.202101375.

[17] T. Shimoboji et al. "Photoresponsive polymer–enzyme switches". In: *Proceedings of the National Academy of Sciences* 99.26 (2002), pp. 16592–16596. ISSN: 0027-8424. DOI: 10.1073/pnas.262427799.

[18] S. L. Oscurato et al. "From nanoscopic to macroscopic photo-driven motion in azobenzene-containing materials". In: *Nanophotonics* 7.8 (2018), pp. 1387–1422. DOI: 10.1515/nanoph-2018-0040.

[19] S. L. Oscurato et al. "Light-driven wettability tailoring of azopolymer surfaces with reconfigured three-dimensional Posts". In: *ACS Applied Materials & Interfaces* 9.35 (2017), pp. 30133–30142. DOI: 10.1021/acsami.7b08025.

[20] F. Pirani et al. "Laser-induced anisotropic wettability on azopolymeric micro-structures". In: *Applied Physics Letters* 110.10 (2017), p. 101603. DOI: 10.1063/1.4978260.

[21] O. M. Wani, H. Zeng, and A. Priimagi. "A light-driven artificial flytrap". In: *Nature Communications* 8.1 (2017), p. 15546. DOI: 10.1038/ncomms15546.

[22] Y. Zakrevskyy et al. "Photosensitive surfactants: micellization and interaction with DNA". In: *The Journal of Chemical Physics* 140.4 (2014), p. 044906. DOI: 10.1063/1.4862678.

[23] Y. Zakrevskyy et al. "Interaction of photosensitive surfactant with DNA and poly acrylic acid". In: *The Journal of Chemical Physics* 140.4 (2014), p. 044907. DOI: 10.1063/1.4862679.

[24] M. R. Banghart, M. Volgraf, and D. Trauner. "Engineering light-gated ion channels". In: *Biochemistry* 45.51 (2006), pp. 15129–41. DOI: 10.1021/bi0618058.

[25] MR. Banghart et al. "Light-activated ion channels for remote control of neuronal firing". In: *Nature Neuroscience* 7 (2004), pp. 1381–1386. DOI: 10.1038/nn1356.

[26] D.B. Konrad, J.A. Frank, and D. Trauner. "Synthesis of redshifted azobenzene photoswitches by late-stage functionalization." In: *Chem Eur J* 22 (2016), pp. 4364–8. DOI: 10.1002/chem.201505061.

[27] A. Goulet-Hanssens and C. J. Barrett. "Photo-control of biological systems with azobenzene polymers". In: *Journal of Polymer Science Part A: Polymer Chemistry* 51.14 (2013), pp. 3058–3070. DOI: 10.1002/pola.26735.

[28] A. Stracke et al. "Gain effects in optical storage: thermal induction of a surface relief grating in a smectic liquid crystal". In: *Advanced Materials* 12 (2000), pp. 282–285. DOI: 10.1002/(SICI)1521-4095(200002)12:4<282::AID-ADMA282>3.0.CO;2-P.

[29] R. Berg, S. Hvilsted, and P. Ramanujam. "Peptide oligomers for holographic data storage". In: *Nature* 383 (1996), pp. 505–508. DOI: 10.1038/383505a0.

[30] A. Natansohn et al. "Azopolymers for reversible optical storage". In: *Macromolecules* 25.8 (1992), pp. 2268–2273. DOI: 10.1021/ma00034a031.

[31] U.A. Hrozhyk et al. "Photoinduced isotropic state of cholesteric liquid crystals: novel dynamic photonic materials." In: *Adv Mater* 19 (2007), pp. 3244–7. DOI: 10.1002/adma.200700209.

[32] M. Eich et al. "Reversible digital and holographic optical storage in polymeric liquid crystals". In: *Die Makromolekulare Chemie, Rapid Communications* 8.1 (1987), pp. 59–63. DOI: 10.1002/marc.1987.030080111.

[33] N. K. Viswanathan et al. "Surface relief structures on azo polymer films". In: *J. Mater. Chem.* 9 (1999), pp. 1941–1955. DOI: 10.1088/1757-899X/49/1/012024.

[34] A. Natansohn and P. Rochon. "Photoinduced motions in azobenzene-based amorphous polymers: possible photonic devices". In: *Advanced Materials* 11 (1999), pp. 1387–1391. DOI: 10.1002/(SICI)1521-4095(199911)11:16<1387::AID-ADMA1387>3.0.CO;2-#.

[35] T. Ikeda and O. Tsutsumi. "Optical switching and image storage by means of azobenzene liquid-crystal Films". In: *Science* 268.5219 (1995), pp. 1873–1875. DOI: 10.1126/science.268.5219.1873.

[36] S. Masiero et al. "The direct conversion of light into continuous mechanical energy by photoreversible self-assembly: a prototype of a light-powered engine†". In: *Angew Chem* 47 (2008), pp. 3184–7. DOI: 10.1002/anie.200705313.

[37] H. S. Kang et al. "Light-powered healing of a wearable electrical conductor". In: *Advanced Functional Materials* 24.46 (2014), pp. 7273–7283. DOI: 10.1002/adfm.201401666.

[38] T. Ikeda, J. Mamiya, and Y. Yu. "Photomechanics of liquid-crystalline elastomers and other polymers". In: *Angew Chem Int Ed Engl* 46(4) (2007), pp. 506–28. DOI: 10.1002/anie.200602372.

[39] M. Camacho-Lopez et al. "Fast liquid-crystal elastomer swims into the dark". In: *Nat. Mater.* 3 (2004), pp. 307–10. DOI: 10.1038/nmat1118.

[40] P. Rochon, E. Batalla, and A. Natansohn. "Optically induced surface gratings on azoaromatic polymer films". In: *Appl. Phys. Lett.* 66.2 (1995), pp. 136–138. DOI: 10.1063/1.113541.

[41] D. Y. Kim et al. "Laser-induced holographic surface relief gratings on nonlinear optical polymer films". In: *Applied Physics Letters* 66.10 (1995), pp. 1166–1168. DOI: 10.1063/1.113845.

[42] N. S. Yadavalli, M. Saphiannikova, and S. Santer. "Photosensitive response of azobenzene containing films towards pure intensity or polarization interference patterns". In: *Applied Physics Letters* 105.5 (2014), p. 051601. DOI: 10.1063/1.4891615.

[43] D. Bublitz et al. "Photoinduced deformation of azobenzene polyester films". In: *Applied Physics B* 70 (2000), pp. 863–865. DOI: 10.1007/s003400000281.

[44] J. Jelken and S. Santer. "Light induced reversible structuring of photosensitive polymer films". In: *RSC Adv.* 9 (2019), pp. 20295–20305. DOI: 10.1039/C9RA02571E.

[45] K. G. Yager and C. J. Barrett. "Confinement of surface patterning in azo-polymer thin films." In: *J. Chem. Phys.* (2007), pp. 1–8. DOI: 10.1063/1.2538787.

[46] A. Sobolewska and A. Miniewicz. "Analysis of the Kinetics of Diffraction Efficiency during the Holographic Grating Recording in Azobenzene Functionalized Polymers." In: *J. Phys. Chem. B* (2007), pp. 1536–1544. DOI: 10.1021/jp067021l.

[47] Z. Wang, C. Hsu, and X. Wang. "Topographical transition of submicron pillar array of azo molecular glass induced by circularly polarized light." In: *Sci Rep 11* (2021), p. 7327. DOI: 10.1038/s41598-021-86794-y.

[48] X. Kong et al. "Photomanipulated architecture and patterning of azopolymer array". In: *ACS Applied Materials & Interfaces* 9.22 (2017), pp. 19345–19353. DOI: 10.1021/acsami.7b04273.

[49] M. Saphiannikova and D. Neher. "Thermodynamic theory of light-induced material transport in amorphous azobenzene polymer films". In: *J. Phys. Chem. B* 109.41 (2005), pp. 19428–19436. DOI: 10.1021/jp053249h.

[50] A. Priimagi and A. Shevchenko. "Azopolymer-based micro- and nanopatterning for photonic applications". In: *Journal of Polymer Science Part B: Polymer Physics* 52.3 (2013), pp. 163–182. DOI: 10.1002/polb.23390.

[51] A. Ambrosio et al. "Cis–trans isomerization and optical laser writing in new heterocycle based azo-polyurethanes". In: *Optical Materials* 34 (2012). DOI: 10.1016/j.optmat.2011.10.009.

[52] S. Loebner et al. "Light induced deformation of azobenzene containing colloidal spheres: calculation and measurement of opto mechanical stresses". In: *The Journal of Physical Chemistry B* 122.6 (2018), pp. 2001–2009. DOI: 10.1021/acs.jpcb.7b11644.

[53] C. J. Barrett, P. L. Rochon, and A. L. Natansohn. "Model of laser-driven mass transport in thin films of dye-functionalized polymers". In: *J. Chem. Phys.* 109.4 (1998), pp. 1505–1516. DOI: 10.1063/1.476701.

[54] J. Kumar et al. "Gradient force: The mechanism for surface relief grating formation in azobenzene functionalized polymers". In: *Appl. Phys. Lett.* 72.17 (1998), pp. 2096–2098. DOI: 10.1063/1.121287.

[55] D. Bublitz, B. Fleck, and L. Wenke. "A model for surface-relief formation in azobenzene polymers". In: *Appl. Phys. B: Lasers Opt.* 72.8 (2001), pp. 931–936. DOI: 10.1007/s003400100596.

[56] V. Toshchevikov, J. Ilnytskyi, and M. Saphiannikova. "Photoisomerization Kinetics and Mechanical Stress in Azobenzene-Containing Materials". In: *Journal of the Society for Information Display* 8 (2017), pp. 1094–1098. DOI: 10.1021/acs.jpclett.7b00173.

[57] A. Ambrosio et al. "Light-induced spiral mass transport in azo-polymer films under vortex-beam illumination". In: *Nature communications* 3 (2012), p. 989. DOI: 10.1038/ncomms1996.

[58] J.J.D. Lange, J.M. Robertson, and I. Woodward. "X-ray crystal analysis of trans-azobenzene." In: *Proc R Soc Lond A* 171 (1939), pp. 398–410. DOI: 10.1098/rspa.1939.0073.

[59] G.C. Hampson and J.M. Robertson. "Bond lengths and resonance in the cis-azobenzene molecule." In: *J Chem Soc Resumed* 0 (1941), pp. 409–13. DOI: 10.1039/JR9410000409.

[60] C. J. A Brown. "A refinement of the crystal structure of azobenzene." In: *Acta Crystallogr* 21 (1966), pp. 146–52. DOI: 10.1107/S0365110X66002445.

[61] M. Sato et al. "Photoinduced conformational transition of polypeptides containing azobenzenesulfonate in the side chains." In: *Macromolecules* 21 (1988), pp. 1612–6. DOI: 10.1021/ma00184a014.

[62] N. Biswas and S. Umapathy. "Density functional calculations of structures, vibrational frequencies, and normal modes of trans and cis azobenzene." In: *J Phys Chem A* 101 (1997), pp. 5555–66. DOI: 10.1021/jp970312x.

[63] N.A. Wazzan, P.R. Richardson, and A.C. Jones. "Cis-trans isomerisation of azobenzenes studied by laser-coupled NMR spectroscopy and DFT calculations." In: *Photochem Photobiol Sci* 9 (2010), pp. 968–74. DOI: 10.1039/C0PP00056F.

[64] T. Naito, K. Horie K, and I. Mita. "Photochemistry in polymer solids. 11. The effects of the size of reaction groups and the mode of photoisomerization on photochromic reactions in polycarbonate film." In: *PMacromolecules* 24 (1991), pp. 2907–11. DOI: 10.1021/ma00010a042.

[65] K. G. Yager and C. J. Barrett. "All-optical patterning of azopolymer films." In: *Solid State Mater. Sci.* (2001), pp. 487–494. DOI: 10.1016/S1359-0286(02)00020-7.

[66] P. Karageorgiev et al. "From anisotropic photo-fluidity towards nanomanipulation in the optical near-field." In: *Nat. Mater.* 4 (2005), pp. 699–703. DOI: 10.1038/nmat1459.

[67] J. Vapaavuori et al. "Nanoindentation study of light-induced softening of supramolecular and covalently functionalized azo polymers". In: *Journal of Materials Chemistry C* 1 (2013), p. 2806. DOI: 10.1039/c3tc30246f.

[68] K.-H. Kim and Y.-C. Jeong. "Nanoindentation study of optically patterned surface relief grating of azobenzene polymers". In: *Opt. Express* (2016), p. 25242. DOI: 10.1364/OE.24.025242.

[69] N. Hurduc et al. "Direct observation of athermal photofluidisation in azopolymer films". In: *Soft Matter* 10 (2014), pp. 4640–4647. DOI: 10.1039/C4SM00397G.

[70] N. Mechau, M. Saphiannikova, and D. Neher. "Dielectric and mechanical properties of azobenzene polymer layers under visible and ultraviolet irradiation". In: *Macromolecules* 38.9 (2005), pp. 3894–3902. DOI: 10.1021/ma0479316.

[71] J. Jelken. "Surface relief and bulk birefringence gratings in photo-sensitive polymer films in-situ probing and manipulation in real time". In: *Dissertation* (2020).

[72] Y. Zhao and T. Ikeda. *Smart light reponsive materials: azobenzene containing polymers and liquid crystals*. John Wiley and Sons. 2009.

[73] N. K. Viswanathan et al. "A detailed investigation of the polarization-dependent surface-relief-grating formation process on azopolymer films". In: *Japanese J. Appl. Physics* 38 (1999), pp. 5928–5937. DOI: 10.1143/jjap.38.5928.

[74] P. Pagliusi et al. "Tunable surface patterning of azopolymer by vectorial holography: the role of photoanisotropies in the driving force". In: *ACS Applied Materials & Interfaces* 11.37 (2019), pp. 34471–34477. DOI: 10.1021/acsami.9b12624.

[75] M. Saphiannikova et al. "Linear viscoelastic analysis of formation and relaxation of azobenzene polymer gratings". In: *The Journal of Chemical Physics* 120.8 (2004), pp. 4039–4045. DOI: 10.1063/1.1642606.

[76] P. Lefin, C. Fiorini, and J. M. Nunzi. "Anisotropy of the photo-induced translation diffusion of azobenzene dyes in polymer matrices". In: *Pure Appl. Opt.* 7.1 (1998), pp. 71–82. DOI: 10.1088/0963-9659/7/1/011.

[77] L. Philippe, F. Céline, and N. Jean-Michel. "Anisotropy of the photoinduced translation diffusion of azo-dyes". In: *Optical Materials* 9.1 (1998), pp. 323–328. DOI: 10.1016/S0925-3467(97)00100-6.

[78] C. J. Barrett, A. L. Natansohn, and P. L. Rochon. "Mechanism of optically inscribed high-efficiency diffraction gratings in azopolymer films". In: *The Journal of Physical Chemistry* 100.21 (1996), pp. 8836–8842. DOI: 10.1021/jp953300p.

[79] C. J. Barrett, A. L. Natansohn, and P. L. Rochon. "Mechanism and model of laser-driven mass transport in thin films of azo polymers". In: *Am. Chem. Soc. Polym. Prepr* 38 (1998), pp. 542–543.

[80] T. Pedersen et al. "Mean-field theory of photoinduced formation of surface reliefs in side-chain azobenzene polymers". In: *Phys. Rev. Lett.* 80.1 (1998), pp. 89–92. DOI: 10.1103/physrevlett.80.89.

[81] T. G. Pedersen and P. M. Johansen. "Mean-field theory of photoinduced molecular reorientation in azobenzene liquid crystalline side-chain polymers". In: *Phys. Rev. Lett.* 79 (13 1997), pp. 2470–2473. DOI: 10.1103/PhysRevLett.79.2470.

[82] M. Saphiannikova and V. Toshchevikov. "Optical deformations of azobenzene polymers: Orientation approach vs. photofluidization concept". In: *Journal of the Society for Information Display* 23 (2015). DOI: 10.1002/jsid.294.

[83] V. Toshchevikov, M. Saphiannikova, and G. Heinrich. "Microscopic theory of light induced deformation in amorphous side chain Azobenzene Polymers". In: *The Journal of Physical Chemistry B* 113.15 (2009), pp. 5032–5045. DOI: 10.1063/1.1603736.

[84] V. Toshchevikov and M. Saphiannikova. "Theory of light-induced deformation of azobenzene elastomers: effects of the liquid-crystalline interactions and biaxiality". In: *The Journal of Physical Chemistry B* 118.42 (2014), pp. 12297–12309. DOI: 10.1021/jp5063226.

[85] J.M. Ilnytskyi, V. Toshchevikov, and M. Saphiannikova. "Modeling of the photo-induced stress in azobenzene polymers by combining theory and computer simulations". In: *Soft Matter* 15 (2019), pp. 9894–9908. DOI: 10.1039/C9SM01853K.

[86] M. Warner and E. M. Terentjev. *Liquid Crystal Elastomers*. International Series of Monographs on Physics. OUP Oxford, 2007. ISBN: 9780199214860.

[87] P. G. de Gennes and J. Prost. *The Physics of Liquid Crystals*. International Series of Monographs on Physics. Clarendon Press, 1993. ISBN: 9780198517856.

[88] M. Dumont and A. El Osman. "On spontaneous and photoinduced orientational mobility of dye molecules in polymers". In: *Chemical Physics* 245.1-3 (1999), pp. 437–462. DOI: 10.1016/s0301-0104(99)00096-8.

[89] G. Pawlik et al. "Kinetics of diffraction gratings formation in a polymer matrix containing azobenzene chromophores: Experiments and Monte Carlo simulations". In: *The Journal of Chemical Physics* 119.13 (2003), pp. 6789–6801. DOI: 10.1063/1.1603736.

[90] M. Dumont, G. Froc, and S. Hosotte. "Alignment and orientation of chromophores by optical pumping". In: *Nonlinear Optics* 9 (1995), pp. 327–338.

[91] A. Kopyshev et al. "Optomechanical scission of polymer chains in photosensitive diblock copolymer brushes". In: *Langmuir* 29.45 (2013), pp. 13967–13974. DOI: 10.1021/la403241t.

[92] A. Ambrosio, P. Maddalena, and L. Marrucci. "Molecular model for light-driven spiral mass transport in azopolymer films". In: *Phys. Rev. Lett.* 110 (2013), p. 146102. DOI: 10.1103/PhysRevLett.110.146102.

[93] P. PERZYNA. "The constitutive equations for rate sensitive plastic materials". In: *Quarterly of Applied Mathematics* 20.4 (1963), pp. 321–332. DOI: 10.1090/QAM/144536.

[94] A. Kozanecka-Szmigiel et al. "On stress-strain responses and photoinduced properties of some azopolymers." In: *Polymer* 140 (2018), pp. 117–121. DOI: 10.1016/j.polymer.2018.02.028.

[95] G. D. Florio et al. "Graphene multilayer as nanosized optical strain gauge for polymer surface relief gratings". In: *Nano Letters* 14.10 (2014), pp. 5754–5760. DOI: 10.1021/nl502631s.

[96] N. S.r Yadavalli et al. "Soft matter beats hard matter: rupturing of thin metallic films induced by mass transport in photosensitive polymer films". In: *ACS Applied Materials & Interfaces* 5.16 (2013), pp. 7743–7747. DOI: 10.1021/am400682w.

[97] R. B. Bird et al. *Dynamics of polymeric liquids, kinetic theory.* 2nd ed. Vol. 2. Dynamics of Polymeric Liquids. New York: Wiley-Interscience, 1987. ISBN: 0-471-80244-1.

[98] M. Doi and S.F. Edwards. *The theory of polymer dynamics.* International series of monographs on physics. Clarendon Press, 1986. ISBN: 9780198519768.

[99] A. Ortega and J. G. dela Torre. "Hydrodynamic properties of rod-like and disk-like particles in dilute solution." In: *J. Chem. Phys.* 119 (2003), pp. 9914–9919. DOI: 10.1063/1.1615967.

[100] M. B. Mackaplow and E. S. G. Shaqfeh. "A numerical study of the rheological properties of suspensions of rigid, non-Brownian fibres". In: *Journal of Fluid Mechanics* 329 (1996), pp. 155–186. DOI: 10.1017/S0022112096008889.

[101] B. Yadav et al. "Orientation approach to directional photodeformations in glassy side-chain azopolymers". In: *The Journal of Physical Chemistry B* 123.15 (2019), pp. 3337–3347. DOI: 10.1021/acs.jpcb.9b00614.

[102] S. Loebner et al. "Local direction of opto-mechanical stress in azobenzene containing polymers during surface relief grating formation". In: *Macromolecular Materials and Engineering* (2022). DOI: 10.1002/mame.202100990.

[103] B. Yadav, J. Domurath, and M. Saphiannikova. "Modeling of stripe patterns in photosensitive azopolymers". In: *Polymers* 12.4 (2020). DOI: 10.3390/polym12040735.

[104] J. Oldroyd. "A rational formulation of the equations of plastic flow for a Bingham solid." In: *Mathematical Proceedings of the Cambridge Philosophical Society.* 43 (1947), pp. 100–105. DOI: 10/1017/S0305004100023239.

[105] ANSYS help. In: (2021). URL: https://ansyshelp.ansys.com/account/secured?returnurl=/Views/Secured/corp/v202/en/wb2_help/wb2_help.html%23wb2_help.

[106] K. M. Lee and T. J. White. "Photochemical mechanism and photothermal considerations in the mechanical response of monodomain, azobenzene-functionalized liquid crystal polymer networks". In: *Macromolecules* 45.17 (2012), pp. 7163–7170. DOI: 10.1021/ma301337e.

[107] F. Pirani et al. "Light-driven reversible shaping of individual azopolymeric micro-pillars". In: *Scientific Reports* 6.1 (2016). DOI: 10.1038/srep31702.

[108] S. Lee et al. "Directional superficial photofluidization for deterministic shaping of complex 3D architectures". In: *ACS Applied Materials & Interfaces* 7.15 (2015), pp. 8209–8217. DOI: 10.1021/acsami.5b01108.

[109] A. Ambrosio et al. "Realization of submicrometer structures by a confocal system on azopolymer films containing photoluminescent chromophores". In: *Journal of Applied Physics* 107 (2010). DOI: 10.1063/1.3382945.

[110] A. Ambrosio. "(CNST@POLIMI - fondazione Istituto Italiano di Tecnologia, Milano, Italy)". In: *Private Communication* (2020).

[111] M. E. Gurtin, E. Fried, and L. Anand. *The mechanics and thermodynamics of continua.* 1st ed. Vol. 53. 9. Cambridge University Press, 2010. ISBN: 978-0-511-76980-1.

[112] A. Kopyshev et al. "Light-induced structuring of photosensitive polymer brushes". In: *ACS Applied Polymer Materials* 1.11 (2019), pp. 3017–3026. DOI: 10.1021/acsapm.9b00705.

List of Figures

2.1 Chemical structure of azobenzene chromophore a) in the straight trans-state and b) in the bent cis-state. 9
2.2 Isomerization between trans- and cis-isomers of azobenzene chromophore in the presence of light. 9
2.3 Representation of the orientation vector $\boldsymbol{u}$ in the polar co-ordinate system. The nematic director $\mathbf{n}$ is along the x axis. 14
2.4 The linearly polarized light is propagating in the z direction and its electric field vector (represented with gray arrows) lies along the y direction. 16
2.5 In left handed circularly polarized light, the electric field vectors, represented by gray color, rotate anti-clockwise with respect to the observer and the light propagates along the z direction. . . . 17
2.6 In right handed circularly polarized light, the electric field vectors, represented by gray color, rotate clockwise with respect to the observer and the light propagates along the z direction. . . . 17
2.7 a) Typical setup for interference patterns where red lines represent the two light beams, whose wavefronts propagate in the shaded incidence plane. b) Representation of SS c) and PP interference patterns, where length of arrow represents the intensity of light and direction gives polarization. 19
2.8 Light-induced orientation of azobenzenes in the plane perpendicular to the light polarization $\boldsymbol{E}$ of the linearly polarized light. . . 22
2.9 a) Representation of the azopolymer Kuhn segment, the orange-colored chromophores are rigidly attached to the main chain via a spacer (both are represented by blue color), the gray arrow represents the orientation vector for the Kuhn segment and b) the electric field vector makes an angle θ with the unit orientation vector. 24

3.1 Light-induced orientation of azobenzenes along the propagation direction $\boldsymbol{k}$ of the circularly polarized light. 27
3.2 Comparison of the linear and hybrid closure approximations with the closure based on the effective orientation potential, as assigned in the legend. 35

3.3 Time evolution of the orientation tensor components: a) $\langle u_x^2 \rangle$ and b) $\langle u_y^2 \rangle = \langle u_z^2 \rangle$ for different strengths of the reduced potential V_r. Time is expressed in the units of λ, rotational time of the rigid segments. 39
3.4 All three components of the orientation tensor corresponding to maximum stress under the SS interference pattern for $\tau_{xx,0} = 25$ MPa. 40

4.1 Dependence of stress on strain in the bilinear isotropic hardening (BISO) model: E is the Young's modulus and E_t is the tangent modulus. 43
4.2 Distribution of stress fields $\boldsymbol{\tau}$ in the block a) hanging at the ceiling and b) lying on the ground, under the effect of gravitational force mg. Here, l is the length of the block, m is the mass and ρ is the density of the block. 45

5.1 Deformations of a) the initial square post in the presence of homogeneous light intensity. Deformed post in the presence of b) vertically polarized light, c) horizontally polarized light and d) circularly polarized light. Modified and reproduced from Ref. [37]. 46
5.2 The time dependent components of the light-induced stress tensor at different strengths of the reduced potential $V_r = -5, -10, -15$: a) τ_{xx} for horizontally and b) τ_{zz} for circularly polarized light. . 47
5.3 The time dependent true plastic strain for the linearly polarized light at different magnitudes of initial equivalent stress τ_{eq}. $\tau_{yield} = 10$ MPa, $\lambda = 50\Delta t$. 48
5.4 The time dependent true plastic strain for the circularly polarized light at different equivalent stress τ_{eq}. $\tau_{yield} = 10$ MPa, $\lambda = 50\Delta t$. 49
5.5 The dependence of stopping time on the initial equivalent stress when the azopolymer sample is illuminated with linearly (blue) and circularly (red) polarized light. 50
5.6 The dependence of stationary plastic strain on the initial equivalent stress when the azopolymer sample is illuminated with linearly (blue) and circularly (red) polarized light. 51
5.7 ANSYS undeformed square post: (a) 3D view of 1/8 of the post and (b) top view. 52
5.8 Plastic strain with respect to time a) for $\tau_{eq} = 30$ MPa with different time step sizes at 0.5 μm mesh size, b) for $\tau_{eq} = 50$ MPa with different mesh sizes at the time step $0.1\Delta t$. 53
5.9 Stationary deformation of 1/8 of the square post in the presence of linearly polarized light: (a) 3D view and (b) the top view shows the elongation along the light polarization $l/l_0 = 2.19$, $\tau_{eq} = 30$ MPa. 54

5.10 Stationary deformation of 1/8 of the square post in the presence of circularly polarized light: (a) 3D view and (b) the top view shows the expansion perpendicular to the light propagation direction $l/l_0 = 1.23$, $\tau_{eq} = 50$ MPa. 55

6.1 The laser beam is represented by the green stick moved in the y-direction (shown by the dotted red line). The formation of a) a groove and b) a protrusion is observed in the thin polymer films for light polarized in the x and y direction, respectively [109, 103]. 57
6.2 The x component of the volume force: (a) stretching for light polarized in x direction and (b) compressive for light polarized in y direction. $\tau_0 = 40$ MPa. The beam radius $w = 2\sqrt{10}\ \mu m$. . . . 59
6.3 The surface represented with the light gray colour is free to move in all three directions and the all four side surfaces represented with dark grey color are restricted to move in the normal direction. 61
6.4 The top surface represented with the light gray colour is free to move in all three directions and the all four side surfaces represented with dark grey color are restricted to move in the normal direction. 62
6.5 The deformations for the upper surface of the material in the presence of x polarized light. $\tau_{max} = 50$ MPa. The film dimensions are $0 \leq x \leq 60\ \mu$m, $0 \leq y \leq 15\ \mu$m, $0 \leq z \leq 15\ \mu$m and the beam radius $w = 2\sqrt{10}\ \mu m$. 63
6.6 The deformations in z direction for light polarized in x direction.The film dimensions are $0 \leq x \leq 60\ \mu$m, $0 \leq y \leq 15\ \mu$m, $0 \leq z \leq 15\ \mu$m and the beam radius $w = 2\sqrt{10}\ \mu m$. 63
6.7 Time-dependent deformations in z direction for light polarized in the x direction. Value of the maximum traction τ_{max} is shown in the legend. The film dimensions are $0 \leq x \leq 60\ \mu$m, $0 \leq y \leq 15\ \mu$m, $0 \leq z \leq 15\ \mu$m and the beam radius $w = 2\sqrt{10}\ \mu m$. 64
6.8 The deformations in z direction for the light polarized in x direction at different values of squared beam radius w^2, shown in the legend. The film dimensions are $0 \leq x \leq 60\ \mu$m, $0 \leq y \leq 15\ \mu$m, $0 \leq z \leq 15\ \mu$m. 65
6.9 The deformations for the upper surface of the material in the presence of y polarized light. $\tau_{max} = 50$ MPa. The film dimensions are $0 \leq x \leq 60\ \mu$m, $0 \leq y \leq 15\ \mu$m, $0 \leq z \leq 15\ \mu$m and the beam radius $w = 2\sqrt{10}\ \mu m$. 66
6.10 The deformations in z direction for light polarized in y direction.The film dimensions are $0 \leq x \leq 60\ \mu$m, $0 \leq y \leq 15\ \mu$m, $0 \leq z \leq 15\ \mu$m and the beam radius $w = 2\sqrt{10}\ \mu m$. 66
6.11 Time-dependent deformations in z direction for light polarized in the y direction. Value of the maximum traction τ_{max} is shown in the legend. The film dimensions are $0 \leq x \leq 60\ \mu$m, $0 \leq y \leq 15\ \mu$m, $0 \leq z \leq 15\ \mu$m and the beam radius $w = 2\sqrt{10}\ \mu m$. 67

6.12 The film area in which the stresses exceed the yield stress rapidly shrinks with decrease of $\boldsymbol{\tau}_{max}$. This example is calculated for the beam radius $w = 2\sqrt{10}\mu$m [103]. 68

7.1 AFM micrograph of the initial and elongated colloid in the presence of linearly polarized light. The light-induced elongation ratios is about 5. Modified and reproduced from Ref. [52]. 70
7.2 AFM micrograph of the SRG inscribed in colloidal particles using a) PP interference pattern and b) SS interference pattern. The arrows show the polarization direction and their length is related to the light intensity. Modified and reproduced from Ref. [102]. 70
7.3 AFM micrographs of the gap edges structured during irradiation with (a) RL and (b) LR polarization pattern. White and black arrows show the distribution of the electrical field vectors. Modified and reproduced from Ref. [102]. 70
7.4 a) Time evolution of equivalent stress corresponding to $\tau_{xx,0} =$ 30 MPa. b) Dependence of stopping time on the initial applied stress. 72
7.5 Initial half of the sphere with diameter 1μm: (a) top view (b) 3D view. 73
7.6 The deformed half-spheroid after 50 s of irradiation for $\tau_{xx,0}$ equal to a) 15 MPa, b) 20 MPa, c) 25 MPa and d) 30 MPa is shown here. e) The time dependence of length of the half-spheroid at different $\tau_{xx,0}$. 74
7.7 The variation of the light intensity with optical period D and light polarization direction in x direction for PP interference pattern is represented by the blue curve. 76
7.8 The deformed half-spheroid after 10 s of irradiation for initial $\tau_{xx,0}$ a) 15 MPa, b) 20 MPa, c) 25 MPa and d) 30 MPa is shown here. 77
7.9 Dependence of a) length and b) radius of half-spheroid on the initial value of $\tau_{xx,0}$ under the PP interference pattern. 77
7.10 The final deformations in y direction at different $\tau_{xx,0}$ under the PP interference pattern. 78
7.11 Directional deformation in y direction under the PP interference pattern after 5 s (red line) and 10 s (blue line) of irradiation time, at $\tau_{xx,0} = 25$ MPa. 79
7.12 a) The deformations in y direction and b) length of half spheroid dependence on the optical period at initial maximal stress $\tau_{xx,0} =$ 25 MPa. 80
7.13 The variation of the light intensity with optical period D and light polarized in y direction for the SS interference pattern is represented by the blue curve. 81
7.14 3D view of wave-like structure developed after 10 s irradiation with the SS interference pattern at $\tau_{xx,0} = 25$ MPa. 82

7.15 Time dependence of half-spheroid sizes for different $\tau_{xx,0}$ under the SS interference pattern: a) radius in the z direction, b) radius in the y direction and c) length of the half-spheroid. 83
7.16 The deformed half-spheroid after 50 seconds of irradiation for initial $\tau_{xx,0}$ a) 15 MPa b) 20 MPa c) 25 MPa d) 30 MPa is shown here. e) The final deformations in y direction depending on initial $\tau_{xx,0}$ under the SS interference pattern. 84
7.17 Directional deformation in y direction at 5 s and at 10 s of irradiation, $\tau_{xx,0} = 25$ MPa. 85
7.18 Directional deformation at the initial value of $\tau_{xx,0} = 25$ MPa under the SS interference pattern for different optical periods D. 86
7.19 The surfaces represented with the light gray colour are free to move in all three directions, the two side surfaces represented with dark grey color are restricted to move in the normal direction and the bottom surface is restricted to move in all three direction. . . 87
7.20 Plastically deformed azopolymer films at $\tau_{xx,0} = 25$ MPa after 80 s irradiation with (a) the RL pattern and (b) LR pattern. Insert shows the rotation of ECS along the period of the optical grating. The light polarization is represented by red arrows. 88
7.21 (a) Under the RL pattern the azopolymer gradually protrudes along the axis y and builds a surface relief along the axis z; $\lambda =$ 1000 s (b) The growth of protrusion reduces with the decrease of rotational time λ of backbone segments; $\tau_{xx,0} = 25$ MPa. 88

List of Tables

7.1 Light-induced changes in the half-spheroid corresponding to the different initial applied stresses $\tau_{xx,0}$ after 50 s of irradiation. . . 75

List of Symbols

This list describes symbols that are used within the body of the thesis.

μ	Biaxial order parameter
η	Viscosity of the plastic flow
γ	Viscosity parameter
λ	Rotational time of the rigid segment
ρ	Density
τ_{eq}	Equivalent stress
τ_{yield}	Yield stress
$\boldsymbol{\delta}$	Unit tensor
$\boldsymbol{\epsilon_{el}}$	Elastic strain tensor
$\boldsymbol{\epsilon_{mech}}$	Mechanical strain tensor
$\boldsymbol{\epsilon_{pl}}$	Plastic strain tensor
$\boldsymbol{\epsilon_{th}}$	Thermal strain tensor
$\boldsymbol{\tau_{light}}$	Light-induced stress tensor
$\boldsymbol{\tau}$	Total stress tensor
$\boldsymbol{E}$	Electric field vector
$\boldsymbol{F}$	Force
$\boldsymbol{f}$	Volume force
$\boldsymbol{k}$	Light propagation vector
$\boldsymbol{n}$	Nematic director
$\boldsymbol{P}$	Polarization

$\boldsymbol{Q}$	Nematic order tensor
$\boldsymbol{u}$	Orientation vector
D	Optical period
D_r	Orientation diffusion coefficient of the azobenzene
E	Young's modulus
e_l	Elongation ratio of half-spheroid
E_t	Tangent modulus
G	Shear modulus of the azopolymer
I	Light intensity
I_0	Total intensity of light
k_B	Boltzmann constant
l	Final edge length of the square post
l_0	Initial edge length of the square post
l_i	Initial length of half-spheroid
m	Number of azobenzenes in the backbone segment
n	Number density of segments
q	Shape factor of the azopolymer
T	Temperature
t	Time
t_{stop}	Stopping time
U	Effective orientation potential
v	Velocity
V_0	Strength of the orientation potential
V_r	Reduced potential
w	Gaussian beam radius
Q	Nematic order parameter

Erklarung

Hiermit versichere ich, dass ich die vorliegende Arbeit ohne unzulassige Hilfe Dritter und ohne Benutzung anderer als der angegebenen Hilfsmittel angefertigt habe; die aus fremden Quellen direkt oder indirekt ubernommenen Gedanken sind als solche kenntlich gemacht. Die Arbeit wurde bisher weder im Inland noch im Ausland in gleicher oder ahnlicher Form einer anderen Prufungsbehorde vorgelegt.
Die Arbeit wurde angefertigt unter Betreuung von Prof. Dr. Jens-Uwe Sommer am Leibniz-Institut fur Polymerforschung Dresden e.V., Hohe Strasse 6, 01069 Dresden.
Es haben betreffend meiner Person keine fruheren erfolglosen Promotionsverfahren stattgefunden.
Weiter erklare ich hiermit, dass ich die Promotionsordnung vom 23.02.2011 der Fakultat Mathematik und Naturwissenschaften der Technischen Universitat Dresden anerkenne.

Unterschrift:

Datum: